

STUDY OF STATE-OF-CHARGE AND DEGRADATION
IN LITHIUM ION BATTERY PACK

A THESIS SUBMITTED TO THE GRADUATE DIVISION OF THE
UNIVERSITY OF HAWAI'I AT MĀNOA IN PARTIAL FULFILLMENT
OF THE REQUIREMENTS FOR THE DEGREE OF

MASTER OF SCIENCE

IN

MECHANICAL ENGINEERING

MAY 2012

By

Cyril A. Truchot

Thesis Committee:

Bor Yann Liaw, Chairperson
Mehrdad N. Ghasemi Nejhad
Lloyd H. Hihara

Keywords: Lithium-ion battery, Battery pack, Battery testing, State-of-charge, Cell-to-cell variations,
Cycle aging, Degradation mechanisms, Incremental capacity analysis

Acknowledgements

I would have never been able to finish my thesis without the guidance of my advisors, help from friends and support from my family and girlfriend.

First and foremost, I owe sincere and earnest thankfulness to my advisor, Prof. Bor Yann Liaw, for welcoming me in his Electrochemical Power Systems Laboratory despite my mechanical engineering background, for his excellent guidance, caring, patience, and support through the good times and bad for the past three years.

I would like to express my deepest gratitude to Dr. Matthieu Dubarry for guiding my research, for the countless fruitful discussions, and for helping me to develop my knowledge in material science, electrochemistry and battery. Also, and most importantly, I would like to thank him for believing in me at all times.

I would like to thank Dr. Shengxi Li for his help in the lab and to all the postdocs, technicians and students that have come and gone through the lab: Dr. Mikael Cugnet, Dr. Kenny Chiu, Dr. Nahong Zhao, Elton Wong and Bernhard Lochner. Besides, I want to thank Dr. Nicolas Gaillard (Thin Films Lab) for letting me borrowing his tools and his equipment at many occasions.

I would also like to show my gratitude to Prof. Mehrdad N. Ghasemi Nejhad and Prof. Lloyd H. Hihara for accepting to serve in my thesis committee.

It is a great pleasure to thank the HNEI staff too, specifically Grace Fujino and Michele Nuibe, for kindly helping me with the administrative work.

I am also very grateful to Anais, Benoit, Melanie, Francois and Volker for boosting me morally.

Finally, I would like to thank my family and my girlfriend, Merica McNeil. She has always been there with me cheering me up through course of my study.

Abstract

Rechargeable batteries in portable electronics, powertrains and energy storage systems need to handle more energy and power that are beyond a single cell's capability. Therefore, in today's battery applications, connecting cells in series/parallel configurations to meet energy and power requirements is a common practice. As the number of cells in the battery configuration increases, the complexity in the control and managing the cells becomes sophisticated as well. There is an urgent need to understand the behavior of multi-cell strings through proper assessments to derive adequate knowledge for the control and management of the battery packs. Here two very important aspects in the string assessments and evaluations in terms of state-of-charge estimation and pack degradation using Li-ion commercial cells are studied. The ability to characterize cell variability using non-destructive electrochemical techniques such as incremental capacity analysis and accurate state-of-charge tracking, enables us to understand the inherent variations among the cells and their impact on the string performance characteristics as well as their degradation mechanisms in different cycle aging processes.

Table of Contents

Acknowledgements.....	ii
Abstract.....	iii
Table of Contents.....	iv
List of tables.....	viii
List of figures.....	ix
List of abbreviations.....	xiv
1 Introduction and background information on Li-ion batteries.....	1
1.1 Why Li-ion batteries?	1
1.1.1 Introduction to commercial Li-ion batteries.....	1
1.1.2 Li-ion batteries among other rechargeable batteries.....	2
1.2 Status of development of Li-ion cells.....	3
1.2.1 Back to battery basics	3
1.2.2 Li-ion battery chemistries	5
1.3 Li-ion battery packs.....	6
1.3.1 Different pack configurations	6
1.3.2 Merits of Li-ion battery packs	7
1.3.3 Additional issues with battery packs	8
2 State-of-charge of a Li-ion cell	9
2.1 State-of-charge according to USABC	9
2.1.1 Definition.....	9
2.1.2 Importance of determining SOC in Li-ion battery and Li-ion battery pack applications	10
2.1.3 Limitations of the USABC definition for SOC	10
2.2 Thermodynamic state-of-charge	11
2.2.1 Binary phase diagrams and electrical potential.....	11
2.2.2 Example: the LiCoO ₂ Li-ion cell.....	14
2.2.3 Definition of thermodynamic state-of-charge	17
2.3 SOC determination.....	18
2.3.1 A literature review: how is SOC determined?.....	18
2.3.2 Experimental validation of “t-SOC” determination using OCV measurements.....	21

2.4	Accuracy on OCV-SOC measurements	22
2.5	What about pack-SOC?	24
3	Cell variability.....	25
3.1	Origins of performance variability of Li-ion batteries.....	25
3.2	Initial conditioning and characterization tests	27
3.2.1	Description of Li-ion cells studied	27
3.2.2	Experimental	27
3.2.3	Experimental results and discussion.....	29
3.3	Cell-to-cell variation conclusions	31
4	SOC of a battery pack.....	32
4.1	Different methods for pack-SOC from OCV measurements	33
4.1.1	Method #1: Pack ps-OCV=f(SOC) curve	33
4.1.2	Method #2: Average relax cell voltages.....	33
4.1.3	Method #3: Average of single cell SOC's	34
4.1.4	Method #4: Single cell minimum SOC.....	34
4.1.5	Method #5: Single cell maximum SOC	35
4.2	Tests on accuracy of each method	35
4.2.1	Experimental	35
4.2.2	Remnant capacity test results.....	36
4.2.3	Pack-SOC analysis and discussion	37
4.3	Discussion of uncertainty of SOC estimation using ps-OCV=f(SOC) curves for pack and single cell	41
4.4	Conclusion on pack-SOC	42
5	Ageing analysis of Li-ion battery packs	43
5.1	Degradation of Li-ion battery pack	43
5.2	Stress factors impacting performance and degradation of commercial Li-ion cells in a string configuration.....	43
5.3	Ageing of commercial Li-ion cell in a string configuration.....	45
5.3.1	Ageing of commercial Graphite/spinel Li-ion cell in a string configuration with temperature gradient within the string.....	45
5.3.2	Ageing of commercial Graphite/composite [NMC+spinel] Li-ion cell in a string configuration with initial capacity variability and initial SOC imbalance.....	57

5.3.3	Ageing of commercial Graphite/NMC Li-ion cell in a string configuration with imbalance on polarization resistance	69
5.4	Conclusions on pack degradation	78
6	Conclusion and future directions	79
7	Appendix	82
7.1	Li-ion cell chemistries.....	82
7.1.1	Material properties and atomic structures.....	82
7.1.2	Atomic structures and capacity of Li-ion cells	83
7.1.3	Experimental illustration of performances of diverse Li-ion chemistries using ps-OCV=f(SOC)curve	84
7.1.4	Li-ion cells studied in thesis work	86
7.2	Origins of cell variability.....	87
7.2.1	Influence of redox couples.....	87
7.2.2	Influence of crystal structure of active material.....	88
7.2.3	Influence of synthesis conditions of active materials.....	89
7.2.4	Influence of the electrode architecture.....	89
7.2.5	Influence of electrode processing.....	90
7.2.6	Electrode loading	92
7.2.7	Electrode separator.....	93
7.2.8	Influence of casings.....	93
7.2.9	Importance of formation cycle	94
7.3	Cell variability.....	95
7.3.1	Amount of material involved and capacity ration	95
7.3.2	Rate capability and Peukert coefficient	97
7.3.3	Resistance variations.....	103
7.4	Methods for determining the SOC in Li-ion batteries.....	105
7.4.1	Accuracy of the ps-OCV=f(SOC) curves	105
7.4.2	Techniques to derive model for SOC estimation	107
7.4.3	Summary	112
7.4.4	Uncertainty of SOC estimation using ps-OCV=f(SOC) curves for pack and single cell.....	115
7.5	Pack SOC.....	117
7.5.1	Summary of the 5 pack SOC methods.....	117

7.5.2	SOC results per method	118
7.5.3	Pack capacity ration results per method	121
7.6	Incremental capacity and cell degradation mechanisms analysis	124
7.6.1	Incremental capacity concept.....	124
7.6.2	Incremental capacity peak indexation.....	127
7.7	Test equipment.....	129
7.7.1	Arbin.....	129
7.7.2	Maccor Series 4300.....	129
7.7.3	BioLogic VMP3	130
8	References	131

List of tables

Table 1 Li-ion cell chemistry summary.....	5
Table 2 Average values of attributes for each cell type.....	29
Table 3 Standard deviations for each attribute of the cell-to-cell variation for each cell type.....	30
Table 4 Capacity ration per rate per method	39
Table 5 IMR cell selection for pack configuration (based on their similarity)	45
Table 6 INL cell selection for pack configuration (based on maximum capacity).....	57
Table 7 IHR cell selection for pack configuration (based on polarization resistance)	70
Table 8 Cell chemistry properties and applications.....	82
Table 9 Positive electrode crystal structures	83
Table 10 Manufacturer specs of studied cells	86
Table 11 Capacity ration averages and standards deviation	96
Table 12 Manufacturer and experimental discharge capacities of IHR and INL cells.....	98
Table 13 Peukert coefficient of studied cells.....	100
Table 14 Q5/Q2 ratio averages and standard deviation.....	102
Table 15 Resistance averages and standards deviation	104
Table 16 Equivalent system to each pack-SOC estimation method	117
Table 17 Advantages and drawbacks summary.....	117
Table 18 C/25 capacity correction using the resistance in the circuit.....	118
Table 19 EOC and EOD SOCs from method #1.....	119
Table 20 EOC and EOD SOCs from method #2.....	120
Table 21 EOC and EOD SOCs from method #3.....	120
Table 22 EOC and EOD SOCs from method #4.....	121
Table 23 Capacity ration from method #1	122
Table 24 Capacity ration from method #2	122
Table 25 Capacity ration from method #3	123
Table 26 Capacity ration from method #4	123
Table 27 Capacity ration from method #5	123

List of figures

Figure 1 Commercial Li-ion cells	1
Figure 2 a) Energy density per unit mass and volume for common secondary cells ⁴ ; b) Electrochemical cell voltages.....	2
Figure 3 Electrochemical system	4
Figure 4 Pack: A) series; B) parallel; C) mixture	6
Figure 5 Equivalence in voltage of a 6-cell lead acid pack and a 3-cell Li-ion battery pack.....	7
Figure 6 a) gas gauge, b) SOC gauge	9
Figure 7 Limitations of SOC definition from USABC: capacity loss neglected.	10
Figure 8 Schematic binary phase diagram	12
Figure 9 Schematic variation of electrical potential with composition across the binary phase diagram shown in Figure 8.....	12
Figure 10 Open circuit voltage of a graphite electrode during Li insertion.....	14
Figure 11 Open circuit voltage versus amount of lithium in a LiCoO ₂ electrode	15
Figure 12 The first charge/discharge cycle of a graphite electrode	16
Figure 13 a) Li insertion in each electrode.....	17
Figure 14 Illustration of t-SOC.....	18
Figure 15 SOC measurement from open circuit voltage.....	20
Figure 16 Accuracy issues in SOC determination.....	21
Figure 17 (a) Uncertainty of SOCs on LFP cell full SOC range. (b) Zone of uncertainty on LFP cell ps-OCV=f(SO) curves).....	23
Figure 18 Performance variability in Li-ion battery manufacturing processes.....	26
Figure 19 A) Arbin Universal Battery Holder, B) Arbin High Current Battery Holder	27
Figure 20 Method 1: 3-cell pack considered as one cell.....	33
Figure 21 Method 2: 3-cell pack reduced to one single cell	33
Figure 22 Method 3: 3-cell pack SOC from independent single cell.....	34
Figure 23 Method #4: 3-cell pack SOC is single cell's lowest SOC within the string.....	34
Figure 24 Method #5: 3-cell pack SOC is single cell's greatest SOC within the string	35
Figure 25 Pack circuit	36
Figure 26 SOC range per rate per method (summary)	37
Figure 27 Zoom of pack EOC and EOD SOCs	37
Figure 28 Remnant capacity.....	38
Figure 29 Predicted SOC vs. Experimental SOC	39

Figure 30 Predicted SOCs vs. Experimental SOCs (validation on 2 other chemistries).....	40
Figure 31 Comparison of SOC uncertainty from single cell ps-OCV=f(SOC) curve and pack ps-OCV=f(SOC) curve	41
Figure 32 (a) Pack capacity evolution at different C-rate. (b) Capacity evolution as a function of cycle number for single cell cycling at identical conditions.....	47
Figure 33 (a) Peukert curves of single cell and pack. (b) RPVs evolution at the EOD and EOC at different C-rate.	47
Figure 34 (a) Pack evolving ps-OCV=f(SOC) curves. (b) EOC and EOD SOCs from the pack evolving ps-OCV=f(SOC) curves.....	48
Figure 35 IMR pack capacity ration evolution during cycle aging	49
Figure 36 IMR pack Peukert curves during cycle aging.....	50
Figure 37 (a) Relax cell voltages (RCVs) of each IMR cell in the pack versus cycle number as measured during the cycle aging at the beginning- and end-of-charge. (b) Evolution of the end-of-charge and end-of-discharge SOC of each IMR cell during cycle aging.	51
Figure 38 (a) EOD voltage before relaxation of each cell during cycle aging. (b) EOD voltage before relaxation of IMR pack during cycle aging.	51
Figure 39 Capacity ration evolution per cell in IMR pack with temperature gradient.	52
Figure 40 IC curves at C/25-rate in discharge for (a) cell#1, (b) cell #2, and (c) cell #3.....	53
Figure 41 Evolution of IC peak intensity for (a) peak #1, and (b) peak #2.....	53
Figure 42 IC curves at C/25-rate in charge for (a) cell#1, (b) cell #2, and (c) cell #3.	54
Figure 43 Comparison of IC curves at C/25-rate in discharge on cycle #4 and #10 for (a) cell #1, (b) cell #2, and (c) cell #3.	55
Figure 44 Evolution of cell ps-OCV=f(SOC) curves for (a) cell #1 and #3, and (b) cell #2.	55
Figure 45 Comparison of ps-(OCV)=f(SOC) curves according to cell capacity rations evolution	56
Figure 46 (a)Capacity variations as a function of cycle number measured during cycle aging and from reference performance tests using different C/n rates; (b) Peukert curves of single cell and pack	59
Figure 47 Capacity variation comparison between pack and single cell at (a) 2C, and (b) C/25.....	59
Figure 48 (a)Rest pack voltages (RPVs) versus cycle number as measured during the cycle aging and from RPTs at the BOD and EOD; (b) Relax cell voltages (RCVs) from the single cell study	60
Figure 49 (a) The ps-OCV=f(SOC) curves as a function of cycle for (a) the pack and, (b) the single cell	61
Figure 50 (a) Pack SOC evolution from floating pack ps-OCV=f(SOC) curves. (b) Comparison of capacity ration evolution between pack and single cell	62
Figure 51 (a) RCVs of each cell in the pack versus cycle number as measured during the cycle aging at the beginning- and end-of-discharge. (b) Evolution of the end-of-charge and end-of-discharge SOC of each cell determined during cycle aging.	63

Figure 52 (a) End-of-charge SOC _s for each cell in the pack determined from the evolving ps-OCV=f(SOC) curves of each cell. (b) End-of-discharge SOC _s for each cell in the pack determined from the evolving ps-OCV=f(SOC) curves of each cell.....	63
Figure 53 Evolution of capacity ration for each cell in the string calculated from the ΔSOC _s given by the evolving ps-OCV=f(SOC) curves.....	64
Figure 54 IC curves at C/25-rate for (a) cell #1, (b) cell #2, and (c) cell #3	65
Figure 55 (a) EOD voltage before relaxation. (b) EOC voltage before CV step.....	66
Figure 56 (a) Polarization resistance in discharge. (b) Polarization resistance in charge.....	67
Figure 57 IC curves at C/2-rate for (a) cell #1, (b) cell #2, and (c) cell #3	68
Figure 58 (a) Spinel Resistance. (b) Spinel peak intensity evolution.	68
Figure 59 (a) Capacity variations as a function of cycle number measured during cycle aging and from reference performance tests using C/25-rates. (b) Rest pack voltages (RPVs) versus cycle number as measured during the cycle aging and from RPTs at the BOD and EOD.	71
Figure 60 (a) Peukert curves of single cell and pack; (b) Capacity evolution as a function of cycle number for single cell cycling at identical conditions.....	71
Figure 61 (a) Pack evolving ps-OCV=f(SOC) curves. (b) Pack SOC _s from the evolving ps-OCV=f(SOC) curves determined with 3 different methods.....	72
Figure 62 Pack capacity ration evolution during C/2-rate cycle aging.....	73
Figure 63 (a) Relax cell voltages (RCVs) of each cell in the pack versus cycle number as measured during the cycle aging at the beginning- and end-of-discharge. (b) Evolution of the end-of-charge and end-of-discharge SOC of each cell determined during cycle aging.	74
Figure 64 Capacity ration evolution per cell in IHR pack with initial imbalance base on the polarization resistance.....	74
Figure 65 IC curves at C/25-rate in discharge for (a) cell #1, (b) cell #2, and (c) cell #3.....	75
Figure 66 (a) Cell voltage at the end of discharge before relaxation per cell. (b) NMC peak intensity evolution per cell.	76
Figure 67 IC curves at C/2-rate in charge for (a) cell #1, (b) cell #2, and (c) cell #3	77
Figure 68 USABC SOC definition limitation: capacity loss not considered	80
Figure 69 SOC gauge evolution during cycle aging	80
Figure 70 Comparison of ps-OCV=f(SOC) curve for two different chemistries (Nickel Zinc and Li-ion)	85
Figure 71 Comparison of ps-OCV=f(SOC) curve of two Li-ion cells with different positive electrode materials	85
Figure 72 Comparison of ps-OCV=f(SOC) curve for two Li-ion cell with different NE/PE ratio	86
Figure 73 From redox couples to battery packs	87
Figure 74 Diverse redox couples used in Li-ion batteries	88
Figure 75 Potential vs. capacity of lithium insertion in a) LiCoPO ₄ and b) LiCoO ₂	88

Figure 76 Capacity evolution for a vanadium oxide active material obtained from different synthesis processes.....	89
Figure 77 Schematic drawing indicating the impact of carbon black distribution on the kinetics of Li+/electron electrochemical insertion into active material ⁵⁴	90
Figure 78 Tape casting process	91
Figure 79 Evolution of the discharge capacity with the solvent concentration expressed in mL/mg of dried material ⁵⁶	91
Figure 80 Comparison of two cells using same active material but different electrode loading	92
Figure 81 Cylindrical cell components	93
Figure 82 Capacity ration distribution for (A) IMR, (B) IHR, (C) IBR, (D) INL	96
Figure 83 Peukert curves of (a) INL cell, (b) IHR cell, (c) IHR and INL manufacturer specs, and (d) IHR and INL experimental data.....	99
Figure 84 Peukert curves of (a) IBR cells and, (b) IMR cells	100
Figure 85 Q5/Q2 ratio distribution for (A) IMR, (B) IHR, (C) IBR and (D) INL cells	102
Figure 86 Incremental capacity curve used for polarization resistance calculation.....	103
Figure 87 Resistance distribution for (A) IMR, (B) IHR, (C) IBR, (D) INL	104
Figure 88 GITT cycle with zoom on relax cell voltages used for ps-OCV=f(SOC) curve	105
Figure 89 C/25 and C/2 rate cycles	106
Figure 90 Comparison of OCV vs. SOC curves obtained from GITT and C/25-rate cycle.....	107
Figure 91 Artificial Neural Network	108
Figure 92 Nyquist plot obtained with impedance spectroscopy frequency response, (a) and parameters identification (b).....	109
Figure 93 Li-ion battery equivalent circuit model.....	109
Figure 94 Principle of Kalman filter.....	110
Figure 95 Membership functions for (a) temperature and (b) SOC	111
Figure 96 A complete fuzzy inference system	112
Figure 97 ps-OCV=f(SOC) curve of IHR pack	119
Figure 98 RCT for capacity ration calculation and comparison	122
Figure 99 Incremental capacity analysis on major modes of capacity fade	125
Figure 100 (a) Schematic illustrates the potential scale of the reactions occur in the composite positive electrode that comprises [NMC+Spinel]. (b) Convolution and index of the incremental capacity peaks as a function of cell voltage according to the composite positive electrode against the graphite negative electrode.	126
Figure 101 Peak indexation for IHR cell	127
Figure 102 Peak indexation for IBR cells.....	128

Figure 103 Peak indexation for IMR cells..... 128

List of abbreviations

Δ SOC: SOC Range	LFP: Lithium Iron Phosphate
ANN: Artificial Neural Network	Li-ion: Lithium Ion
Ah: Ampere-hours	LIB: Lithium Ion Battery
BOC: Beginning-of-Charge	LTO: Lithium Titanium Oxide
BOD: Beginning-of-Discharge	NE/PE ratio: ratio of Negative Electrode over Positive Electrode
CC: Constant Current	NiCd: Nickel Cadmium
CV: Constant Voltage	NiMH: Nickel Metal Hydride
DOD: Depth-of-Discharge	NMC: Nickel Manganese Cobalt Oxide
EKF: Extended Kalman Filter	NSC: Nominal Sample Cell
EOC: End-of-Charge	OCV: Open Circuit Voltage
EOD: End-of-Discharge	PITT: Potentiostatic Intermittent Titration Technique
EOL: End-of-Life	Pk: Peukert coefficient
e-SOC: engineering State-of-Charge	Ps-OCV=f(SOC): pseudo-OCV versus SOC
EV: Electric Vehicle	Q: Capacity
GITT: Galvanostatic Intermittent Titration Technique	Q _R : Capacity ration
HEV: Hybrid Electric Vehicle	RCT: Remnant Capacity Test
IC: Incremental Capacity	RCV: Relax Cell Voltage
IBR: Molicel [®] cell with composite positive electrode	RPT: Reference Performance Test
IHR: Molicel [®] cell with NMC positive electrode	RPV: Relax Pack Voltage
IMR: Molicel [®] cell with spinel positive electrode	SEI: Solid Electrolyte Interphase
INL: Sanyo [®] cell with composite positive electrode	SOC: State-of-Charge
KF: Kalman Filter	SOH: State-of-Health
LCO: Lithium Cobalt Oxide	t-SOC: thermodynamic State-of-Charge
	USABC: United States Advanced Battery Consortium

1 Introduction and background information on Li-ion batteries

1.1 Why Li-ion batteries?

1.1.1 Introduction to commercial Li-ion batteries

Lithium ion (Li-ion) batteries (LIB) are attractive for portable and stationary applications due to their high specific energy, high efficiency and long life. It is known that LIBs could handle hundreds (to a couple of thousands) of charge/discharge cycles with high coulombic efficiency, have acceptable loss of charge when not in use and little memory effect. These properties have made them a power source of choice for consumer electronics with a global production of a few billions of cells per year; currently accounting for 67% of worldwide sales value in portable rechargeable batteries¹, LIBs are being developed to power an increasingly diverse range of applications, from microchips to electrified cars. Therefore, to date a significant number of battery manufacturers are developing and commercializing LIBs and packs as shown by the variety of cell configurations in Figure 1. However, to our knowledge, few reported the evolution and degradation mechanisms in these commercial cells and packs in the literature. Although many of the commercial electrode materials have been investigated in the laboratories, these batteries are complex systems to understand, and the processes of their ageing are even more complicated². As a matter of fact, capacity loss and power fading do not originate from one single cause, but from number of various processes and interactions. Moreover, most of these processes cannot be studied independently and do not occur at similar timescales, without talking about the variability among the same cells, complicating the investigation of ageing mechanisms of single cells and battery packs³.



Figure 1 Commercial Li-ion cells

1.1.2 Li-ion batteries among other rechargeable batteries

There are two types of electrochemical storage devices: disposable and rechargeable batteries also referred as primary and secondary batteries. In the first case the chemical energy cannot be restored after it has been converted to electrical energy, whereas, in the second case, the electrochemical reaction is reversible. In fact, a larger voltage applied in the opposite direction can cause the batteries to recharge and allow them to be reused hundreds to thousands of times. Rechargeable batteries come in many different ways from button cell to megawatt systems using several different combinations of chemicals. Four main different chemical reactions dominate the industry. They are: lead-acid, nickel-cadmium (NiCd), nickel-metal-hybrid (NiMH) and lithium batteries.

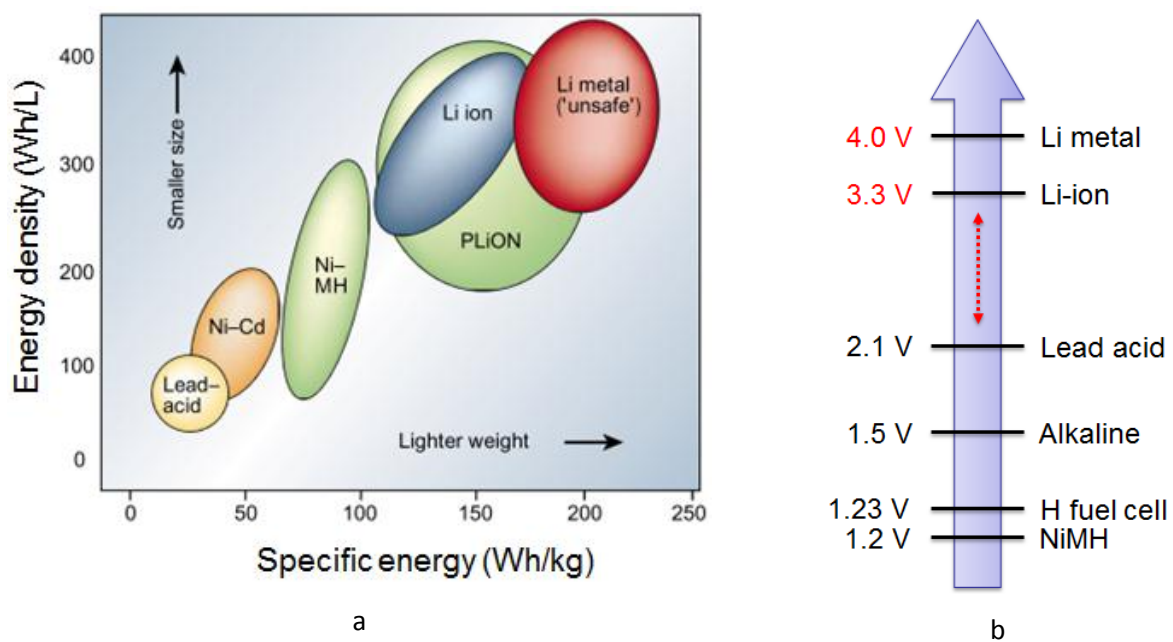


Figure 2 a) Energy density per unit mass and volume for common secondary cells⁴; b) Electrochemical cell voltages

Batteries are often compared on their specific energy (Figure 2a), which is a measure of the amount of electrical energy that the battery can deliver: the higher the specific energy, the longer the runtime will be. It is expressed either per unit of weight (W.h.kg^{-1}) or per unit of volume (W.h.dm^{-3}). It depends on the cell voltage (V) and the capacity (A.h.kg^{-1}) that are both directly linked to the chemistry of the system (Figure 2b). The lead-acid battery finds application in almost every vehicle for engine start-up due to its high power, but normalized to its weight and volume the energy density is very low. For less power demanding electrical gadgets the NiCd batteries have proven most suitable, but are more and more replaced by the more environment friendly NiMH batteries. Both cell types exhibit a cell voltage of 1.2 V. The lithium metal cells exhibit a voltage of 3.5 V to 4 V because it uses lithium (Li) which

has the most negative reduction potential⁴ (-3.04 V versus standard hydrogen electrode). However, the use of pure lithium metal was rapidly given up for safety reasons, notably due to the formation of dendrites at the metal surface that can short circuit the battery and cause an explosion. The suggested solution to that problem is to replace the metallic lithium electrode by insertion reaction materials (see Chapter 2: State-of-charge of Li-ion cells) to the detriment of the performances, which leads us towards LIBs. Due to the high voltage and the low density of lithium ($\rho = 0.5 \text{ g.cm}^{-3}$), the amount of energy incorporated in Li-ion cells, scaled to its mass or volume, exceeds all other rechargeable battery types and make them the best technology for portable devices.

1.2 Status of development of Li-ion cells

The casual battery user may think there is only one type of LIB. As there are many species of apple trees, so do also LIBs vary and the difference lies mainly in their active materials^{5,6}. Usually, batteries are named by their chemical name and the material used. A description of the most common ones is presented below.

1.2.1 Back to battery basics

A battery is made up of one or more electrochemical cells. Each cell contains four main components⁷: a negative electrode and a positive electrode kept apart by a separator soaked in a conductive electrolyte. The electrolyte allows ions, but not electrons, to travel between the electrodes⁸. The separator is a thin porous medium that separates the negative from the positive electrode. It is an electrical insulator that does not allow electrons to flow between the positive and negative electrode. However, being porous, the separator allows ions to pass through it by means of the electrolyte. The two electrodes have different chemical potentials, dictated by the chemistry that occurs at each. When these electrodes are connected by means of an external device, a chemical reaction begins: negatively charged electrons flow from the negative to the positive electrode through the external circuit; a proportional number of positively charged ions take the same journey through the electrolyte, as illustrated in Figure 3. Therefore the charge balance is maintained and the chemical energy is converted to electrical energy resulting in an electric current⁷ in the external circuit. During the discharge of the electrochemical system, an oxidation reaction (loss of electrons, (1)) occurs at the negative electrode (sometimes referred as anode) and a reduction reaction (gain of electrons, (2)) occurs at the positive electrode (sometimes referred as cathode)⁹.

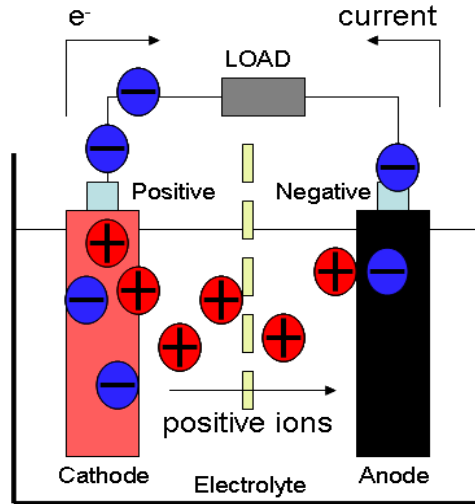
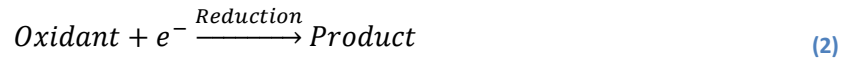
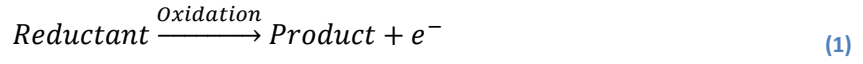


Figure 3 Electrochemical system

As mentioned previously, the electrical energy that a battery can deliver is a function of the cell's voltage and capacity, which are dependent on the chemistry of the system:

- The cell voltage, measured in volts (V), is determined by the potential difference of the redox reactions occurring simultaneously at the positive and negative electrodes. It is also called the electromotive force of the cell.
- The battery capacity, noted Q , measured in ampere-hours (Ah), represents the amount of electrical energy (i.e. the amount of transferred electrons) provided by the electrochemical reactions. In other words, the capacity of a battery delivering a current I_{dis} is the total amount of electronic charge $Q(I)$ transported to the positive electrode over the time Δt_{dis} for a complete discharge of the chemical energy available¹⁰.
- Another important parameter is power, measured in watts (W), which also depends on the chemicals the battery contains because it is calculated using Joule's law, i.e. the product of the voltage measured at the terminal of the battery with the current going through the battery. It indicates the rate at which electric energy can be delivered.

1.2.2 Li-ion battery chemistries

The different insertion reaction materials that are used at the positive electrodes of Li-ion batteries confer different properties in term of voltage and capacity to the cell. Most LIBs for portable applications are cobalt based. The system consists of a cobalt oxide positive electrode that has a 2-D layered structure allowing the intercalation of the Li^+ ions in two directions. Its high specific energy and, thus, long run-time, made Li-cobalt the popular choice for cell phones, laptops and digital cameras¹¹. However cobalt is expensive and resources are limited. Therefore manganese-based compounds (spinel LiMn_2O_4) are now of main interest for battery manufacturers¹², since manganese is more abundant, safer, cheaper and offers a better kinetics due to an intercalation on three directions (3-D structure). Unfortunately, the use of lithium manganese spinel is limited by some operational issues, the most serious being manganese dissolution into the electrolyte upon cycling in lithium cells which leads to a shorter lifespan than that of lithium cobalt oxide¹³. Another material of interest, which also allows high rate, is the lithium iron phosphate (LiFePO_4), where Li^+ ions are intercalated through tunnels (1-D structure). Its additional advantages are the low cost and the abundance of its elements. However the voltage is a little lower than that of the other chemistries and it has a relatively low energy. Therefore, depending on the application for which Li-ion cells are needed, choices have to be made regarding the active materials to figure out which one is the most appropriate. Nowadays battery manufacturers are developing composite positive electrodes. The concept is attracting attention in recent years because it promises the combination of several active materials into a hybrid electrode to allow performance optimization in term of power and energy. Table 1 summarizes the several Li-ion cell chemistries described above.

Chemical name	Material (short form)	Specific capacity (mAh/g)	Cell voltage (V)	Notes
Lithium Cobalt Oxide	LiCoO_2 (LCO)	170	3.7	High capacity, low rate capability
Lithium Manganese Oxide	LiMn_2O_4 (LMO)	120-140	3.9	Most safe, lower capability but high power
Lithium Nickel Manganese Cobalt Oxide	LiNiMnCoO_2 (NMC)	160-170	3.7	High capacity, low rate capability
Lithium Iron Phosphate	LiFePO_4 (LFP)	130	3.3	Low capacity, high rate capability

Table 1 Li-ion cell chemistry summary

Regarding negative electrodes, the most common materials found in commercial Li-ion batteries are carbon-based (i.e. graphite) since it has a high capacity and a very light weight. Another one which is of interest is the lithium titanium oxide ($\text{Li}_4\text{Ti}_5\text{O}_{12}$ or LTO) because it offers a longer lifespan but comes with a lower voltage. The next generation of anode will most likely be Silicon based and Nano-sized^{14,15}.

1.3 Li-ion battery packs

Depleting fossil fuels as well as growing awareness of sustainability have created an enormous interest in renewable energy technologies. Rechargeable LIBs are now of interest for much larger scale applications such as, electric cars, powertrains and energy storage systems. However, these applications having energy and power requirements that are beyond a single cell's capability, multi-cell configurations are now needed. In fact, the voltage of a LIB being of approximately 3.7 V, huge electric currents would be needed for high power requirements, according to Joule's law for direct resistive circuits. Hence a connection of several cells in series/parallel configurations becomes necessary, which leads us to the battery packs.

1.3.1 Different pack configurations

In order to meet energy and power requirements, connecting identical cells in a pack following different configurations such as: series, parallel and series-parallel, became of common practice (Figure 4). Therefore, higher voltage, capacity, and thus power density can be delivered.

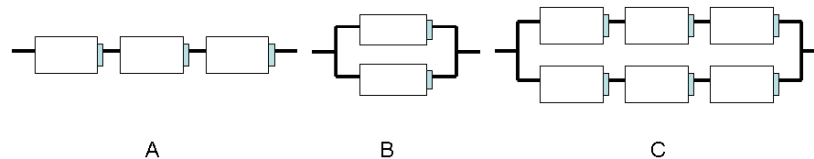


Figure 4 Pack: A) series; B) parallel; C) mixture

Following Kirchhoff's first law stating that at any node (i.e. junction) in an electrical circuit, the sum of currents flowing into that node is equal to the sum of currents flowing out of that node: if higher current (or higher capacity) is needed, cells have to be plugged in parallel. On the other hand, if higher voltage is needed, cells must be assembled in series according to Kirchhoff's second rule in which the directed sum of the electrical potential differences around any closed circuit is zero. Hence, the energy and voltage requirements can be met for high power applications such as electric vehicles (EV) and hybrid electric vehicles (HEV)¹⁶.

1.3.2 Merits of Li-ion battery packs

LIB packs have very strong advantages over other types of advanced batteries for high energy and high power applications since Li-ion cells come with the highest voltage. For instance, nickel-based cells provide a nominal cell voltage of 1.25 V, a lead acid cell delivers 2 V and most Li-ion cells are rated above 3.6 V. Thus, a five-cell nickel-based battery delivers 6 V (6.25 V with 1.25 V/cell marking) and a six-cell pack has 7.2 V (7.5 V with 1.25 V/cell marking); on the other hand the portable lead acid comes in 3 cell (6 V) and 6 cell (12 V) formats for motor engine starter. As for the Li-ion family with 3.6 V for a single cell, it has either 7.2 V for a two-cell pack or 10.8 V for a three-cell pack¹¹. The LMO and Li-ion polymer systems use even higher potentials with approximately 3.9 V as the designated cell voltage. This is the reason of the often unfamiliar voltages, such as 11.7 V for a three cell pack of spinel chemistry in a string configuration. Consequently, fewer cells are needed to reach high voltages when Li-ion technology is used compared with others as it is illustrated in Figure 5. Packs with fewer cells in series have generally better performance than those with twelve cells or more: similar to a chain, the more links that are used the greater the odd of one breaking is.

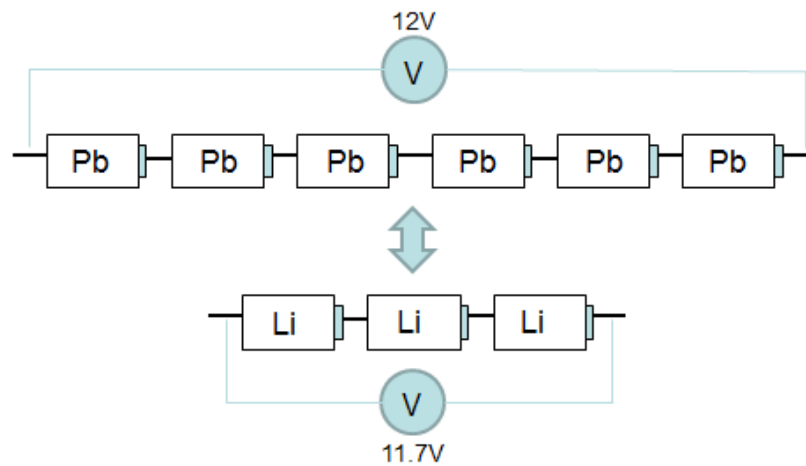


Figure 5 Equivalence in voltage of a 6-cell lead acid pack and a 3-cell Li-ion battery pack

Parallel connections are used to obtain higher ampere-hour ratings. When possible, pack designers prefer using larger cells. This may not always be practical because new battery chemistries come in limited sizes. Often, a parallel connection is the only option to increase the battery rating. Paralleling is also necessary if pack dimensions restrict the use of larger cells. Among the battery chemistries, Li-ion lends itself best to parallel connections as well.

1.3.3 Additional issues with battery packs

As the number of cells in the battery configuration increases, the complexity in the control and managing the cells becomes sophisticated as well. Consequently, there is an urgent need to understand the behavior of multi-cell strings through proper assessments to derive adequate knowledge for the control and management of battery packs. Furthermore, the integration of Li-ion cells in such configurations is not as straight forward as other more conventional and well-known battery systems such as lead acid batteries, notably regarding safety. Therefore a better comprehension of their performance and degradation is necessary to ensure reliable, effective and secure operations as scaling up LIB pack technology is still problematic. This thesis presents some recent progress made in the string assessments and evaluations by focusing on two very important aspects in multi-cell string configuration assessments and evaluations: state-of-charge estimation and degradation using Li-ion commercial cells.

2 State-of-charge of a Li-ion cell

2.1 State-of-charge according to USABC

Mobile phones, laptop computers, cameras, camcorders are devices using batteries that are now part of our daily life. Their use brings a big contribution to our mobility, our comfort and our freedom. However, they also bring new questions: will my battery last long enough to give a phone call, to take more pictures? Also, for the luckiest of us that drive electric cars: will I be able to drive home? Therefore, in all these systems using rechargeable batteries, a key point is the knowledge of the state-of-charge (SOC) or more simply: how long do I have until my device stops working?

2.1.1 Definition

In comparison with the gas gauge of a conventional car using gasoline, state-of-charge estimation is intended to be used as the "fuel gauge" of an electric vehicle, Figure 6. Knowing the amount of energy left in a battery compared with the energy it had when it was full gives the user information of how much longer a battery will perform before it needs to be recharged^{9,17}.



Figure 6 a) gas gauge, b) SOC gauge

According to the United States Advanced Battery Consortium¹⁸ (USABC) manual that summarizes the procedural information needed to perform battery testing as well as the battery terminology, SOC is defined as "the ratio of the Ampere-hours remaining in a battery at a given rate to the rated capacity under the same specified conditions". Its unit is the percent and it can be described as a function of the depth-of-discharge (DOD), which is the ratio of the net Ampere-hours discharged from a battery at a given rate to the rated capacity ((3)).

$$SOC = 100\% - DOD \quad (3)$$

2.1.2 Importance of determining SOC in Li-ion battery and Li-ion battery pack applications

In addition to immediately displaying the amount of energy left to the user, the knowledge of the remaining capacity is of importance for battery management systems. As a matter of fact, Li-ion cells are very sensitive to deep discharge and overcharge because of their operating principles (i.e. intercalation of Li^+ ions in the electrode insertion materials); and, these states of too high or too low SOC can lead, in best case scenario, to irreversible damages of the cell, and in worst case scenario to thermal runaway that can destroy the cell and provoke leaks and projections of electrolyte acids. Thus, an accurate estimation of the SOC of battery systems is very important in order to prevent degradation from over and under-(dis)charges, facilitate safe and efficient utilization of the cells, minimize degradation and maximize battery life.

2.1.3 Limitations of the USABC definition for SOC

The SOC described by USABC is purely engineering and empirical. Therefore we shall call it the “engineering-SOC” or “e-SOC”¹⁹ since it is determined by capacity based methods. By this definition, e-SOC comes with a few limitations. First of all, it does not take into consideration the capacity loss over aging. This leads to issues such as a non-reliable SOC gauge that would claim that the battery can still perform when no more capacity is available. In other words, it is equivalent with a car running out of gasoline while the fuel gauge displays a non-empty tank, Figure 7.



Figure 7 Limitations of SOC definition from USABC: capacity loss neglected.

Secondly, the e-SOC suffers a common problem in its inability to accurately define the battery' state function, because it does not correspond to a well-defined relationship with the battery's composition and the extent of redox reactions in the active materials under thermodynamic equilibrium.

2.2 Thermodynamic state-of-charge

The true state-of-charge of a battery is supposed to be a state function which represents the thermodynamic property of the electrochemical system^{19,20}. Therefore, it should be defined by thermodynamic conditions and constraints; in other words, by the lithium content in each electrode. In the case of lithium metal batteries, it is very easy to determine the lithium content since pure metallic lithium is used for the negative electrodes. However, we face a dilemma for LIBs since they use intercalation host materials instead, in which Li^+ ions are intercalated and de-intercalated during the subsequent charges and discharges. We shall call state-of-charge determined by the thermodynamic constraints "thermodynamic-SoC" or "t-SoC".

2.2.1 Binary phase diagrams and electrical potential

Electrodes used in Li-ion batteries are insertion reaction materials, which means they can accept and release Li^+ ions in their crystal lattice. Therefore they are pseudo-binary systems that can be described with binary phase diagrams. A binary phase diagram is a representation of the equilibrium state of a chemical system in a two-dimensional plot of temperature vis-à-vis the overall composition of materials composed of two different components. It shows temperature-composition conditions for the stability and composition ranges of the various phases that can form in a given system, and is commonly used in materials science²¹.

Figure 8 shows a phase diagram for a hypothetical binary alloy system A-B. Its binary phase diagram is a map that represents the relationships between temperature and the compositions and quantities of phases at equilibrium, which influence the microstructure of the A-B alloy. Many microstructures develop from phase transformations. These may involve the transition from one phase to another or the appearance or disappearance of a phase. For this system, there are four single phase regions, more particularly three solid solution phases: α , β , γ , and hypothetical one liquid phase. The single phases are all separated by two-phase regions (e.g. $\alpha+\beta$, $\beta+\gamma$, $\alpha+L$, $\beta+L$, $L+\gamma$)²¹.

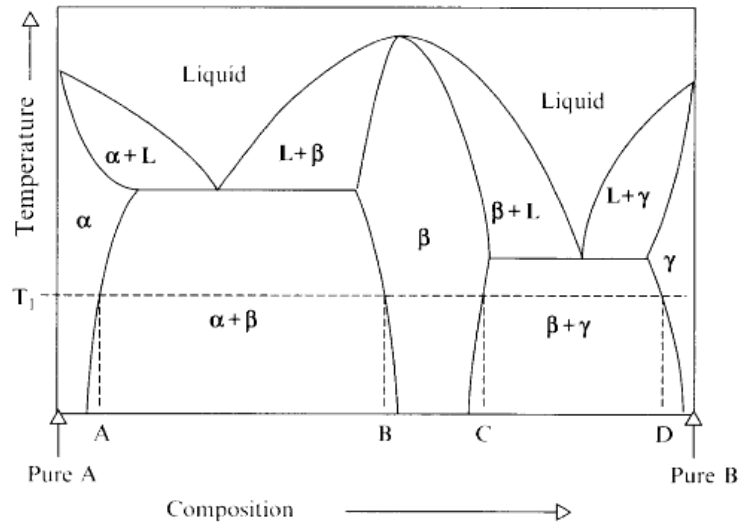


Figure 8 Schematic binary phase diagram

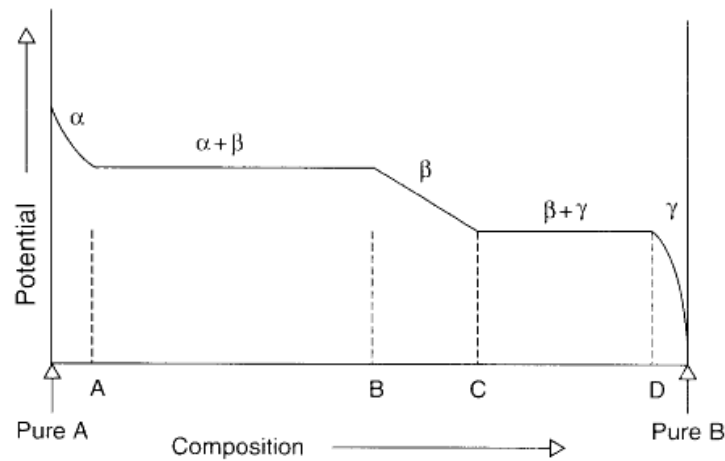


Figure 9 Schematic variation of electrical potential with composition across the binary phase diagram shown in Figure 8

At a constant temperature, the variation of electrical potential with overall composition in a binary system alternates between composition regions in which it is constant (potential plateaus) and those in which it varies. The Gibbs Phase Rule proves that the electrical potential varies continually with the composition within single-phase regions in binary system and is constant when two phases are present in the binary system²². It is often written as in (4):

$$F = C - P + 2 \tag{4}$$

in which C is the number of components present and P the number of phases in the system. The quantity F is the number of degrees of freedom, i.e. the number of intensive thermodynamic

parameters that must be specified to define the system and all its associated properties, one of which is the electric potential. When the temperature and pressure are constant, for binary system, i.e. $C=2$, if there is only one phase present (i.e. $P=1$), F is one. With one degree of freedom, the lithium activity has a degree of freedom to vary; therefore its potential is not fixed (according to Nernst equation). When two phases exist, $P=2$, and $F=0$, the degree of freedom is fixed, consequently the lithium activity is also fixed; therefore, the potential is fixed and there is a voltage plateau for the composition, in which two phases co-exist. Figure 9 is the schematic variation of electrical potential with composition associated to the phase diagram at temperature T_1 , Figure 8. At this temperature, two phase transformations occur from a pure A composition to a pure B composition. If B atoms are added to pure element A, the overall composition is initially in the solid solution (i.e. single phase α) and the electrical potential varies with the composition. When α solubility limit is reached, indicated as composition A, addition of B causes the nucleation and growth of the β phase. Two phases are then present, and the potential maintains a fixed value (phase transformation #1). When the overall composition reaches B, all the α -phase will have been consumed and only phase β will remain. Upon further compositional change electrical potential again becomes composition dependent. At composition C, the upper compositional limit of the β phase at that temperature, the overall composition again enters a two-phase (β and γ , phase transformation #2) range and potential is again composition-independent. On reaching composition D the potential again varies with composition²¹.

Driving current through a Li^+ ion cell from an external source will involve the reversible extraction and insertion of lithium ions between the two electrodes with a concomitant removal and addition of electrons. During discharging, lithium ions will leave the negative electrode, pass through the electrolyte, and arrive at the positive electrode. When they reach the positive electrode surface, they are incorporated into the bulk of the electrode lattice crystal structure, changing its composition (from pure A to pure B). As a result the potentials of each electrode will evolve and the cell voltage will be reduced from the open circuit value. Therefore, changing the composition of the electrodes in a Li-ion cell will be accompanied with a voltage change. In other words, the voltage will change with the SOC. During charging, the reversible process will occur and the voltage will be increased. This to-and-fro approach gave to LIBs the nickname of “rocking chair” batteries: Li^+ ions are reversibly exchanged between the two intercalation electrodes.

2.2.2 Example: the LiCoO₂ Li-ion cell

As a concrete example, consider a LCO Li-ion cell which has the following composition: a lithium cobalt oxide positive electrode LiCoO₂ and a graphitic negative electrode.

2.2.2.1 Graphite electrode

The negative electrode used in the cell is made of graphite. Its electrochemical behavior versus a lithium electrode is well known^{23,24} and several phase transformations occur throughout the intercalation or de-intercalation of Li⁺ ions in the structure. The potential profile of graphite vs. Li⁺/Li is shown on Figure 10. As mentioned in the previous paragraph, phase transformations are characterized by voltage plateaus. In this case, there are five voltages plateaus, noted ① to ⑤ on Figure 10, indicating that the graphite will be subjected to five phase transformations when Li⁺ ions are intercalated in its structure.

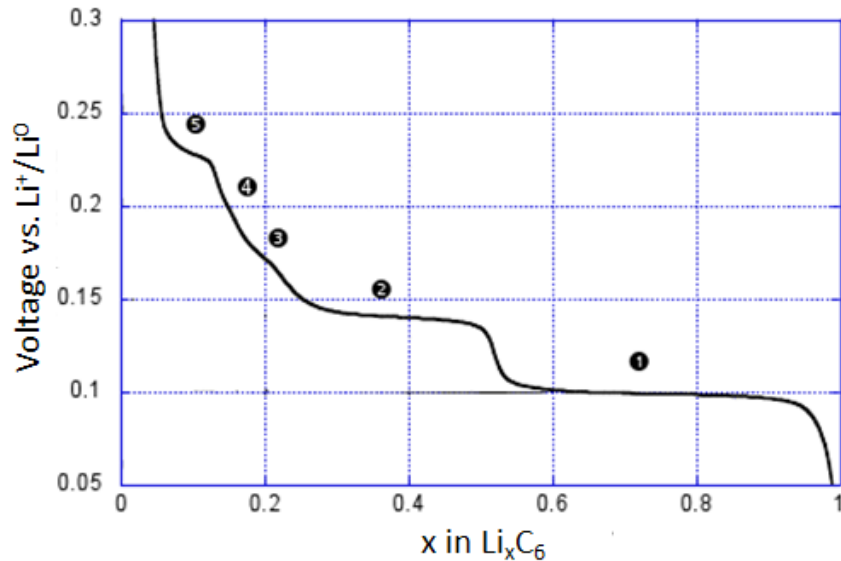


Figure 10 Open circuit voltage of a graphite electrode during Li insertion

2.2.2.2 Positive electrode

Assuming that the positive electrode used in the cell is LiCoO₂, the potential of Li_xCoO₂ (against metallic lithium) varies with the lithium content x, Figure 11. When the cell is being discharged, Li⁺ ions are incorporated in the cobalt oxide intercalation host (CoO₂) of the positive electrode. On the other hand, during charging of the cell, Li⁺ ions are extracted from its host while the basic CoO₂ lattice structure remains intact. In reality, the Li⁺ ions between Li₀CoO₂ and Li_{0.5}CoO₂ should not be extracted otherwise the structure of the electrode would become unstable and the electrode would reach potentials greater than that of the electrolyte voltage window limits, leading to electrolyte

decomposition. Those ions will be referred as “structural Li⁺ ions”. Since the reversible intercalation range is thus only for x from 0.5 and 1 (i.e. from Li_{0.5}CoO₂ and Li₁CoO₂), the percent of exchanged lithium for the positive electrode will only vary from 0% to 50% (i.e. Δx=0.5).

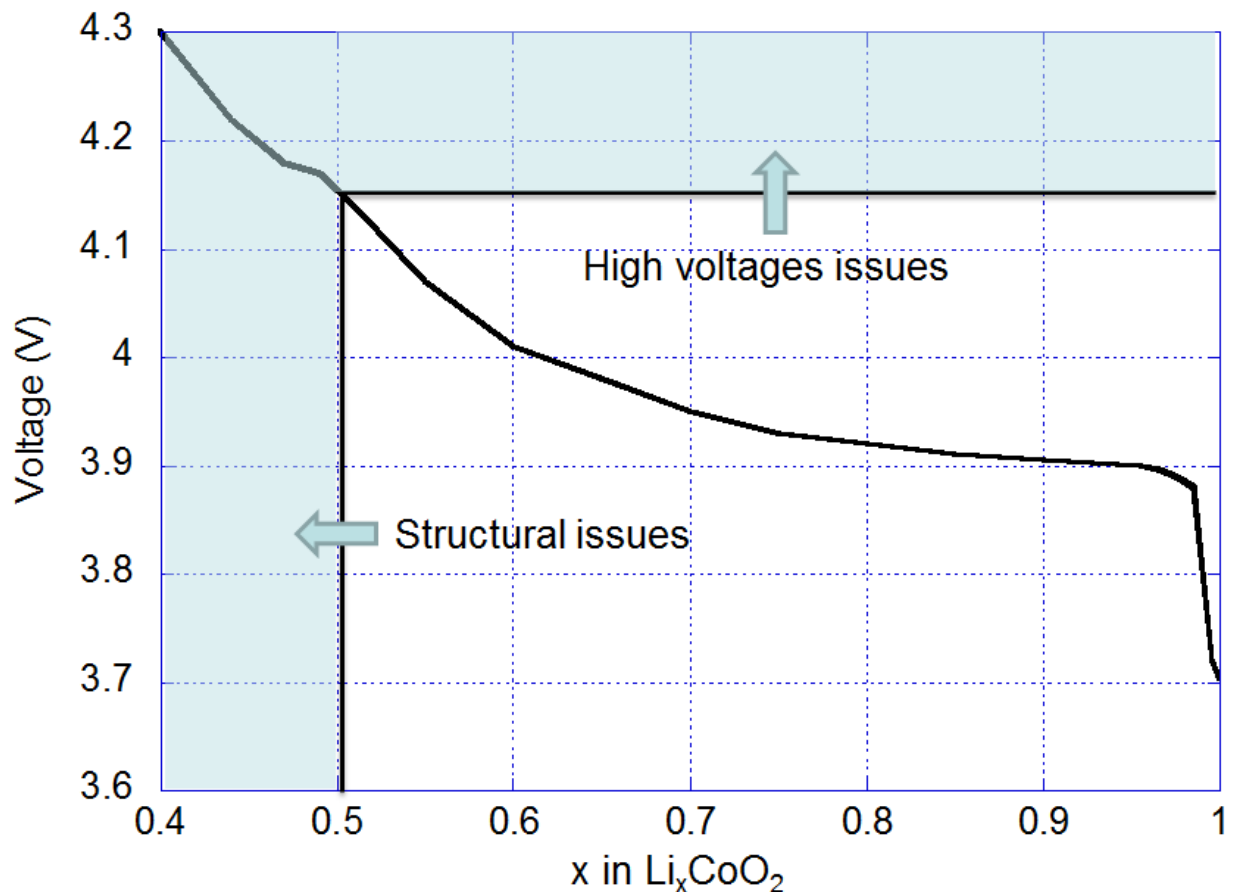


Figure 11 Open circuit voltage versus amount of lithium in a LiCoO₂ electrode

2.2.2.3 Voltage signature of a Li-ion cell and Li⁺ ion composition

LIBs are assembled in their discharged state, with all the lithium present in the positive electrode (e.g. LiCoO₂ electrode in this case). During the first charge, some of the electrolyte is reduced at the negative electrode (i.e. graphite electrode). As a result, a surface film is formed on the graphite surface. Fortunately, this film conducts ions and is an electronic insulator. Thus it is not too bad for the functioning of the cell. However, this reduction of electrolyte is an irreversible process which consumes lithium and leads to a lithium loss, as well as a capacity loss C_{irr} , between 5-30%, and allow only between 70 and 95% of the total amount of Li⁺ ions to be exchanged reversibly for the next charge/discharge cycles for the negative electrode^{23,25}. This film, which acts as a passivating layer, is most often referred

to as a Solid Electrolyte Interphase (SEI layer). The potential profile of graphite vs. Li^+/Li during the first and subsequent discharge is shown in Figure 12.

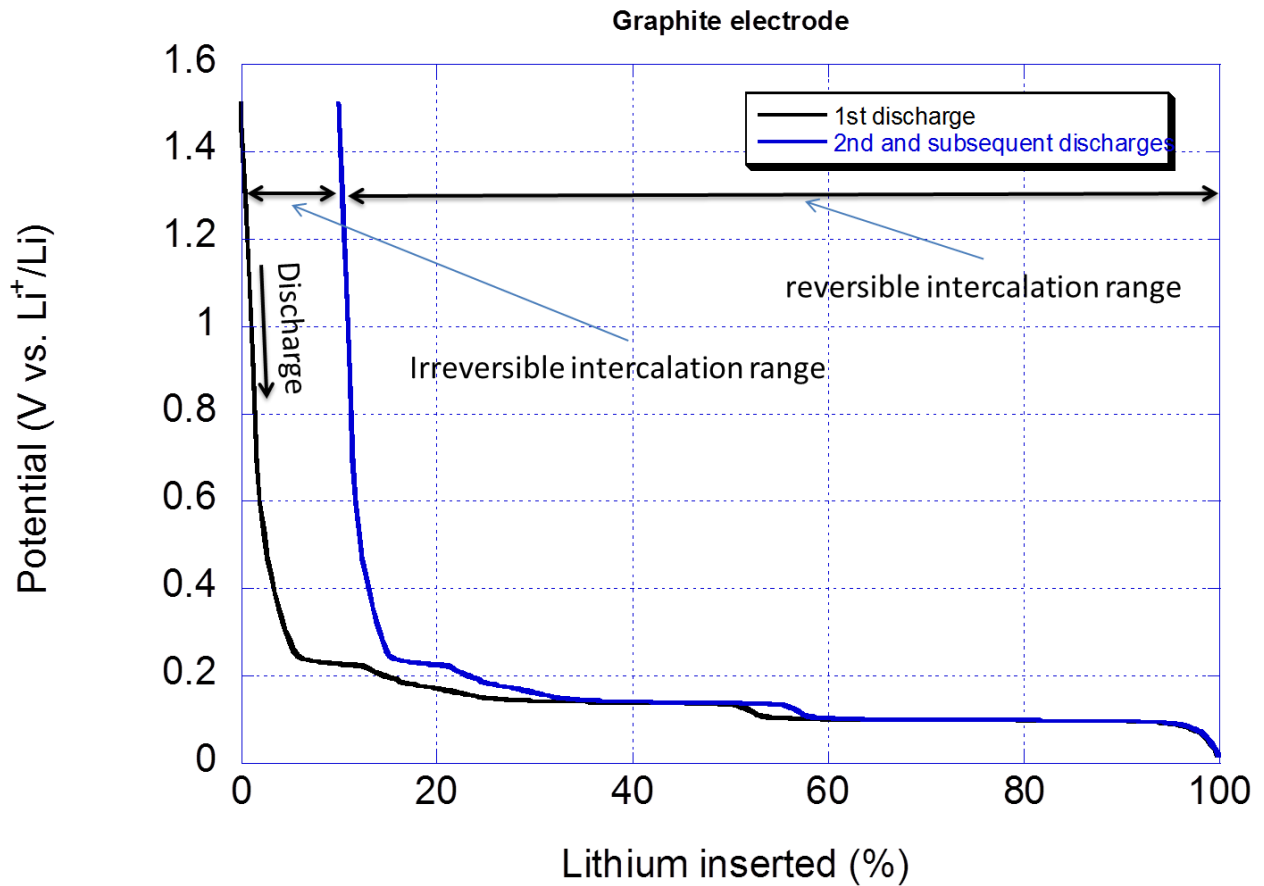


Figure 12 The first charge/discharge cycle of a graphite electrode

When the electrode potential according to the amount of Li^+ ions that can be reversibly inserted and extracted for each electrode are known (i.e. electrode signatures), as well as the electrode loading (i.e. the ratio of the amount of negative electrode over positive electrode), the voltage signature of the Li-ion cell can be obtained by subtracting the potentials of the each half-cell, since one is releasing its Li^+ ions while the other one receives them. Therefore, a relationship between the voltage of the LiCoO_2 Li-ion cell and the exchangeable lithium concentration can be determined in a stable potential window as it is illustrated on Figure 13.

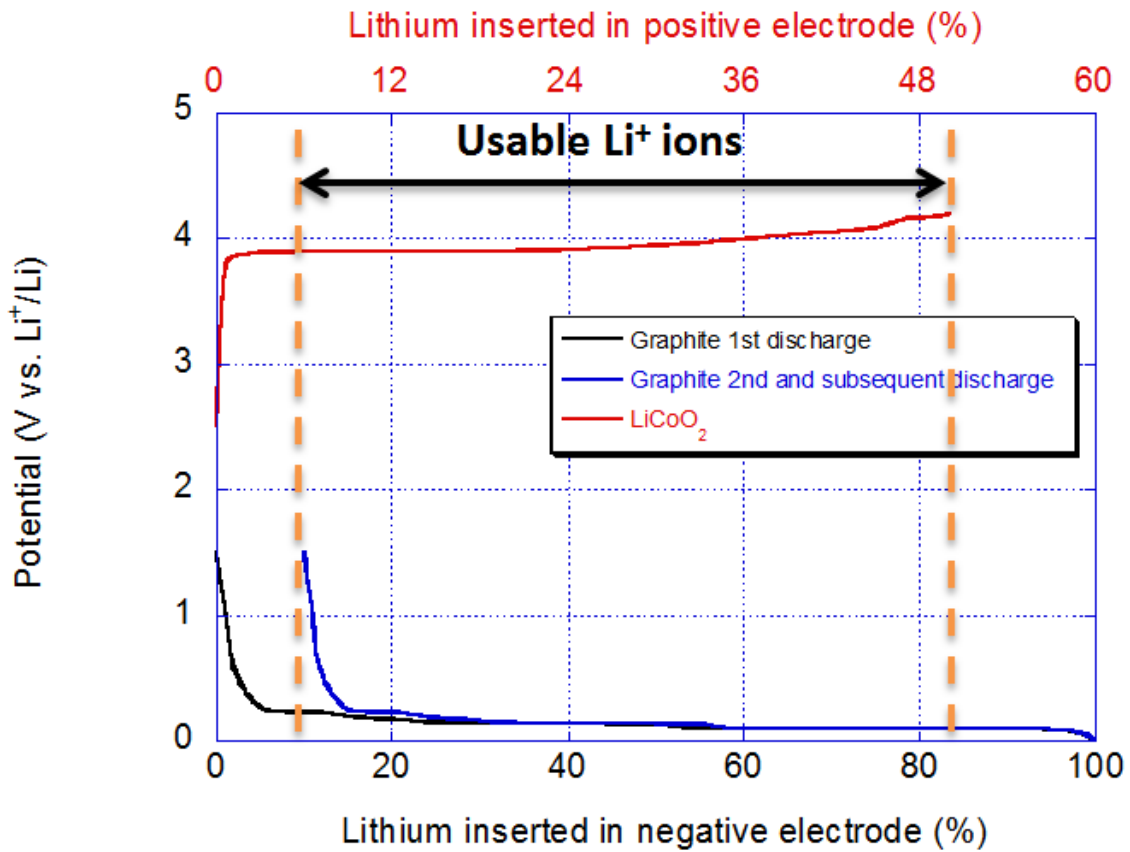


Figure 13 a) Li insertion in each electrode

2.2.3 Definition of thermodynamic state-of-charge

T-SOC for Li-ion cells being defined by the lithium content in each electrode, the knowledge of the exchangeable lithium concentration in a stable potential window should allow its determination. As a matter of fact, 0 % SOC will be reached when all the exchangeable Li^+ ions are out of the negative electrode and, vice versa, 100 % SOC will be reached when all the “nonstructural” Li^+ ions will be out of the positive electrode. Therefore, a first expression for the t-SOC, based on the lithium composition, can be formulated as the ratio of remaining exchangeable Li^+ ions over the total exchangeable Li^+ ions, as shown in (5).

$$SOC = \frac{\text{Remaining Exchangeable Li}^+}{\text{Total Exchangeable Li}^+} \quad (5)$$

Figure 14 illustrates this concept on a very simplified example: if it is assumed that only 12 Li^+ ions can be reversibly exchanged between the two electrodes during cycling, the t-SOC when only 4 Li^+

ions remain in the negative electrode is 33 % (because the Li^+ ions flow from the negative to the positive electrode when discharging the battery).

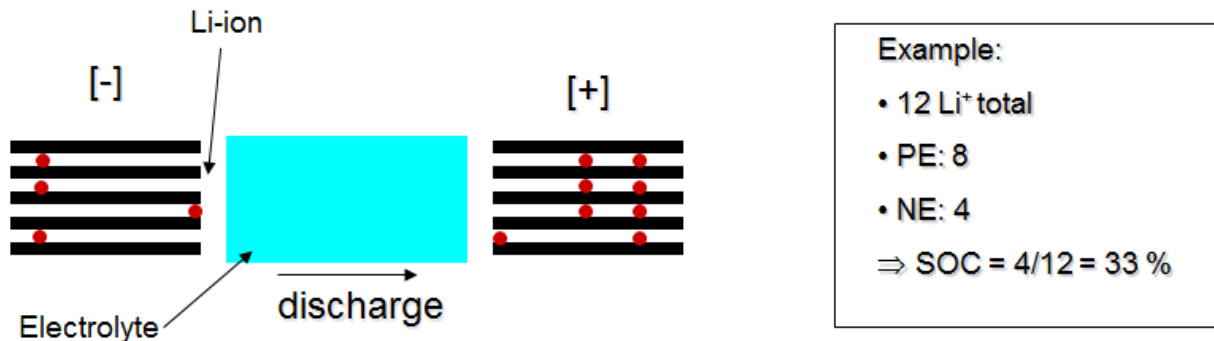


Figure 14 Illustration of t-SOC

Since the exchange of Li^+ ions through the electrolyte is always accompanied with an exchange of electrons to ensure the electroneutrality of the system, the t-SOC definition given previously can be converted to capacity. In fact, measuring the amount of electrons transferred in the external circuit or, in other word, the electrical energy which is also referred as the capacity when dealing with batteries, is equivalent to measuring the lithium composition evolution in the electrode. Consequently, a second definition for the t-SOC, now capacity based, can be written as the ratio of remaining capacity over maximum capacity that a Li-ion cell can provide, (6).

$$SOC = \frac{\text{Remaining capacity}}{\text{Maximum capacity}} \quad (6)$$

As a conclusion, two equivalent definitions of the t-SOC can be drawn and both are matching material scientist and engineer's visions. T-SOC for Li-ion system is thus related to the lithium content in each electrode and the cell capacity corresponds to the quantity of Li^+ ions that can be exchanged reversibly in the intercalation processes.

2.3 SOC determination

2.3.1 A literature review: how is SOC determined?

A multitude of methods and techniques to derive model for SOC estimation have been introduced since the 1980s^{17,26}, the adoption of which has been gradual in various academic research and industrial applications. Only two of these methods are described below since one is the most used (i.e. coulomb counting) and the other one the most accurate (i.e. open circuit voltage). All the other

estimation methods, algorithms and technologies that are used for single cells are itemized and discussed in appendix 7.4.2.

2.3.1.1 Coulomb counting

Coulomb counting, or Ampere hour counting, is the most common technique for calculating the SOC by measuring the current flowing through the battery and integrating it with the duration according to (7) where C_N is the rated capacity and I the current flowing through the battery. If a starting point $SOC(t=0)$ is given, the value of the current integral is a direct indicator of the SOC.

$$SOC(t) = SOC(t = 0) + \frac{1}{C_n} \int_0^t I(t) dt \quad (7)$$

Coulomb counting is the most used technique at this time for all systems and applications^{27,28}. Indeed, the method is direct, easy to implement and reliable as long as the current measurement is accurate and good reference points are available. The nominal capacity, however, is measured at a constant discharge rate under controlled temperature. These conditions seldom occur in real-world applications. Therefore, the use of nominal capacity as the total capacity remains controversial. Furthermore, this method does not accommodate capacity fade during aging. Besides the nominal capacity, two other main issues arise with coulomb counting: firstly, since the approach requires dynamic measurement of the cell current, incorrect current measurement could add a large error, and accurate current measurements are very expensive; secondly, reference points are necessary to avoid adding large errors. The first point can be overcome by investing money in measuring equipment. For the second one, the errors can be kept low if points for re-calibration are reached, e.g. the SOC is set to 100 % if full charge is detected or open circuit voltage measurement (see below) is used to correct the SOC value¹⁷.

2.3.1.2 Open circuit voltage

Open circuit voltage (OCV) versus SOC (OCV vs. SOC) curves are used for the inference of the SOC from the OCV measured at the terminal of the cell^{19,29-31}. These curves, that represent the voltage signature of a full cell at equilibrium (i.e. OCV), are specific to the battery chemistry (i.e. electrode materials and loading ratio). The principle of the method is easy and straight-forward: since the correlation between SOC and voltage at equilibrium is known, the voltage value directly measured at the terminals of the cell at an equilibrium state just needs to be reported on the curve to obtain its equivalent in SOC, Figure 15. It allows more direct inference than the coulomb counting, mostly because a voltage measurement is more accurate than a current measurement. As a matter of fact, to measure

current, we generally convert it to a voltage by running it through a known resistance. This is an invasive measurement, because series resistances have to be added to the circuit to measure the current. This often can change the current, so resistances as small as possible are usually used for the measurement. But this makes the measurement less accurate, so in making a current measurement, there is often a tradeoff between the invasiveness of the measurement, and its accuracy. This confirms why, contrary to the coulomb counting, OCV measurement is not expensive. Nevertheless, this method needs long rest times (and thus, cannot be used dynamically) because the cell needs time reach an equilibrium because of diffusion, and results can vary widely depending on actual voltage level, temperature, discharge rate and the age of the cell. Compensation of these factors needs to be provided to achieve a reasonable accuracy. In addition, because of numerous phase transformations occurring at each electrode during charging and discharging processes, the OCV vs. SOC curves of LIBs present some voltage plateaus. As a result, the inferred SOC may contain uncertainty issues as it is pointed out on Figure 16 with an inferred SOC between 68% and 92% at 3.34V. This issue may not be extremely relevant for portable electronics; however, if used in larger scale applications such as EV, an early cut-off during the charging process, that would stop the charge when the SOC is only 68 %, could lead to a loss of 25 % of usable capacity, which is not negligible when knowing that the mile range of EV is not greater than 150-200 miles currently (and would be thus reduced to 110-150 miles).

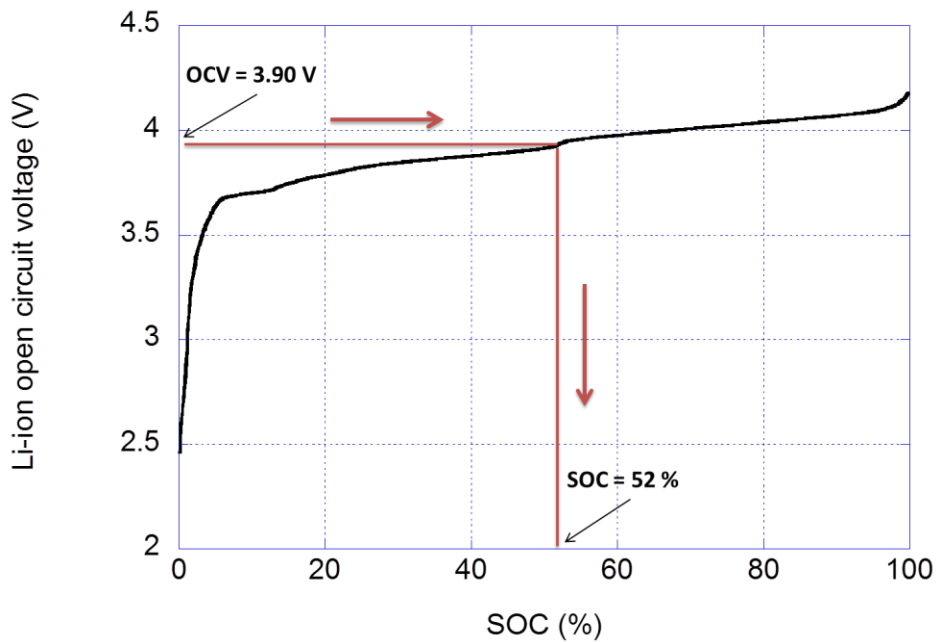


Figure 15 SOC measurement from open circuit voltage

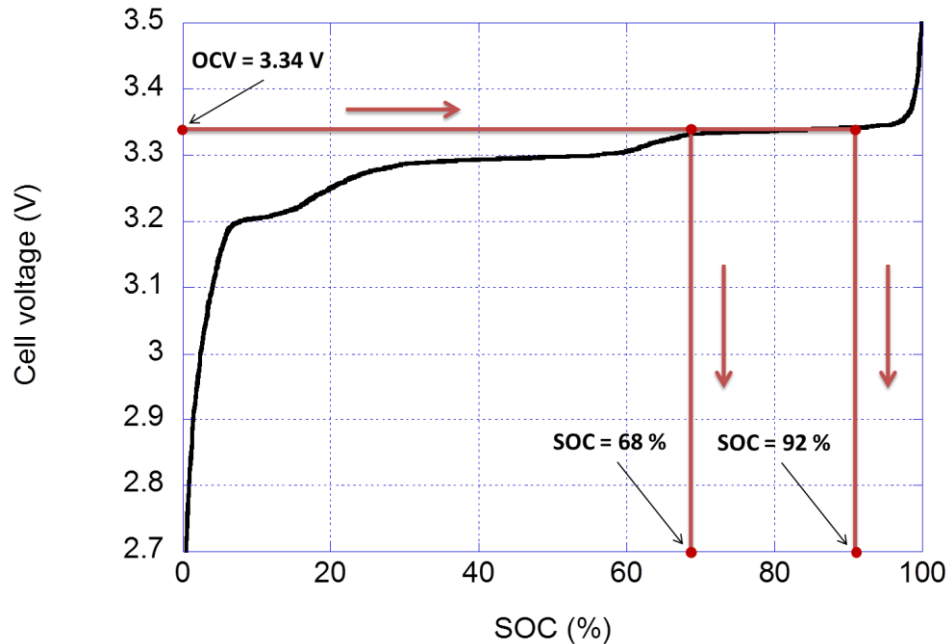


Figure 16 Accuracy issues in SOC determination

The rapid drop in cell voltage at the end of the discharge could be used as an indication of imminent, complete discharge of the battery, but an earlier warning is required for many applications. In fact, fully discharging Li-ion cells can dramatically shorten their cycle life and most applications will impose a limit on the depth of discharge to which the cell is submitted in order to prolong cells cycle life. Another drawback of this method is obtaining the OCV vs. SOC curve. It is time consuming, costly and laborious (see next paragraphs). In addition these curves evolve during cycle aging of the cells because of electrodes degradation^{13,32}.

2.3.2 Experimental validation of “t-SOC” determination using OCV measurements

There are different existing techniques to determine the OCV vs. t-SOC curve experimentally. A known one is the equilibrium coulombic titration, which usually involves changing the composition of the active material of each electrode in the system potentiostatically or galvanostatically, followed by an equilibrium OCV measurement to determine the voltage of the system against a well-established state at the reference electrode. The potentiostatic intermittent titration technique (PITT) and the galvanostatic intermittent titration technique (GITT) are two well-established techniques suitable for this purpose. Basically, their concept is to successively charge and discharge the battery intermittently using very low and short constant voltage or constant current phases for regular capacity intervals, for example 1% of the nominal capacity. These phases are separated with sufficiently long relaxation

periods for the cell to reach a uniform open circuit voltage. This is performed on the whole SOC-range of the battery (i.e. from fully charge state to fully discharged state and reversibly) in charge and discharge. Thus, the composition becomes homogeneous throughout the electrode materials at each step; the open circuit voltage reaches a steady state value and allows information to be obtained about the equilibrium chemical potential as well as the activity of electro-active species as a function of composition²¹.

However, even though a precise OCV vs. SOC curve should be determined by PITT or GITT, a sufficiently accurate approximation might be obtained by taking the average potential between the charge and discharge voltage branch at a sufficiently low C-rate. In fact, the longer in time will be the charge/discharge, the lower will be the current and the closer the cell will be to its equilibrium. Then the normalized capacities can be taken as a “close-to-equilibrium” SOC to yield a cte-OCV versus SOC curve and use it as a good faith OCV vs. SOC curve. It will be referred as “pseudo-OCV vs. SOC” curve and noted ps-OCV=f(SOC) curve. A comparison of the GITT and C/25-rate methods is available in appendix 7.4.1.

2.4 Accuracy on OCV-SOC measurements

When SOC estimations within ± 1 % of uncertainty are claimed³³, a few precisions have to be added with regard to measurement accuracy, especially when using ps-OCV=f(SOC) curves. In point of fact, the SOC accuracy is more often discussed whereas voltage measurement accuracy should be of interest. For example, most battery testers or voltage measurement systems have 8 to 16 bits resolution, which means that the precision of a measure has 256 increments in the case of 8 bits, or 65536 increments in the case of 16 bits, out of the range of the measurement. In the case of a voltage meter with a 5 V range, this is equivalent to an accuracy of approximately 20 mV (i.e. 5/256), or 0.07 mV (i.e. 5/65536). By keeping this in mind, let us take a look at a LFP Li-ion cell. This chemistry is not studied in this thesis but its particular OCV vs. SOC curve comprising two wide voltage plateaus as well as its popularity within Li-ion battery applications make a relevant example, Figure 17(b). When the equilibrium voltage at the terminal of the cell is approximately 3.33 V, the SOC that can be inferred is 45 %. However since the battery tester that was used has a voltage range of 0 V to 15 V ± 3 mV, 3 mV of uncertainty has to be considered and can have drastic influence on SOC estimations. Figure 17(a) highlights the amplitude of uncertainty that can arise with such measurement precisions as well as 1 mV and 5 mV measurement precisions. Depending on the SOC of the cell, uncertainty up to 15 % can be inferred if voltage measurement oscillates of 3 mV and up to 25 % if the voltage measurement oscillates

of 5 mV. Therefore, before claiming very low uncertainty on SOC estimations from voltage measurements, attention must be paid to the error measurement of the tester as well as the bit depth (which directly correspond to the resolution) of the test equipment.

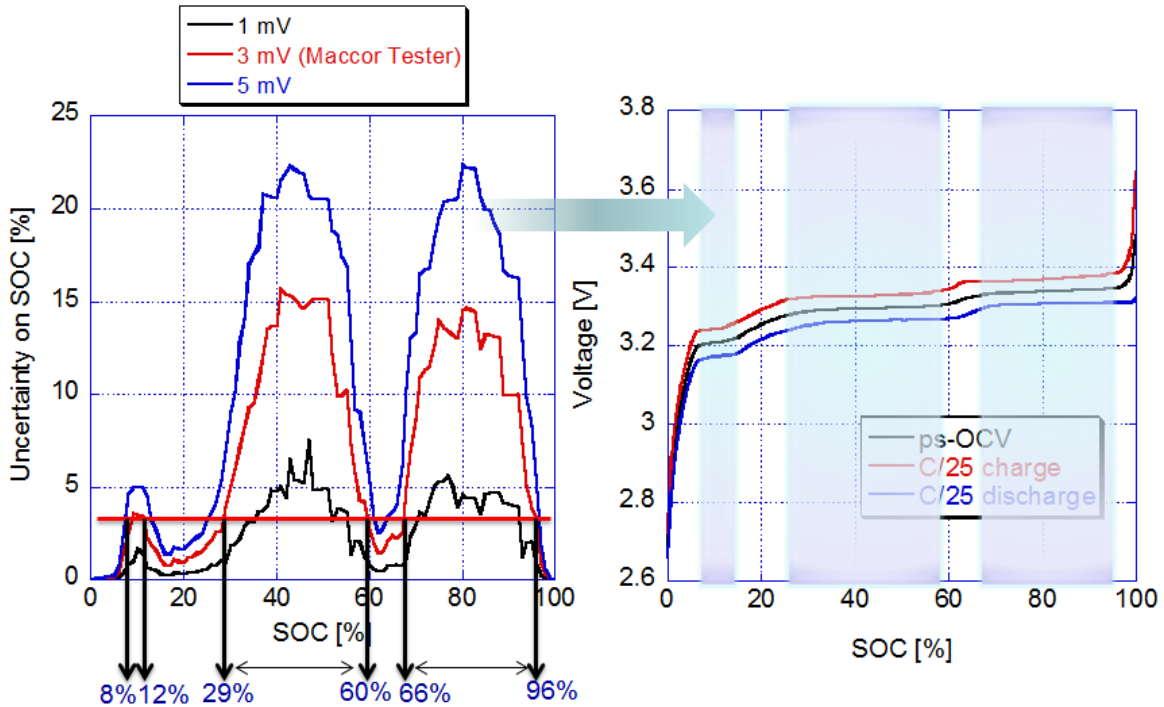


Figure 17 (a) Uncertainty of SOC on LFP cell full SOC range. (b) Zone of uncertainty on LFP cell ps-OCV=f(SOC) curves

Zones where uncertainty on SOC estimation is above 3 % (red line, Figure 17(a)) can be highlighted on the ps-OCV=f(SOC) curves, Figure 17(b). Indeed, biggest uncertainties are for voltage plateaus. In application such EV, the SOC is often controlled between 30 % and 80 %. Therefore, SOC estimation using ps-OCV=f(SOC) is controversial for LFP Li-ion cell since it corresponds to its most uncertain areas. In addition, when dealing with battery pack in string configuration, the precision errors on the voltage measurements are emphasized since the voltage range increases (contrary to what H. He claimed when saying that OCV difference of only 0.41 V could be ignored compared to the 32 V of a LFP battery pack³⁴).

Same representations of uncertainty for all Li-ion cell chemistries introduced in chapter 1 are presented in Appendix 7.4.4. Li-ion cells using pure spinel as a positive electrode also show large zones of inaccuracy because of the two phase transformations of the spinel material. However, cells using NMC and composite (NMC+spinel) positive electrodes display much better results due to the presence

of large solid solution areas where SOC_s can be inferred precisely with less than 1.5 % of uncertainty on the whole SOC range.

2.5 What about pack-SOC?

This chapter was dedicated to the description and the determination of SOC for single cells only. Regarding battery pack SOC, new matters have to be considered, intrinsic to the pack on one hand and to the cells on the other hand. In fact, differences in cell performance as well as cell variability do not allow speaking about content of lithium in the electrodes, which questions the t-SOC definition for pack applications. The next chapter will introduce the origins of the cell variability as well as experimental data emphasizing the variations between different batches of Li-ion cells from diverse battery manufacturers.

3 Cell variability

With anticipated growing usage of LIBs for powering mobile devices and tools, dispatched energy storage systems, and electric hybrid vehicles; complicated battery pack configurations and operations are expected. Nevertheless, reliable battery management remains as challenging issue for engineers that need to perform battery system integration for mobile or stationary energy storage applications. To manage such applications, battery modeling and simulation can be an effective tool in predicting battery response and behavior and providing a performance baseline in assisting diagnosis of battery behavior. However, an immediate obstacle exists in battery management and modeling, which comes from cell-to-cell variations, inherited from battery manufacturing processes and packaging. Being able to identify and quantify the sources that lead to cell-to-cell variations within a batch of batteries is a prerequisite to effective battery management and to account for cell imbalance within a pack³⁵.

The cell variability inspection is obtained with the initial conditioning and characterization tests, a modified version of test protocols and procedures was derived from those defined in the USABC Electric Vehicle Battery Test Procedures Manual¹⁸. The intent of such tests is to establish the baseline performance matrix for the cell chemistry, including cell-to-cell variations which are critical to us in several aspects, such as³⁰:

- To quantify the cell quality in performance.
- To quantify such variability in performance in multi-cell applications.
- To establish the confidence level for interpreting test results from a large matrix of cells that will undergo various test conditions.
- To estimate possible errors in model accuracy.
- To estimate possible escalation of errors in subsequent aging tests.

3.1 Origins of performance variability of Li-ion batteries

As explained in chapter 1, differences in positive electrode materials confer different performance to the cells in term of voltage, capacity and rate capability. However, the chemistry is not the only parameter that has to be taken into account when choosing cells for diverse applications. In fact, huge performance variability is observed within batteries using the same positive electrode active material. It mostly results from manufacturing processes from the active material selection and synthesis to the battery assembly through electrode morphology. Figure 18 highlights the different processing steps and

selections that have an influence on the cell performance from the redox couple selection to the pack design. These steps are all described in detail in appendix 7.2.

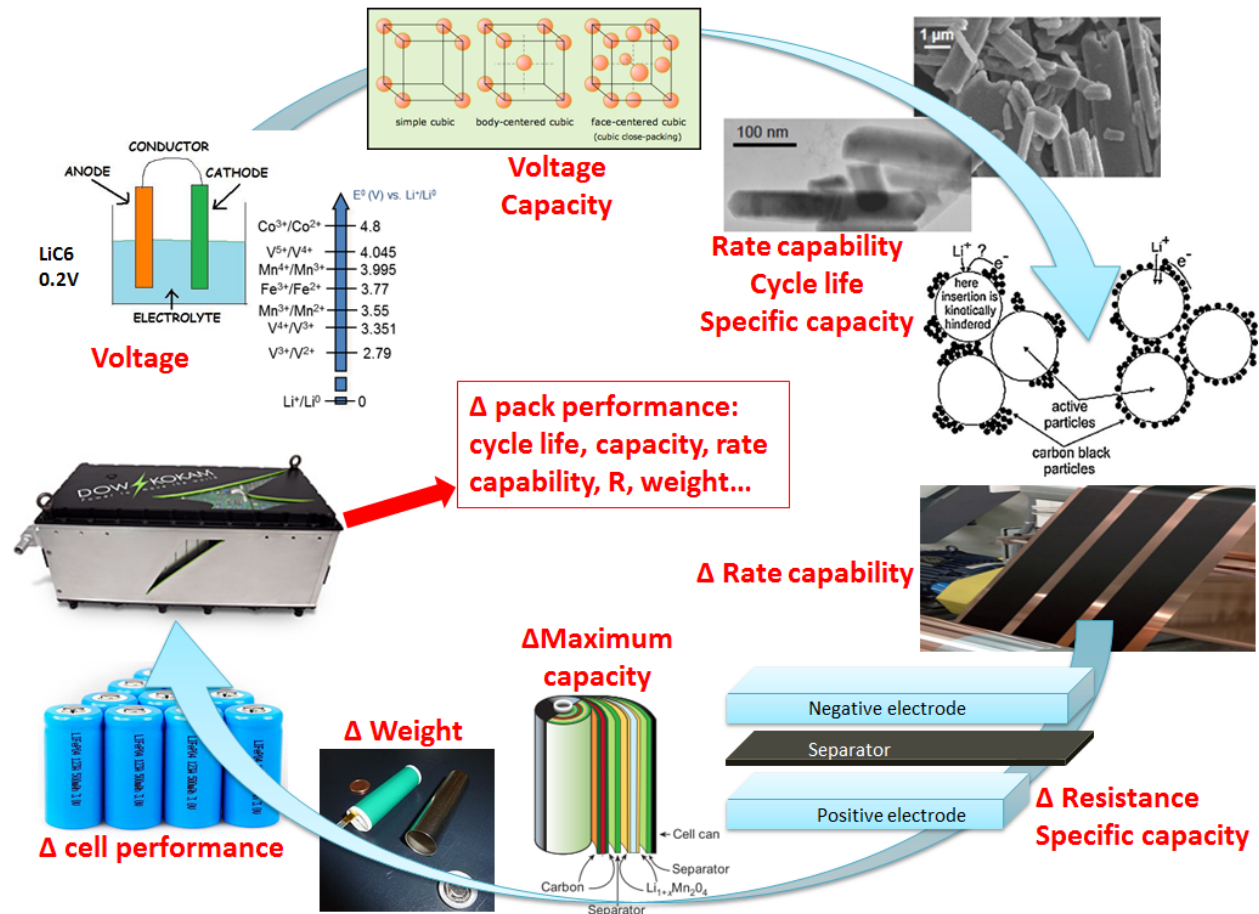


Figure 18 Performance variability in Li-ion battery manufacturing processes

To sum up, measures of Li-ion cells performance, such as cell potential, capacity or energy density, are related to the intrinsic property of the materials that form the positive and the negative electrodes. The cycle-life and lifetime are dependent on the nature of the interfaces between the electrodes and electrolyte, whereas safety is a function of the stability of the electrode materials and interfaces⁴. Pack designing should consider all of these points in order to limit the variability between cells so the pack can actually be considered as a single cell.

The aim of this thesis is to understand all these variations of properties, being able to take them into account when designing pack, as well as forecasting and anticipating cycle life and degradation. Chapter 4 and 5 will be devoted to such purposes.

3.2 Initial conditioning and characterization tests

3.2.1 Description of Li-ion cells studied

In this thesis work, a logical approach to detect cell-to-cell variations by testing and analyzing performance characteristics is illustrated and applied to three different Li-ion cell chemistries. Their specifications are presented in appendix 7.1.4.

- The first one uses a positive electrode composed of lithium manganese oxide LiMn_2O_4 , also referred as spinels, and a negative electrode made of graphite. They have been provided by Molice[®] and will also be referred as IMR cells.
- The second one has a Lithium-Manganese-Cobalt oxide $\text{LiMn}_{1/3}\text{Ni}_{1/3}\text{Co}_{1/3}\text{O}_2$ positive electrode and a graphitic negative electrode. They were also provided by Molice[®] and will be denoted IBR cells.
- The third one has a composites positive electrode comprised $[\text{LiMn}_{1/3}\text{Ni}_{1/3}\text{Co}_{1/3}\text{O}_2 + \text{LiMn}_2\text{O}_4]$ and a negative graphite electrode. In this case, two batches from different manufacturer, Molice[®] and Sanyo[®] (provided by Idaho National Laboratory), will be documented. They will be designated IHR and INL cells respectively.

3.2.2 Experimental

3.2.2.1 Cell-to-cell variations

All cells were surveyed by weight and open circuit voltage (OCV) measurements as received and then subjected to the initial conditioning tests using a Maccor 4300[®] system and an Arbin HVBT 5560[®] system. All cells were tested with Arbin Universal Battery Holders and Arbin High Current Battery Holders, Figure 19. Attention was paid to minimize variations in physical contact to avoid influences of contact variations on cell performance characteristics in any significant manner and in order to achieve better consistency in test results and improve fidelity.



Figure 19 A) Arbin Universal Battery Holder, B) Arbin High Current Battery Holder

Upon the initial survey, the cells were subjected to a conditioning process using a series of repetitive charge and C/2 discharge regimes, with no rest between each regime, which was terminated when the cell capacity was stabilized within $\pm 0.2\%$ between two consecutive cycles. The cells could be conditioned within 3 to 6 cycles typically. All cells were recharged using a constant current (CC) at C/2 step to 4.2 V, followed by a constant voltage (CV) step at 4.2 V until the termination current of C/25 was reached. Unless specified, the discharge cutoff voltage was generally 2.6 V for INL cells based on composite positive electrode and 2.5V for all other cells (IHR, IMR and IBR Molice[®]). The cells were then subjected to two discharge regimes: either C/5 and C/25 respectively for composite cells from INL; or C/5 and C/2 respectively for IMR, IHR and IBR cells from Molice[®]. Full recharge by the CC-CV steps was performed after each discharge to determine the corresponding capacity. A 4-h rest between each charge and discharge regime was imposed to determine the relax cell voltages (RCVs). The polarization resistance of the cell is calculated from the difference of the voltage drops between the two discharge regimes using Ohm's law; i.e. $\Delta V = R\Delta I$, assuming that the polarization in the cell follows a pseudo-Ohmic relationship below C/2-rate. After these tests, the cells were recharged to 50 % SOC for storage at -10°C in a freezer³⁰.

3.2.2.2 Initial characterization on nominal sample cell

A "nominal sample cell" or NSC was selected from each batch and subjected to further evaluation via a simplified reference performance test (RPT) with charge-discharge cycles at C/25, C/5, C/2, 1C, 2C and 5A to determine their performance characteristics. In these cycles, the cells were discharged and charged at specific rates until the cutoff condition were reached. The cells were set for 4-h rest to measure the relax cell voltages (RCV) at end-of-charge (EOC) and end-of-discharge (EOD) for each given rate. Remnant capacity was measured following the previous regime with a C/25 discharge or charge step to the respective cutoff condition, followed by another 4-h rest. The RCV measured at the end of this rest shall provide the SOC of the starting point for the next regime, either noted as the beginning-of-charge (BOC) or as the beginning-of-discharge (BOD), when appropriate. As explained before, the SOCs were inferred by locating the RCVs on the ps-OCV=f(SOC) curve for each chemistry³⁰. The latter was calculated from averaging the voltages against normalized capacity of the C/25 charge and discharge curves measured from the NSC. For accuracy purposes another cell was subjected to a C/100-rate cycle with an extended range voltage [1.9V 4.25V] on a VMP3 BioLogic[®]. Its charge and discharge voltage curves were also averaged to obtain another ps-OCV=f(SOC) curve.

3.2.3 Experimental results and discussion

From a previous analysis of the conditioning cycles and characterization tests on a lot of 100 commercial Li-ion cells bought from the same manufacturer, three independent attributes that contribute to cell variations have been identified³⁶. Namely they are:

- The amount of material involved: a thermodynamic factor denoted by the capacity ration that describes the content of primary and secondary active materials, noted Q_R .
- The polarization resistance: a kinetic factor derived from the voltage differences among C/25, C/5 and C/2 at a given SOC, noted R.
- And additional kinetics constraints summarized by the Peukert coefficient, which depicts the rate capability, noted P_k .

Since all the batteries tested in this work have the same 18650 size but involve different positive electrode chemistries, we expect to notice their differences through the three previously described attributes. Table 2 highlights the averaged values of each of them calculated from the conditioning tests performed on each cell of each type of Li-ion chemistry studied.

Cell type	Max. C-rate	Q_R (mAh.%SOC ⁻¹)	P_k	R (mΩ)
IHR	2	21.60	1.035	261.8
IMR	15	11.37	1.003	39.4
IBR	15	15.12	1.001	37.0
INL	3	20.06	1.0125	102.9

Table 2 Average values of attributes for each cell type

A detailed description of their variability as well as a comparison of the cell performance through initial conditioning and characterization tests are documented in appendix 7.3. Results are interesting and prove that these cells are made for different purposes and applications. For example, from the specification sheets, some are supposed to be high energy cells, e.g. NMC positive electrode cells from Molicel® (i.e. IHR cells) and composite positive electrode cells from INL (i.e. INL cells); and the others high power cells, e.g. spinel and composite positive electrode cells from Molicel® (i.e. IMR and IBR cells), which is confirmed with the experimental results. As a matter of fact, IHR and INL have a high capacity

ration with a relatively low maximum C-rate in discharge, they are high energy cells; IMR and IBR present a low capacity ration and a Peukert coefficient almost equal to one on a wide range of C-rates, they are high power cells.

Cell type	Q_R (%)	P_k (%)	R (%)
IHR	± 0.6	± 0.2	± 40
IMR	± 0.2	± 0.05	± 4.6
IBR	± 0.63	± 0.13	± 4.8
INL	± 0.4	± 0.14	± 6

Table 3 Standard deviations for each attribute of the cell-to-cell variation for each cell type

Table 3 summarizes the standard deviations in percent of each of the three attributes for each cell type in order to quantify their variability. As it can be judged by the reported values, variations are very low and even negligible in most cases. Nevertheless, cell selection for pack applications still needs to be performed and these attributes allow good basis for initial characterizations. As a matter of fact, small variability can lead to drastic impacts on pack performance on one hand and degradation on the other hand. In chapter 4 and 5, four battery packs consisting of 3-cell string configuration have been tested. For each of them, cells have been selected using the values presented above on the following way:

- The IHR cells presenting the greatest spread in term of polarization resistance, they have been chosen to establish the resistance influence in 3-cell string configurations. Results and discussions are provided in section 5.3.1. These cells have also been used for the pack-SOC investigation in section 4.2.
- The IMR cells are the ones that show the lowest variability for all parameters. Therefore, they represent good basis to study the influence of exterior parameters, such as the temperature as reported in section 5.3.1.
- The INL cells also have very limited variations for all parameters; they have thus been utilized to investigate the influence of cell topology and cell selection in term of initial SOC when placed in the pack configuration (see section 5.3.2). The very low disparity in term of capacity was also examined.

3.3 Cell-to-cell variation conclusions

Four batches of commercial 18650 cells with different positive active material were investigated to characterize their baseline performance and intrinsic cell-to-cell variations. It was found that the cells are of high quality with little, and sometimes negligible, cell-to-cell variations, thus establishing a high confidence level for analyzing and interpreting test results from a large matrix of cells that undergo various test conditions. Moreover, these cell variations can be incorporated and accommodated into future cell and pack performance models and simulations to enhance accuracy in prediction^{30,37,38}. However, even if all these observed variations among cells from a cell batch seem insignificant at first sight the next chapters will show that they can have drastic consequences when cells are put in a pack configuration on the pack-SOC determination on one hand (chapter 4), and on the pack performance and degradation on the other hand (chapter 5).

4 SOC of a battery pack

In chapter 2 and appendix 7.4, different methods and techniques have been reported to measure and estimate the SOC of single cells, each having its relative merits and drawbacks. The most common ones include the current integration technique, which is often recalibrated by the equilibrium open circuit voltage technique. The latter being the one that's considered to give the result the closest to the t-SOC defined in chapter 2.

From there, new questions raise: how about the pack SOC? Can the pseudo-OCV method be applied to battery packs? If yes, are the cells in the pack supposed to be treated separately? Or again, should the pack be considered as a single cell system? In the literature, everyone agrees on the fact that knowing SOC is essential. As a matter of fact, SOC is considered as a vital parameter followed carefully by the battery management systems (BMS) which are needed to accommodate the operating conditions and thus facilitate safe and efficient utilization of the battery packs. Their main roles are to prevent under- or over- charging conditions and to maintain optimum performance. Thereby, the pack lifetime will be maximized and the progressive permanent damages will be prevented if SOC is monitored accurately during cycle aging.

Some people say that "pack-SOC" is meaningless because of the non-homogeneity among cells included in the pack^{39,40}. As it is known, for the vehicular operations, due to the voltage and power/energy requirements, the battery packs are always composed of up to thousands of cells connected in series or parallel. For example, the Tesla roadster contains 6,831 Li-ion cells arranged into 11 "sheets" connected in series; each sheet contains 9 "bricks" connected in series; each "brick" contains 69 cells connected in parallel. Because of differences in electrochemical characteristics among Li-ion cells, manufacturing variability, production technology and tolerances, material defects and contaminations, cell architecture, and degradation with use, individual cells in a pack will typically show some variations in performance depending on the specific operating conditions (see chapter 4). G. Plett even uses an extreme illustrative example: "Consider a pack comprising two cells wired in series, one of which has SOC equal to 0 % and the other having SOC equal to 100 %. What then is the pack SOC? Is it 0 %? Is it 50 %? Is it 100 %? It cannot be 0 % because that would indicate that the pack can be charged, but the pack cannot be charged without overcharging the cell that is at 100 %. It cannot be 100 % because that would indicate that the pack can be discharged, but the pack cannot be discharged without over-discharging the cell that is at 0 %. Similarly, it cannot be 50 %"⁴⁰.

However, in all this journal papers, the right question may not have been asked. If SOC estimation is considered accurate when using the $ps\text{-OCV}=f(\text{SOC})$ method for single cell, how could this be applied for determining SOC of a battery pack? The aim of this chapter is to investigate and analyze all the different possible solutions.

4.1 Different methods for pack-SOC from OCV measurements

4.1.1 Method #1: Pack $ps\text{-OCV}=f(\text{SOC})$ curve

The first method would be to consider the pack as a single cell system. Thus the cell voltages are added up and SOC is determined by using the pack $ps\text{-OCV}=f(\text{SOC})$ curve, Figure 20. The latter is obtained on the same way as the one of single cells: by averaging the charge and the discharge of C/25-rate cycle (or lower for even more accuracy). Then SOC can be inferred directly from the relax pack voltages (RPVs).

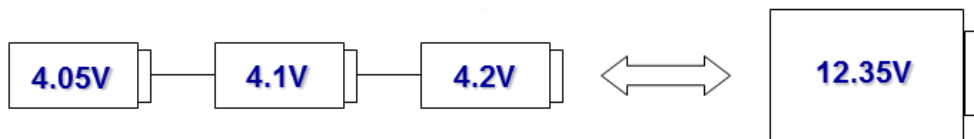


Figure 20 Method 1: 3-cell pack considered as one cell

As for single cells, the advantages of this method for SOC determination are the accuracy that can be get from voltage measurement (greater than that of current for coulomb counting) and its direct inference if the pack is at an equilibrium state. However, it requires having C/25-rate cycles for every pack at every SOH (i.e. at different points in the pack life).

4.1.2 Method #2: Average relax cell voltages

A second method would be to divide the RPVs by the number of cells within the string and then use the $ps\text{-OCV}=f(\text{SOC})$ curves of a reference single cell from the same batch and same chemistry. Thus, the pack is treated as a single cell, Figure 21.

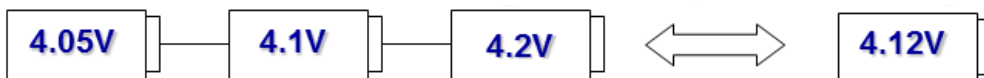


Figure 21 Method 2: 3-cell pack reduced to one single cell

The advantage of averaging the voltages is to reduce the pack to only one cell. Therefore, data on single cells of the exact same chemistry can be used for pack degradation studies. Unfortunately, this involves a few drawbacks in the use of the following assumptions: all the cells in the pack are considered identical to the NSC; cells within the pack degrade the same way and at the same rate since the same $ps-OCV=f(SOC)$ curve is used for all the cells; and, the SOC of each cell is the same at each step (i.e. no SOC imbalance). Therefore, if the degradation comes from the increase of imbalance within the pack, it will never be taken into account during the whole pack life. In other words, cells are assumed to degrade on the exact same way during calendar or cycle aging.

4.1.3 Method #3: Average of single cell SOC

The third method differs from the previous one in the sense that single cells SOC are now averaged instead of the relax pack voltages, Figure 22. Thus the cells are also treated separately as independent single cells and the pack SOC is inferred using the $ps-OCV=f(SOC)$ curve of a reference single cell from the same batch and same chemistry.



Figure 22 Method 3: 3-cell pack SOC from independent single cell

Like previously, if the same $ps-OCV=f(SOC)$ curve is used for all the cells, then the degradation of single cells is assumed to be the same during aging of the pack. However, imbalance of SOC among the cells is taken into account and limiting cells can be detected.

4.1.4 Method #4: Single cell minimum SOC

The fourth method appears easier on a conceptual point of view. In fact, cells are also treated separately like in method #3 but we now make the assumption that the pack is driven by the cell that shows the minimum SOC.



Figure 23 Method #4: 3-cell pack SOC is single cell's lowest SOC within the string

Therefore, the pack SOC is considered to be the one of the limiting factor within the string, which means the battery with the lowest capacity or the lowest capacity ration (assuming that it is the

one driving the pack capacity). Here again, the degradation of all the cells is assumed to be identical during cycle aging.

4.1.5 Method #5: Single cell maximum SOC

The fifth and last method is similar to the previous one except that the assumption is now that the pack is driven by the cell that shows the maximum SOC. Similar advantages and drawbacks than that of method #4 are involved.



Figure 24 Method #5: 3-cell pack SOC is single cell's greatest SOC within the string

4.2 Tests on accuracy of each method

All these methods should give identical SOC for the pack if and only if the Li-ion cells were all identical. However, following what has been introduced in chapter 3, cells taken from a same batch exhibit variations that have to be considered in pack applications. In order to find out which of the five presented methods gives the best pack-SOC estimation, a test referred as “remnant capacity tests” (RCT) has been conducted. Its aim is to give information on the accuracy of each estimation method by measuring the maximum capacity of the pack.

4.2.1 Experimental

After the initial conditioning and characterization tests presented in chapter 4, three cells were chosen from the 24-cell batch of Molicel® IHR 18650A (NMC positive electrode), put in a string configuration and subjected to the RCT test. The choice was made in order to have approximately the same polarization resistance and the same amount of active material (i.e. same capacity ration) between cells. Also, an imbalance in SOC was included initially on a voluntary basis: one cell was charged to only 90 % SOC while the other ones were fully charged (i.e. 100 % SOC) before being put into the string. This was supposed to create an imbalance between cells for emphasizing the accuracy of each method and highlighting the best one. The cells were charged separately to the desired initial SOC using an Arbin HVBT 5560® system before being put in a string configuration and subjected to the RCT test on a Maccor 4300® system. This test consists, firstly, in three successive discharges at 2C, C and C/2 rates with remnant capacity measurements (i.e. an additional C/25 discharge or charge step to the same cutoff condition followed by another 4-h rest). Secondly, three other discharge rates, 5/2C (5 A), 3/2C and C/5, were considered. The charges were done following the protocol recommended by the

manufacturer with a constant current (CC) step at C/2 followed by a constant voltage (CV) step at 12.6 V (4.2*3) with C/25-rate cutoff. Between each RCT test, a C/25-rate cycle was performed with the same cut-off conditions in order to follow the evolution of the ps-OCV=f(SOC) curves (of the pack and each individual cell). For safety reasons the pack cut-off voltages in charge and discharge were set to 12.6 V (4.2*3) and 8.1 V (2.7*3) respectively, i.e. ~4.2 V and ~2.7 V for each cell. In addition, auxiliary channel voltages were recording the voltage of each cell at each time and some extra safety cut-off voltages of 2.5 V in discharge and 4.25 V in charge were used. Besides, a ceramic resistance of 1.025 Ω 10 W was plugged in series with the battery pack. Its voltage was recorded by an auxiliary voltage channel in order to monitor the current flowing through the 3-cell string at each time during the test, Figure 25. The test facility was air-conditioned to maintain a stable temperature.

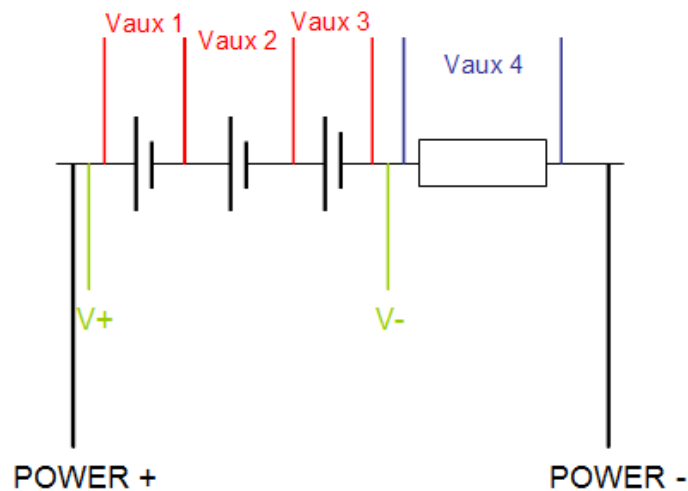


Figure 25 Pack circuit

4.2.2 Remnant capacity test results

Results for each method are meticulously described in Appendix 7.5.2 and plotted on Figure 26. This figure summarizes the SOC ranges used for the six calculated rates with the five different methods presented above on the same experiment. As we can judge, variations of SOC range are very important depending on the approach taken and the differences are far from being negligible in term of SOC determination. According to methods #2, #3 and #5, SOC is more than 10% at the end of discharge at each rate (and almost 20% for #5); whereas SOC is only ~5% for methods #1 and #4. Regarding the end of charge SOC, the pack is fully charged according to methods #1 and #5 (i.e SOC is almost 100%); 90% charged for method #2 and #3; and 85% charged for #4. A closer look at the end-of-charge (EOC) and

end-of-discharge (EOD) SOC is offered on Figure 27. The EOC SOC for all rates present much less variations than the EOD SOC per methods because the charging rate was always C/2 followed by a CV step at 12.6 V. In order to figure out which of those methods gives the actual pack SOC, the remnant capacities at each rate is analyzed in the next paragraph.

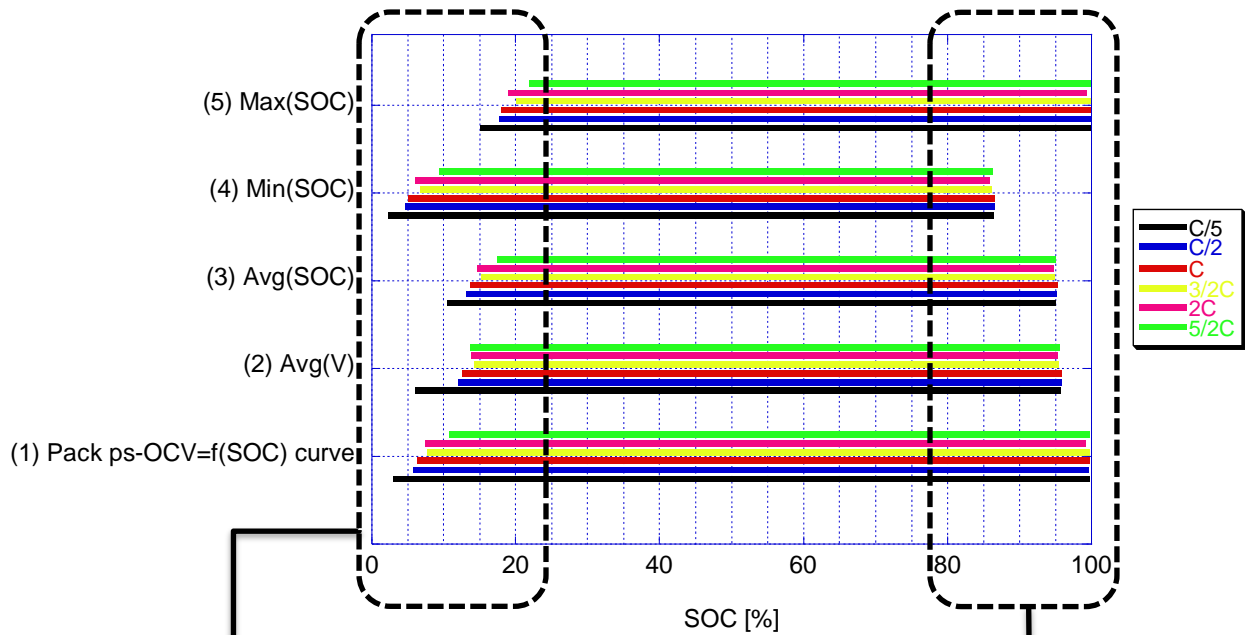


Figure 26 SOC range per rate per method (summary)

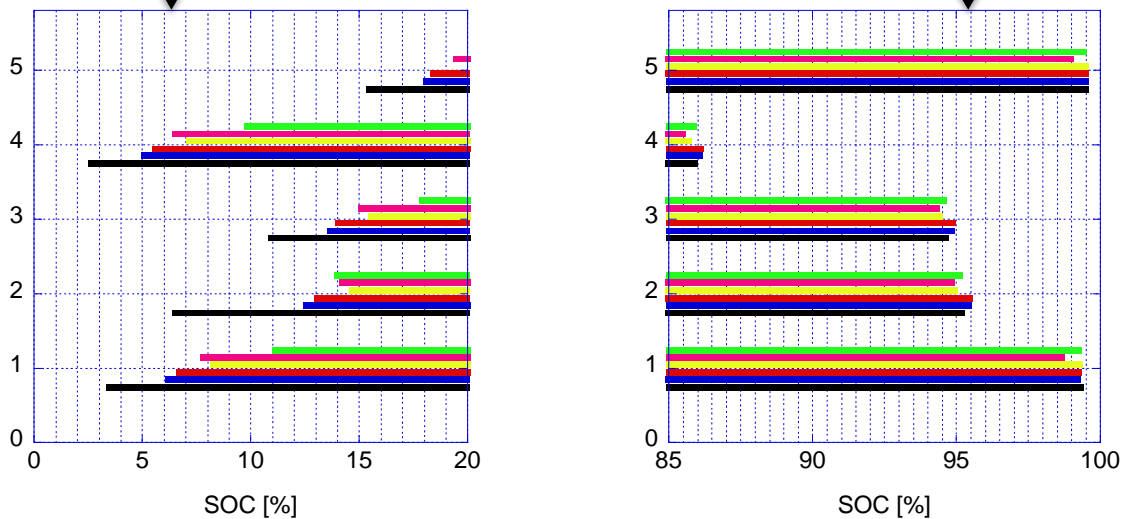


Figure 27 Zoom of pack EOC and EOD SOC

4.2.3 Pack-SOC analysis and discussion

The principle of the RCT test is to measure the pack remnant capacity at the EOD (and at the EOC). This can be done by discharging (or charging) at a very low rate, i.e. C/25-rate or lower, after each

one of the successive C/n-rate discharges (or charges). As a matter of fact, because of diffusion limitations, the maximum capacity cannot be obtained from all rates. For example, when discharging at a 2C-rate, the capacity is lower than the one at C/100-rate, as it is illustrated by the yellow area of the Peukert curve on Figure 28. Considering that the pack will reach 0 % SOC at the end of this low rate discharge step (or 100 % SOC at the end of the low rate charge), the remnant capacity will be obtained. By dividing the remnant capacity by the maximum capacity, the experimental SOC can be obtained and compared to the SOC predicted by each of the five different methods. Therefore, the one that gives the best accuracy on pack-SOC should be easily deciphered.

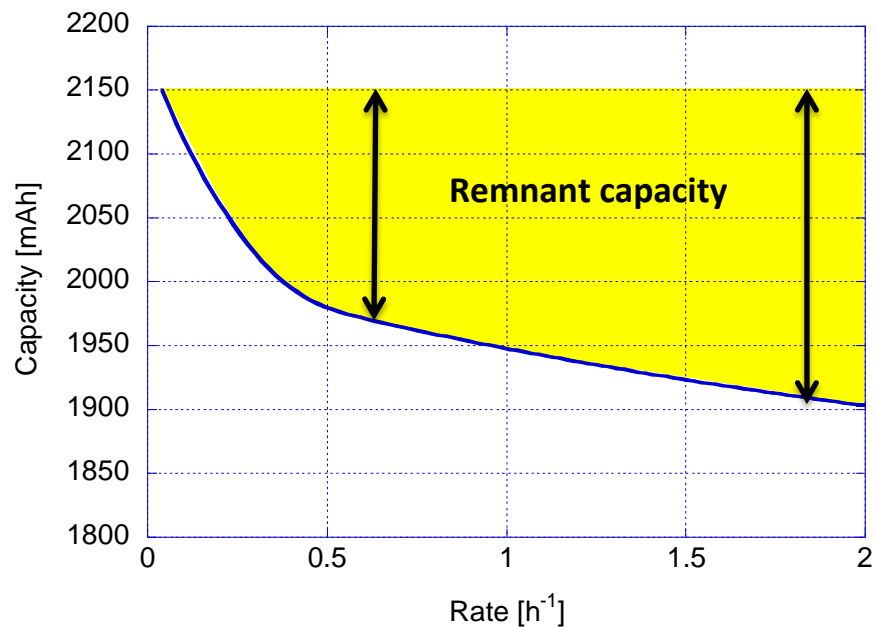


Figure 28 Remnant capacity

Table 4 summarizes the different ratio of remnant capacity over total capacity calculated at different rates with the five methods and Figure 29 illustrates the comparison of the predicted SOC with the experimental SOC in term of absolute value of their difference. On this representation, the closer to 0 % the better it is. More details on these values can be found in Appendix 7.5.3 (in term of capacity ration only). Method #1 using the pack pseudo OCV vs. SOC curve seems to be the one that give the most accurate results since the deviation between the two SOC is always lower than 0.8 % both in charge and in discharge. Methods #2 and #3, which are the most used in the literature, cannot provide less than 5 % of error on SOC for all rates. Method #4 using the cell reaching the minimum SOC offers quite accurate results, but it is important to note that all these values were obtained for the remnant capacities measured in discharge. As a matter of fact, method #4 becomes the method giving the lowest

accuracy at the EOC since the cell reaching the maximum SOC will be the one limiting the pack during the charging process. Reciprocally, method #5 using the cell reaching the maximum SOC provides accurate values at the EOC but not at the EOD.

Rate	$\frac{\text{Remnant } Q}{\text{Total } Q}$	SOC _{Predicted} - SOC _{Experimental} (%)				
		Method #1	Method #2	Method #3	Method #4	Method #5
C/5	3.61	0.14	4.91	7.3	1.15	11.85
C/2	6.71	0.50	5.82	6.96	1.62	11.37
C	7.44	0.75	5.65	6.65	1.84	11.00
3/2C	7.58	0.64	7.06	7.92	1.25	12.81
2C	8.31	0.52	5.89	6.76	1.79	11.13
5/2C	10.46	0.70	5.56	7.5	1.7	11.87
C/2 EOC	6.52	0.38	5.49	7.00	11.50	1.83

Table 4 Capacity ration per rate per method

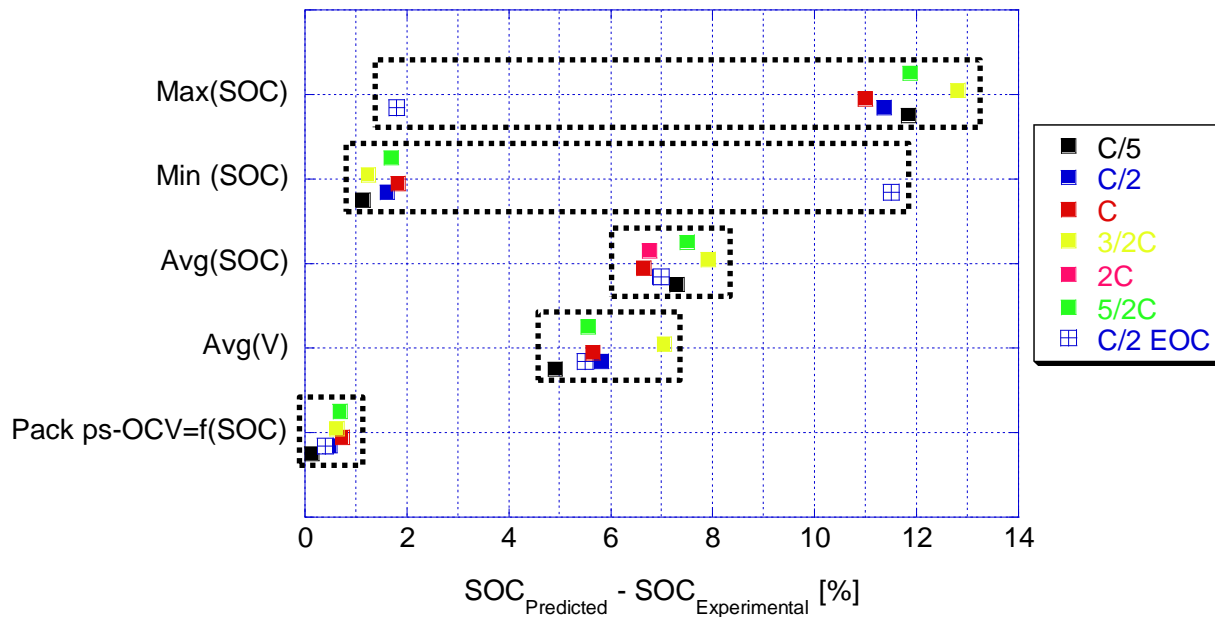


Figure 29 Predicted SOC vs. Experimental SOC

This RCT tests involved a significant imbalance of more than 10 % on the initial SOC among cells so the results show disparities and the accuracy of each method can be emphasized and discussed. However, same results can be obtained when imbalance is limited (i.e. cells are placed in the string with identical initial SOC). Figure 30 displays the same information as Figure 29 but on two different pack tests using different Li-ion cell chemistries. These 3-cell strings were subjected to cycle aging and will be studied in chapter 5. Nevertheless, the presence of remnant capacity measurements in their reference performance tests (RPTs) allowed comparison and validation of the outcomes presented in this chapter. Conclusions are similar to the ones obtained with the RCT tests: method #1 that uses the evolving pack ps-OCV=f(SOC) curves gives predicted SOC that are the closest to the SOC calculated experimentally both in charge and discharge processes. Therefore, it can be concluded that the pack ps-OCV=f(SOC) curve method is the one that estimates the pack-SOC with the highest precision for all cases (i.e. including any kind of imbalance and for any type of Li-ion cell chemistry considered). For these reasons, it will be used for SOC determination in the next chapter. Method #2 and #3, based on the voltage and SOC average respectively, also provide acceptable accuracy and will still be considered in the next chapter as well. Regarding method #4 and #5, they have been discarded because of their inability to supply low uncertainty on SOC determination on the whole SOC range.

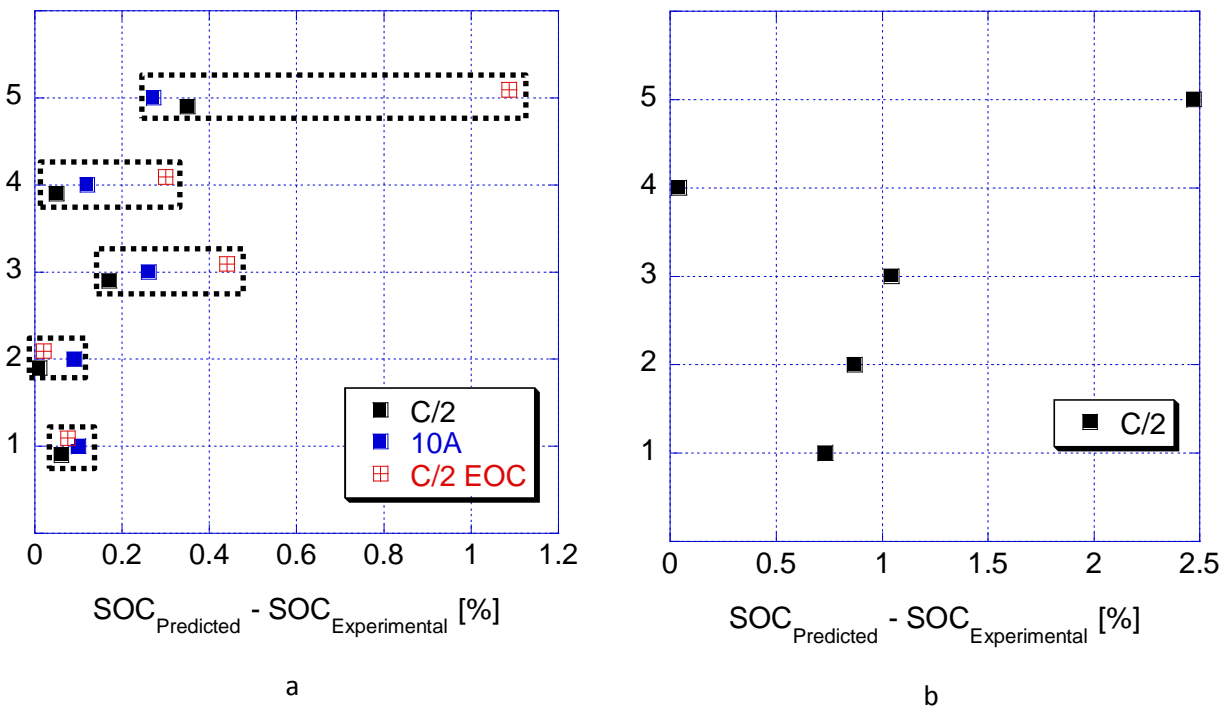


Figure 30 Predicted SOC vs. Experimental SOC (validation on 2 other chemistries)

4.3 Discussion of uncertainty of SOC estimation using ps-OCV=f(SOC) curves for pack and single cell

In chapter 2, a study on the accuracy of the SOC determination has been reported regarding the precision of the voltage measurement. How about such matters for battery pack in string configuration?

Among all the different Li-ion cell chemistries, it has been shown that cells using LFP and spinels positive electrode presented low accuracy in some areas; however the use of these cells for pack applications presents a few advantages. One of them is the rapid voltage turns at the EOD and at the EOC. As a matter of fact, if one of the cells in the pack is experiencing overcharge, it would be only a voltage overcharge which is not as bad as a capacity overcharge (i.e. the cell would raise to high voltage relatively quickly without big increase of capacity). On the other hand, high voltages for NMC, LCO or (NMC+spinel) composite Li-ion cell would mean capacity overcharge, which can lead to safety issue and fast degradation. All ps-OCV=f(SOC) curves as well as their uncertainty areas are documented in chapter 2.4 and appendix 7.4.4.

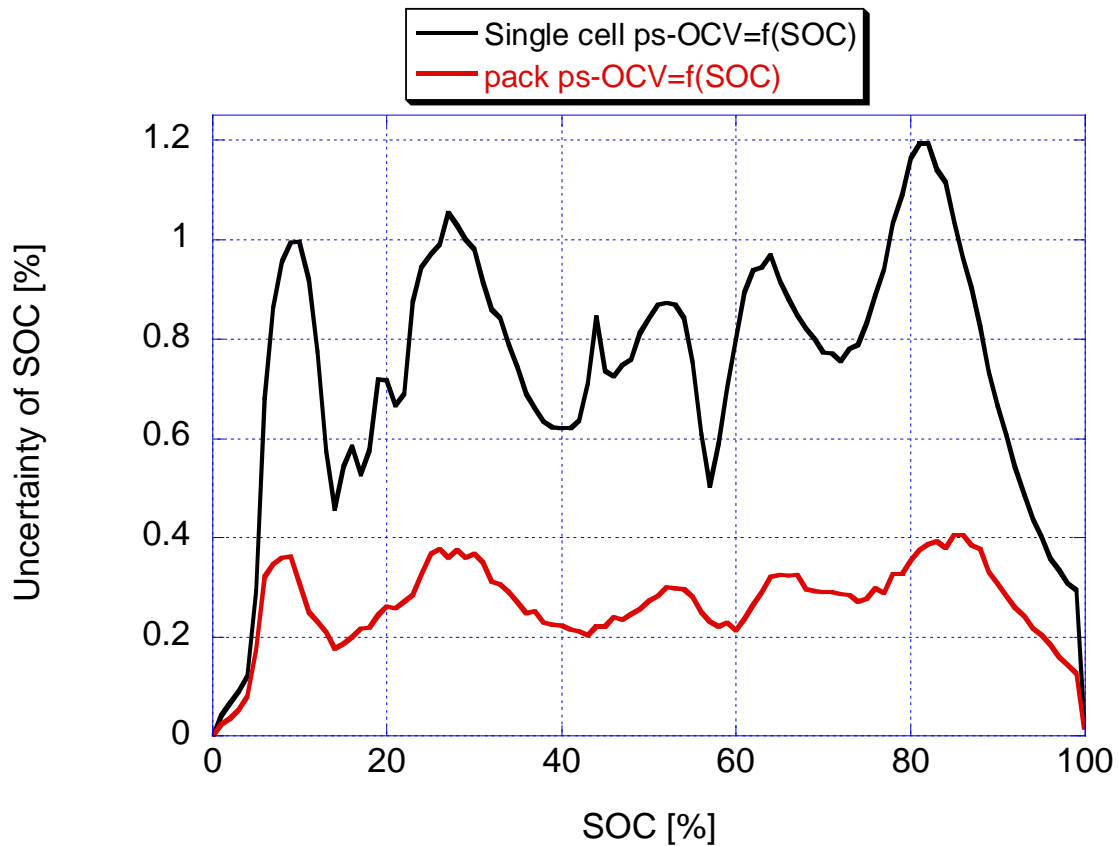


Figure 31 Comparison of SOC uncertainty from single cell ps-OCV=f(SOC) curve and pack ps-OCV=f(SOC) curve

Besides, it appears that pack ps-OCV=f(SOC) curves give better results for SOC estimation than that of single cells because the length of the voltage plateaus seems to be reduced due to the cell imbalance within the pack (uncertainty divided by three, Figure 31). This reinforces the conclusion of the RCT test performed previously: pack SOC must be determined using pack ps-OCV=f(SOC) curves rather than that of single cell. Nevertheless, even if the pack is considered as a “single cell system”, it is very important to monitor each cell separately to identify causes of degradation during cycle aging.

4.4 Conclusion on pack-SOC

In this chapter, five methods based on the SOC determination from the OCV measurements have been tested on three 3-cell string configurations using different types of Li-ion cell chemistry. In all cases, it has been proved that the pack-SOC is the most accurately determined when using the pack ps-OCV=f(SOC) curves. The two methods that are the most used in the literature, i.e. methods based on voltage or SOC averages, give good SOC precision but not in all cases, as it has been highlighted by the 10 % imbalance in the initial SOC's originally included.

Therefore, the SOC gauge of electric cars or any other kind of electric device using Li-ion batteries can now be claimed to be reliable at the beginning of life of the battery pack, no matter what cell chemistry comes into play. Nevertheless, the first limitation of the USABC definition has not been solved yet. In other words, the capacity loss is still not taken into consideration by the gauge during cycle aging. The next chapter will be devoted to such concerns with three different degradation case studies.

5 Ageing analysis of Li-ion battery packs

5.1 Degradation of Li-ion battery pack

Ageing and degradation phenomena that contribute to decrease the battery lifetime are numerous, and are specific to the cell chemistry. They can be either of mechanical or chemical origin. Active-particle isolation from the electrode matrix because of expansion/contraction during successive intercalations and de-intercalations of Li^+ ions during cycling is an example of mechanical degradation, while the SEI growth on graphitic anodes as a consequence of electrolyte decomposition is an example of chemical degradation. Many studies^{2,13,32,41} showed that cell capacity fade may be the result of the loss of cyclable Li^+ ions (i.e. loss of lithium inventory) and of the loss of active materials (e.g. particle isolation, phase transition towards an inactive phase, material decomposition). An impedance increase of the cell can also lead to a decrease of its capacity when measured at substantial current density as well as under-discharges and under-charges. Additionally, it has also been mentioned that the electrode kinetics can be hampered causing an acceleration of capacity loss². All of these degradation origins have to be considered when working on battery pack. As a matter of fact, one cell within the pack showing a quicker degradation may result in a complete failing of the whole pack. Therefore, each cell must be monitored in order to foresee degradations and take actions to avoid failure. This chapter is devoted to this effort from the cell selection to the failure modes of each of them when they are placed in a string configuration.

5.2 Stress factors impacting performance and degradation of commercial Li-ion cells in a string configuration

The variability among cells from a same batch will be a determining factor in the pack design, its performances and its degradation. Therefore, a precise cell matching is extremely important; especially on high voltage battery packs when high load currents are drawn or if the pack is operated in different temperature conditions. As the cells age, cell capacities diverge and this affects charge and discharge times. On charge, a weak cell reaches full charge first, and without limit the voltage would rise further. On the other hand, on discharge, the weak cell discharges first and needs protection from voltage depletion. To sum up weak cells are at a disadvantage; they get stressed the most and lose capacity quicker than the strong cells in a pack, which underlines the importance of the cell-to-cell variations for selecting the batteries that will be put in a pack configuration for optimal pack performance.

There are three main origins for cell variability. In chapter 2, only the intrinsic attributes were introduced. They are:

- The initial maximum capacity,
- The polarization resistance,
- The rate capability (i.e. Peukert coefficient),
- The capacity ration (or amount of active material involved in cell reactions).

Some variability can be induced by external parameters or conditions. These extrinsic attributes are:

- The path dependence during calendar aging (storage conditions of cells),
- The path dependence during cycle aging,
- The temperature,
- The connections.

Besides, the cell selection and topology can also contribute to the introduction of variability in the pack. The main criterion that must be taken into account is:

- The OCV matching (i.e. the initial SOC of each cell when placed in the pack).

All these factors may be source of imbalance when cells are put in a string configuration. Some of them can appear initially on the performance, such as the initial SOC; whereas others can take more than 500 cycles to manifest themselves, such as the amount of active material. Furthermore, as the number of cells in the battery configuration increases, the complexity in the control and managing the cells becomes sophisticated as well. Therefore, there is an urgent need to understand the behavior of a multi-cell string through proper assessments to derive an adequate strategy for the control and management of the string. Battery management systems become critical for maintaining safe and optimum performance. The best that the pack management system can achieve is to accommodate the intrinsic SOC imbalance and minimize the impact from the external attributes (such as temperature or connections) to reduce the risk of degradation and failure of the cells. As a result, the reliability of the energy storage device will be enhanced and the product life extended¹⁶. In the next paragraphs, three imbalances will be studied: one from intrinsic parameters, i.e. the polarization resistance, one from the cell selection and topology, i.e. the OCV matching, and one from extrinsic parameter, i.e. the temperature. Results and discussions for each of them regarding pack performance and degradation are documented through SOC tracking and incremental capacity analysis.

5.3 Ageing of commercial Li-ion cell in a string configuration

5.3.1 Ageing of commercial Graphite/spinel Li-ion cell in a string configuration with temperature gradient within the string

Some pack imbalances are not especially related to cell intrinsic parameters but more to operating condition disparities, or, in other words, external constraints such as path dependence or temperature variations⁴³. In this first case, we are interested in the temperature gradient effect within a string. The spinel material having been proved to be very sensitive to high temperature⁴⁴⁻⁴⁸, cells with pure spinel positive electrode (Molicel® IBR) have been selected for the test. The cells have been chosen so they have the closest maximum capacity, polarization resistance and capacity ration. Table 5 summarizes their initial characteristics. The imbalance of this pack was then induced by the temperature: two cells were at room temperature (~25°C) while the third one was placed in an incubator set to 60°C during cycle aging. The temperature difference being not negligible, the cell at 60°C was obviously expected to show some weakness signs sooner than the two others, and thus, to be at the origin of the pack failure⁴⁹.

Polarization resistance	Cell 1: 37.5 mΩ Cell 2: 35.8 mΩ Cell 3: 34.1 mΩ
Q ₅	Cell 1: 1.1343 Ah Cell 2: 1.1365 Ah Cell 3: 1.1396 Ah
Q _R	Cell 1: 11.5 mAh/%SOC Cell 2: 11.5 mAh/%SOC Cell 3: 11.5 mAh/%SOC

Table 5 IMR cell selection for pack configuration (based on their similarity)

5.3.1.1 Experimental

Following the weight survey as well as the initial open circuit voltage (OCV) measurements, the conditioning cycles and the reference performance test (RPT), the three 1.20 Ah 18650 cells with pure spinel positive electrode chosen from a 32-cell batch provided by Molicel® have been placed into a string configuration. The string was then subsequently subjected to cycle aging at 10 A (~8.3C) in discharge regime while recharging with the protocol typically recommended by the manufacturer with a constant current (CC) step at C/2 followed by a constant voltage (CV) step at 12.6 V (4.2*3) with 75 mA

cutoff. To reduce test duration, the pack was only allowed to a 6-h rest every 10 cycles to trace the SOC changes in the pack. Upon every 10% of capacity loss, the pack was subjected to a pack-RPT, i.e. charge-discharge cycles at C/16, C and 10 A respectively with remnant capacity measurements, to assess changes in performance. During these RPTs, ps-OCV=f(SOC) curves for each cell and for the pack itself were recalculated since the OCV-SOC correspondence evolve over cycle aging¹³. For safety reasons the pack cut-off voltages in charge and discharge were set to 12.6 V and 7.5 V respectively, i.e. ~4.2 V and ~2.5 V for each cell. In addition, auxiliary channel voltages were recording the voltage of each cell at each time and some extra safety cut-off voltages of 2.0 V in discharge and 4.25 V in charge were used. A ceramic resistance of 0.10 Ω 50 W was plugged in series with the battery pack. Its voltage was also recorded by an auxiliary voltage channel in order to double check the current flowing through the 3-cell string at each time during the test and to be able to correct capacities a low-rate. The tester was a Maccor 4300® system and the test facility was air-conditioned to maintain a stable temperature. Arbin High Current Battery Holders were used since the current in discharge was greater than 5 A.

5.3.1.2 Results

The evolution of the pack capacity fade over 200 cycles with the temperature gradient at different rate is presented on Figure 32(a). Contrary to the two other pack degradation studies (that are analyzed in the next paragraphs) where a drastic drop of the capacity is observed after approximately 15-20 % of capacity loss, here it seems to occur initially, right after the temperature of the cell #2 was setup to 60°C, and then only one linear stage can be identified. What is interesting to note is that the loss is rate dependent for the whole cycle aging. As a matter of fact, low rates (C/16 and C/2, triangles and squares respectively) and the high rate (10 A, 8.3C, circles) show different slopes emphasizing the degradation of the rate capability during cycling: at low rates, the loss is about 17 % per 100 cycles whereas it is 23 % per 100 cycles at high rates (for which these cells have been designed). Consequently, the end-of-life (EOL) was reached relatively early after 60 cycles only. After each RPT, a rapid decline of capacity at 10 A is also observed and its intensity seems to amplify with aging.

Same trends were observed on single cells under cycle aging as it is illustrated on Figure 32(b). The slope at 60°C (black circles) is unsurprisingly steeper than that at 25°C (light green circles). The pack capacity following the same evolution as the single cell one cycling at 60°C, it can thus be claimed that the degradation is due to the intrinsic disparity included in the string as a temperature gradient. It is also important to note that the pack fading rate appears to be faster than the single cell because the pack was cycling at higher rate (i.e. single cell was cycling at 2.5C-rate at elevated temperature while the pack

was subjected to 8.3C-rate at elevated temperature). About the performance at the beginning-of-life (BOL), the pack seems to fall short of capacity compared to the single cell at all rates (Figure 33(a)), which allows claiming that the pack performance are limited by the cell variability as well.

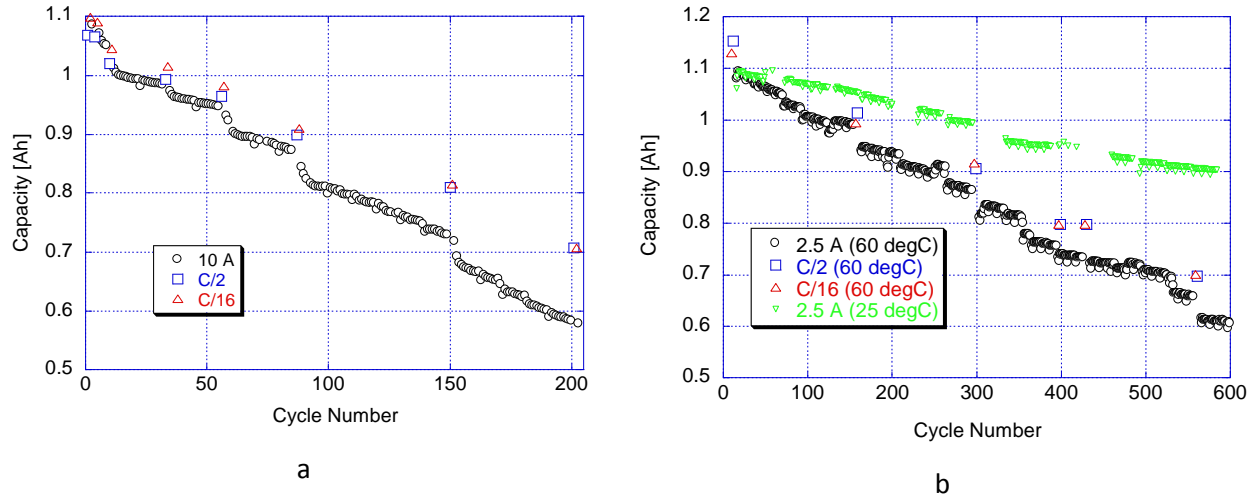


Figure 32 (a) Pack capacity evolution at different C-rate. (b) Capacity evolution as a function of cycle number for single cell cycling at identical conditions.

Relax pack voltages (RPVs) at the end-of-discharge (EOD) do not show any stable behavior but a rapid increase for the first 10 cycles followed by a constant increase over the 200 cycles for all rates are detected, Figure 33(b). Regarding the end-of-charge (EOC), a slight decrease of 200 mV is observed no matter what rate is considered.

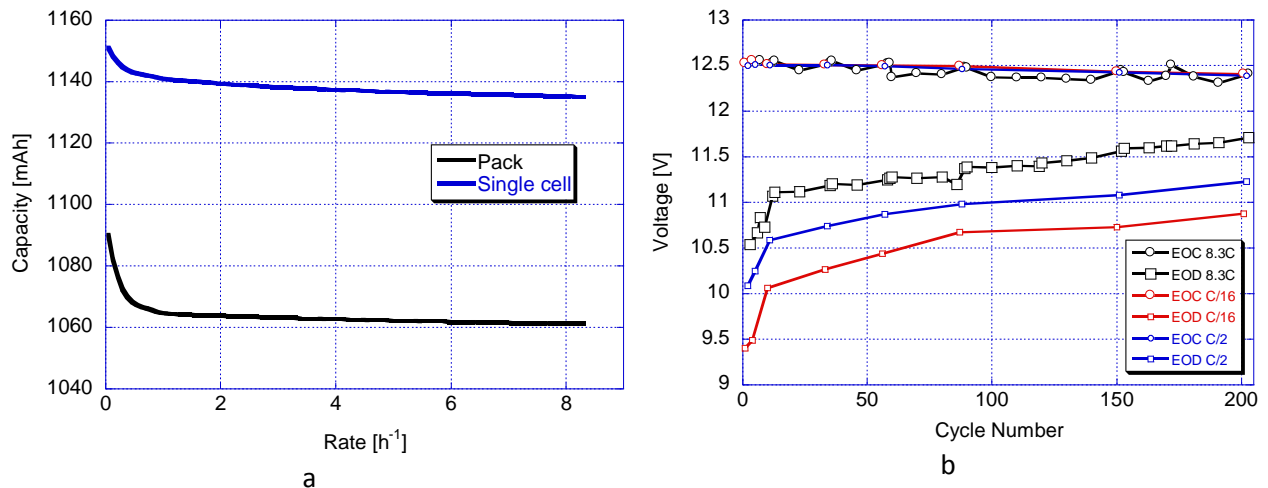


Figure 33 (a) Peukert curves of single cell and pack. (b) RPVs evolution at the EOD and EOC at different C-rate.

The RPTs performed at regular intervals during cycle aging allowed the calculation of the evolving pack ps-OCV= f (SOC) curves, Figure 34(a). Fairly quickly, in less than 10 cycles, the shape of the

curve in the low voltages area exhibited important changes that kept developing until 200 cycles, emphasizing the necessity to use evolving ps-OCV=f(SOC) curves when converting RCVs/RPVs to SOC. Figure 34(b) displays the SOCs determined with the three different methods retained from chapter 4 (i.e. the pack ps-OCV=f(SOC) curve, the voltage average and the SOC average) as well as the experimental SOCs measured from the remnant capacities (green dots). With the imbalance induced from the temperature gradient, only the SOCs obtained from the pack ps-OCV=f(SOC) curves fits with the experimental SOCs during cycle aging. The two average methods can lead to uncertainties of more than 10 % after 200 cycles. Therefore the pack SOCs must be determined from the evolving pack ps-OCV=f(SOC) curves. As for the EOD RPVs, the EOD SOCs follow a linear trend that increases from 4 % to 22 % after 200 cycles, which is thus equivalent to 9% per 100 cycles. At the EOC, because of the CV step, the SOCs are relatively constant.

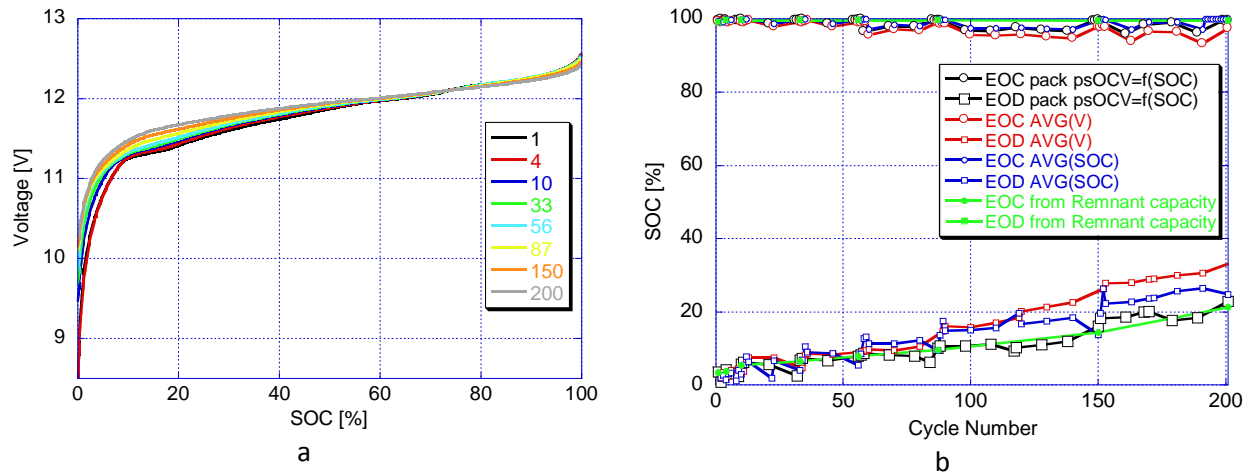


Figure 34 (a) Pack evolving ps-OCV=f(SOC) curves. (b) EOC and EOD SOCs from the pack evolving ps-OCV=f(SOC) curves.

The gradual reduction of the SOC range and the linear decline of the capacity are highlighted with the evolution of the pack capacity ration, Figure 35. The latter deteriorate from 11.3 mAh.%SOC⁻¹ to 7.4 mAh.%SOC⁻¹. This translates a loss of 35 % of the content of active material involved in the cell electrochemical reactions (i.e. lithium inventory and electrode active materials).

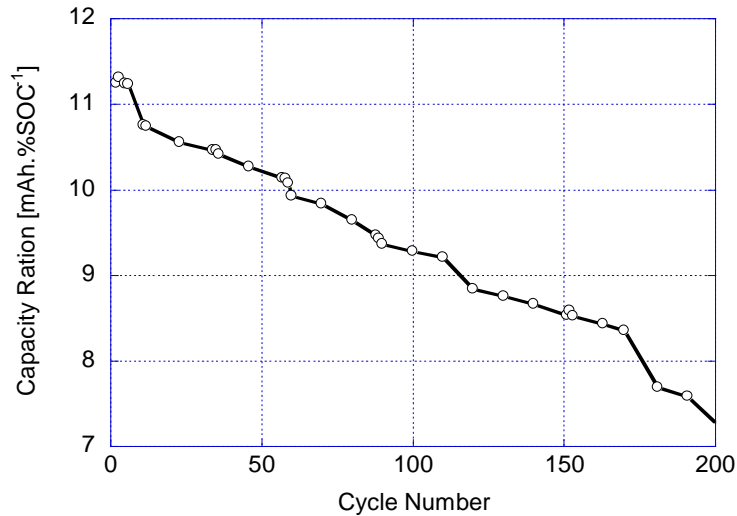


Figure 35 IMR pack capacity ration evolution during cycle aging

Because these IMR spinel cells are designed for high power applications and because the string was subjected to 8.3 C-rate cycle aging, its rate capability is worth investigating. Figure 36 shows the evolution of the Peukert curves calculated from the three discharging rates performed at each RPT. The initial Peukert curve when all cells were at the same temperature is really similar to the second one that was obtained right after the temperature was setup to 60°C for the cell #2. However, all the following ones exhibit constant reduction in term of rate capability. The Peukert coefficient was also obtained by curve power fitting at each RPT, it evolves from almost 1 to 1.038 after 200 cycles. The farther this coefficient is from 1, the less the cell is able to provide high current, which emphasizes the fact that the capacity at 8.3 C has been highly reduced. Before entering into the detailed study on the separate cells in the discussion below, an intriguing fact can be raised on the rate capability. As depicted on Figure 36, the pack clearly follows the Peukert law initially, with a Peukert coefficient of almost 1.0. Such a coefficient usually means that the cell is ideal and can provide the same capacity no matter what rate is requested. Moreover, it also indicates that the active materials are not fully used and that the limiting factor is thus the diffusion of the Li^+ ions in the electrode lattice structures. However, after 200 cycles, the capacities at low rates, i.e. C/16 and C/2, appear almost equal, which is a clear indicator of loss of lithium inventory. As a matter of fact, at low rates, nearly all the available Li^+ ions are retained in the graphite electrode at the EOC. At the EOD, the extent of lithium depletion in this electrode is depending on the discharge regimen and the unused Li^+ ions are considered as the “reserved” capacity. As loss of lithium inventory occurs, as induced by the side reactions in the cycle aging, the amount of Li^+ ions returns to the negative electrode in charging, and thus the “reservoir” of lithium decreases over cycles².

Consequently, it becomes logical that the C/2 capacity becomes equal to the C/16 one when the “reservoir” of lithium is empty. IC curves will be investigated further in the analysis in order to figure out whether what is seen in term of loss of lithium inventory on the pack performance actually occurred on at least one of the cell within the string.

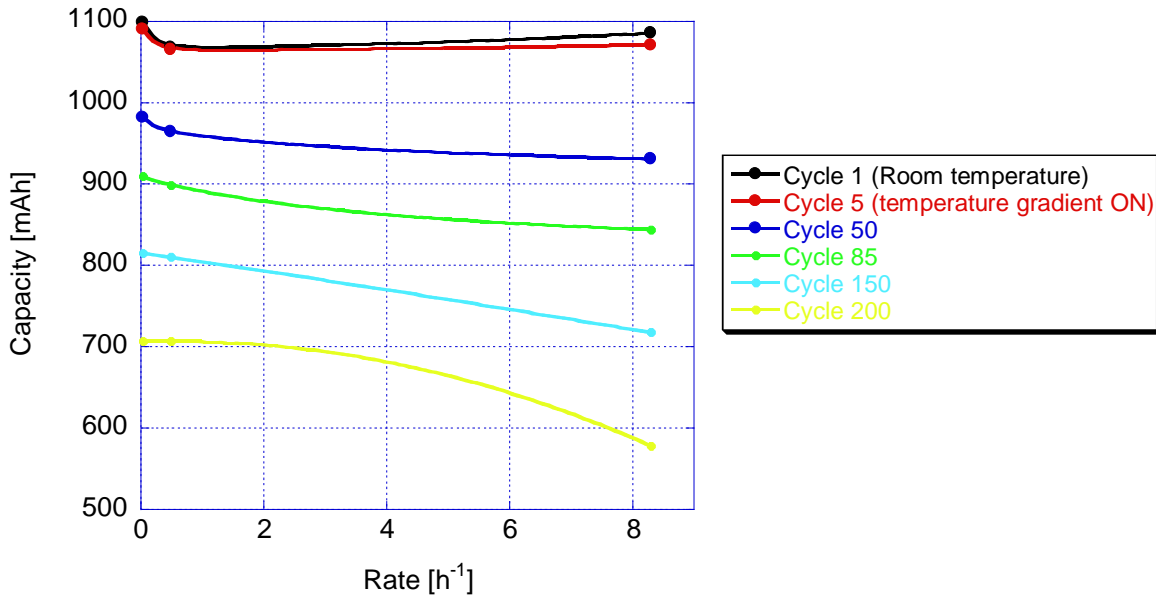


Figure 36 IMR pack Peukert curves during cycle aging

On the cell specs sheet, the manufacturer certifies at least 300 high current cycles before reaching the EOL when respecting the operating temperature range. Therefore the critical temperature of 60°C imposed to one of the cells could be at the origin of the fast degradation observed. Deeper look at the separate cells is indispensable to understand the capacity fading of the pack. A vigorous cell-by-cell analysis using techniques such as IC analysis and SOC tracking is thus proposed in the next paragraphs.

5.3.1.3 Discussion

The RCVs are represented on Figure 37(a), as well as their conversion in SOCs using the evolving ps-OCV=f(SOC) curves of each cell during cycle aging on Figure 37(b). The first notable difference among the three cells is the lower relax voltages in discharge for the cell that was cycling at 60°C. This is easily explained in the literature: as the temperature increases, the resistance becomes lower and the diffusion rate of Li⁺ ions in the lattice structure of the electrode materials rises (since diffusion follows the Arrhenius’law). Therefore, the cell #2 reaches lower voltages earlier than the two others. The phenomenon is straightforwardly observed on Figure 38(a) that illustrates the EOD voltages of each cell

before relaxation. During the three first cycles of the RPT performed at room temperature, cell #2 was getting to approximately 2.9 V when the pack cutoff condition was attained; as soon as its temperature was set to 60°C, the safety cutoff voltage of 2.0 V was ending all discharges at each rate. As a consequence, cell #1 and #3 were subjected to under-discharge and the pack EOD voltage rose from 7.5 V to 8.5 V in 200 cycles, as it is displayed on Figure 38(b).

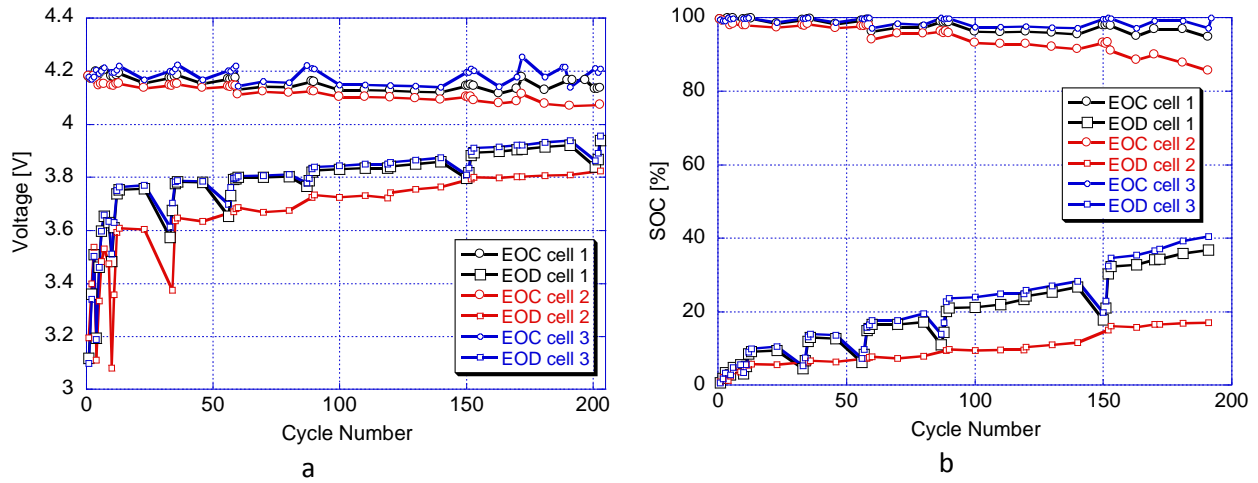


Figure 37 (a) Relax cell voltages (RCVs) of each IMR cell in the pack versus cycle number as measured during the cycle aging at the beginning- and end-of-charge. (b) Evolution of the end-of-charge and end-of-discharge SOC of each IMR cell during cycle aging.

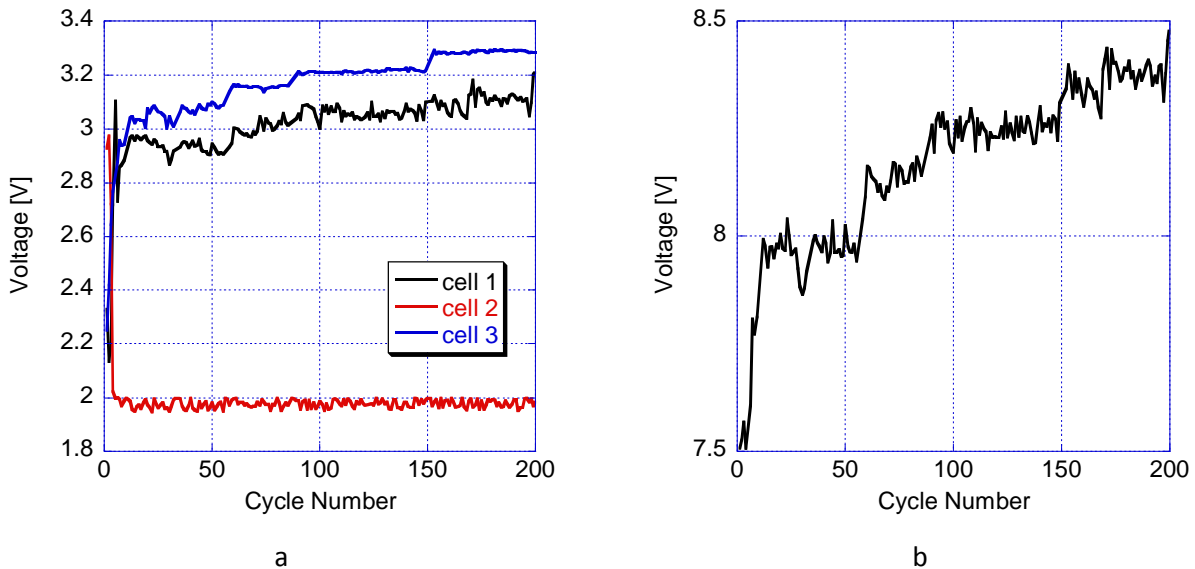


Figure 38 (a) EOD voltage before relaxation of each cell during cycle aging. (b) EOD voltage before relaxation of IMR pack during cycle aging.

Regarding the SOC, as for the RCVs, cell #1 and #3 appeared really similar during the 200 cycles while the cell #2 was following a different trend. The lower voltages reached by the latter imply lower SOC in charge and in discharge. Consequently, the divergence in SOC tendency between the cells has constantly been heightened, leading to approximately 10 % of SOC imbalance between the cells in the string at the EOC and 20 % at the EOD. The SOC range of cell #2 having always been greater than that of cell #1 and #3, and the capacity withdrawn from a pack in series configuration being the same in all cells in the string, the cell capacity ratios show different evolutions as well, Figure 39. After 200 cycles, cell #1 and #2 have lost approximately 9 % of their active materials content whereas cell #3 has lost more than twice as much of involved active materials with a decrease of its capacity ratio greater than 20 %. Besides the rapid drop of capacity ratio in the ten first cycles of the cell #2, the evolutions are constant with $-4.5 \text{ mAh.}\% \text{SOC}^{-1}$ per 100 cycles for cell #1 and #3, and $-10 \text{ mAh.}\% \text{SOC}^{-1}$ per 100 cycles for cell #2.

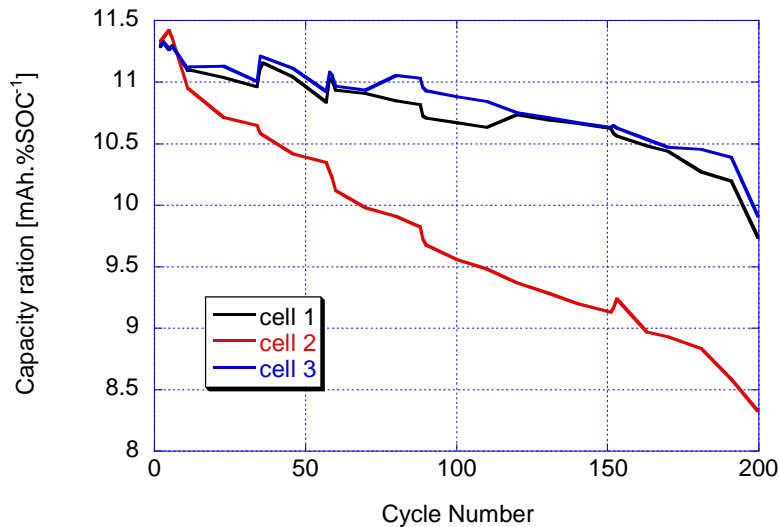


Figure 39 Capacity ratio evolution per cell in IMR pack with temperature gradient.

In order to decipher how the active materials (i.e. either primary or secondary) were affected at a faster rate at 60°C than at 25°C, incremental capacity (IC) analysis must be performed. Figure 40 displays the C/25-rate IC curves in discharge of each cell at each RPT during cycle aging. Since the cell #1 and #3 were both experiencing under-discharge from cycle 87, their IC curves show an early cutoff around 3.8 V, making the comparison of the last IC peaks pointless. Nevertheless, high voltage areas present a diverse evolution for the cell #2 at 60°C compared with the ones at 25°C. As a matter of fact, the first peak at 4.05 V has reduced for cell #1 and #3 and has totally disappeared for cell #2. This reduction is a direct indicator of loss of lithium inventory where the graphite electrode would get less

and less charged with Li^+ ions and would switch from the first to the second phase transformation on the negative electrode sooner than initially, which confirms the assumption made from the pack Peukert curves.

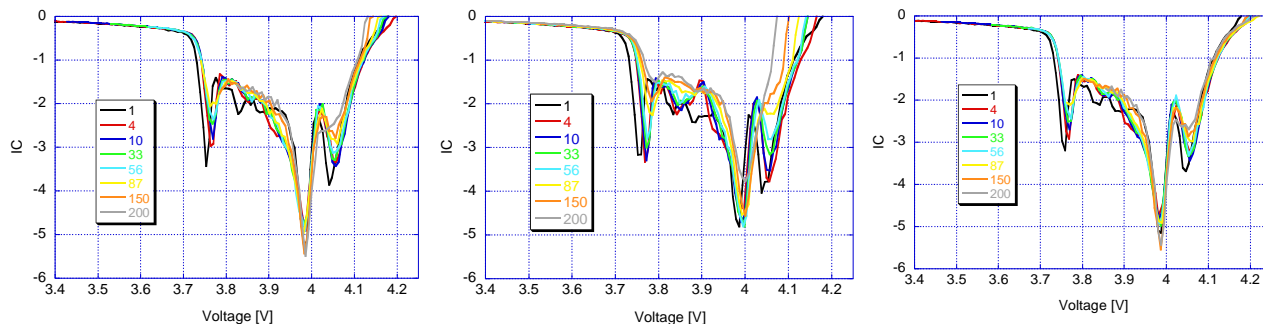


Figure 40 IC curves at C/25-rate in discharge for (a) cell #1, (b) cell #2, and (c) cell #3.

As a result of such a phenomenon the second IC peak, around 3.98 V is usually subjected to a slight increase, which is observed for the two cells at 25°C. For the cell #2 at 60°C, this peak raise was noticed initially but rapidly disappeared to lead to a fast decrease in intensity which could be explained by a much quicker loss of lithium at high temperature than it does at room temperature on one hand, and a loss of active material on the other hands. The evolution of the first and second peaks for each cell are represented on Figure 41(a) and Figure 41(b) respectively.

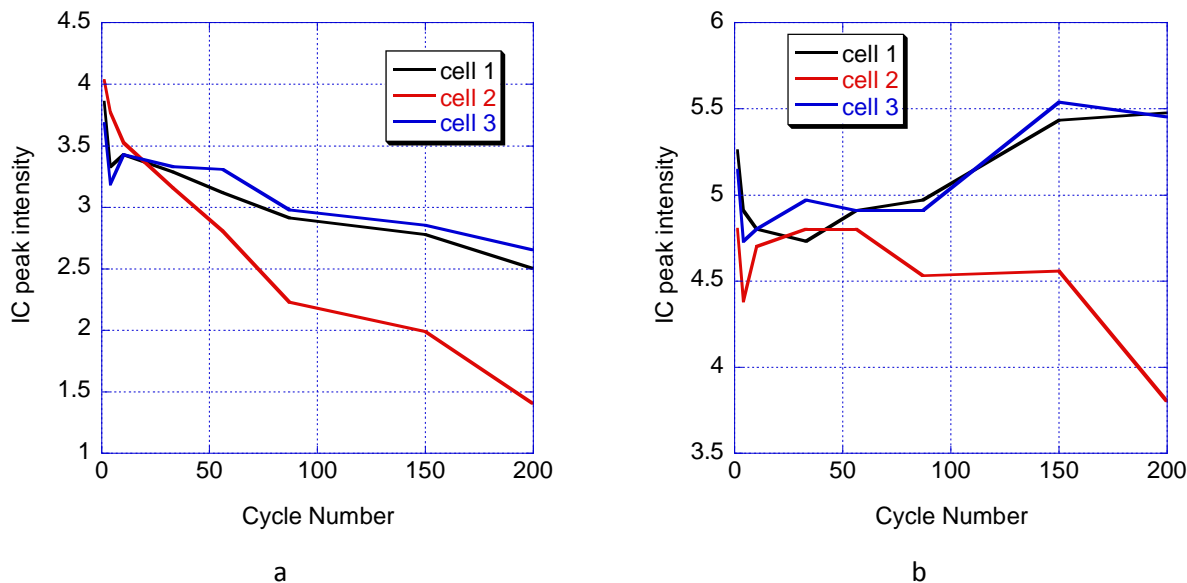


Figure 41 Evolution of IC peak intensity for (a) peak #1, and (b) peak #2

The loss of active material can be either on the positive electrode or on the negative one (or both at the same time). A good way to decipher whether the negative graphitic electrode has been

affected or not is to look at the first peak of the IC curves in charge. The reason why the last peak in discharge is not used for that specific matter is because other electrochemical reactions are included in it in discharge making a broader peak more difficult to interpret. In charge, the latter is much sharper, thus giving a much better understanding of the state of the graphite. Figure 42 shows the IC curves in charge at C/25-rate for the cell cycling at 60°C and confirms that the first peak in charge at 3.8 V has drastically decreased during cycle aging.

Some active material has most likely been lost on the positive electrode as well. However, due to the shape of the spinel electrode signature, it is very difficult to draw exact conclusions on its state from our measurements. The main thing that can be said is that the loss of spinel active material is not the major factor of capacity fade in this case. Otherwise the capacity would have declined very quickly. Loss of lithium inventory and loss of graphitic active material are thus the most coherent explanations.

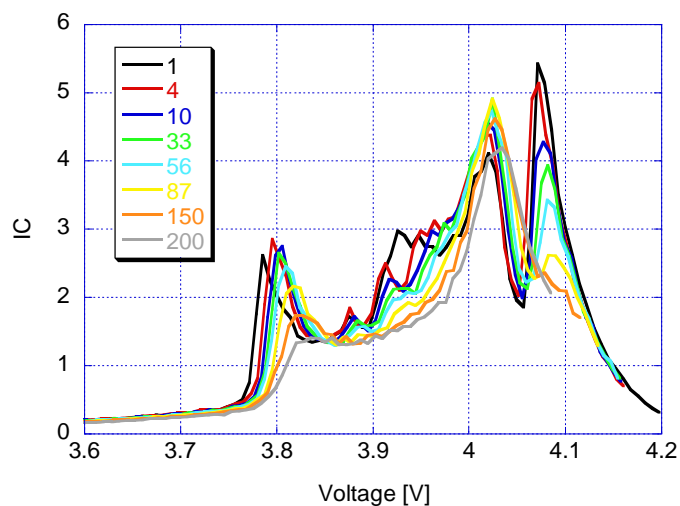


Figure 42 IC curves at C/25-rate in charge for (a) cell#1, (b) cell #2, and (c) cell #3.

The capacity evolution, as well as the capacity ration highlighted a rapid drop when the temperature was setup to 60°C from cycle # 4 to cycle #10. Therefore, it seemed worth to take a closer look at each C/25-rate cell's IC curve at these cycles in order to quantify and confirm the rapid loss of lithium inventory due to high temperature. Results speak for themselves, as they are presented on Figure 43. The two cells at room temperature do not emphasize any particular evolution for the two IC peaks at 4.05 V and 3.98 V. However, the process of loss of lithium inventory clearly shows up for the cell #2 at 60°C since the first peak is being decreased while the other one gets in intensity, which reinforce our first assumption on the primary active material loss at high temperature.

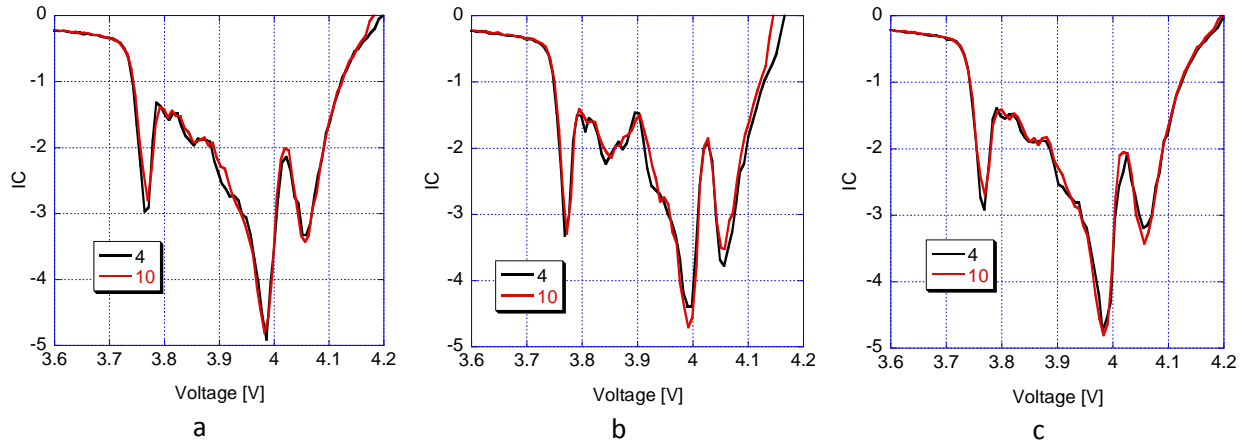


Figure 43 Comparison of IC curves at C/25-rate in discharge on cycle #4 and #10 for (a) cell #1, (b) cell #2, and (c) cell #3.

At this point, it can be claimed for certain that the pack degraded because of the cell that was cycling at a higher temperature which was subjected to a much faster rate of loss of lithium inventory as well as an accelerated degradation of the graphitic negative electrode. Figure 44 represents the evolution of the cell ps-OCV=f(SOC) curves during cycle aging for the cells #1 and #3 on one hand, and the cell #2 on the other hand. Even if the two cells at 25 °C were experiencing under-discharge, their ps-OCV curves do not seem to go through drastic changes and, for example, the plateau at 3.75 V is always noticeable whereas it totally disappeared for the cell at 60°C.

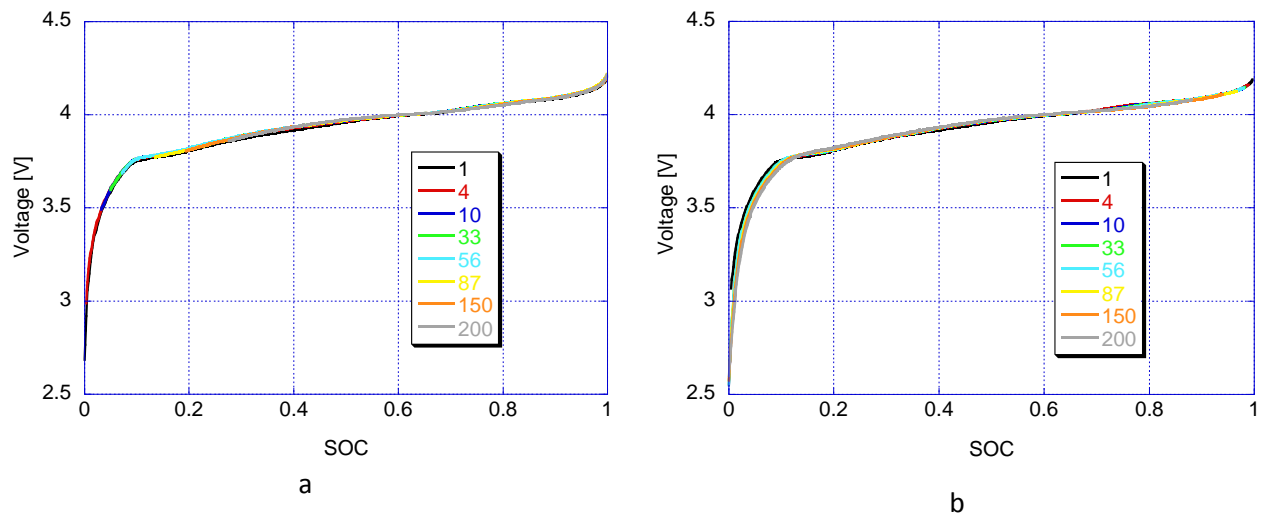


Figure 44 Evolution of cell ps-OCV=f(SOC) curves for (a) cell #1 and #3, and (b) cell #2.

From the capacity ration evolutions per cell, it also appears that the cell #2 degraded twice as fast than cells #1 and #3. The quicker degradation of the cell at higher temperature implies a different evolution of the cell ps-OCV=f(SOC) curves. Therefore we also found interesting to compare the ps-OCV=f(SOC) curves at equivalent stages of capacity ration loss: cell #2 has a capacity ration of 10.5

mAh.%SOC⁻¹ after approximately 40 cycles, while #1 and #3 reach this value after 150 cycles. Figure 45(a) displays this comparison and the curves appear very similar whereas a non-negligible contrast is noticed on Figure 45(b) where ps-OCV=f(SOC) curves of all the cells at the same cycle are represented. This confirms that cell #1 and #3, cycling at 25°C, needed three times as much cycle to reach the same stage of degradation than that of cell #2.

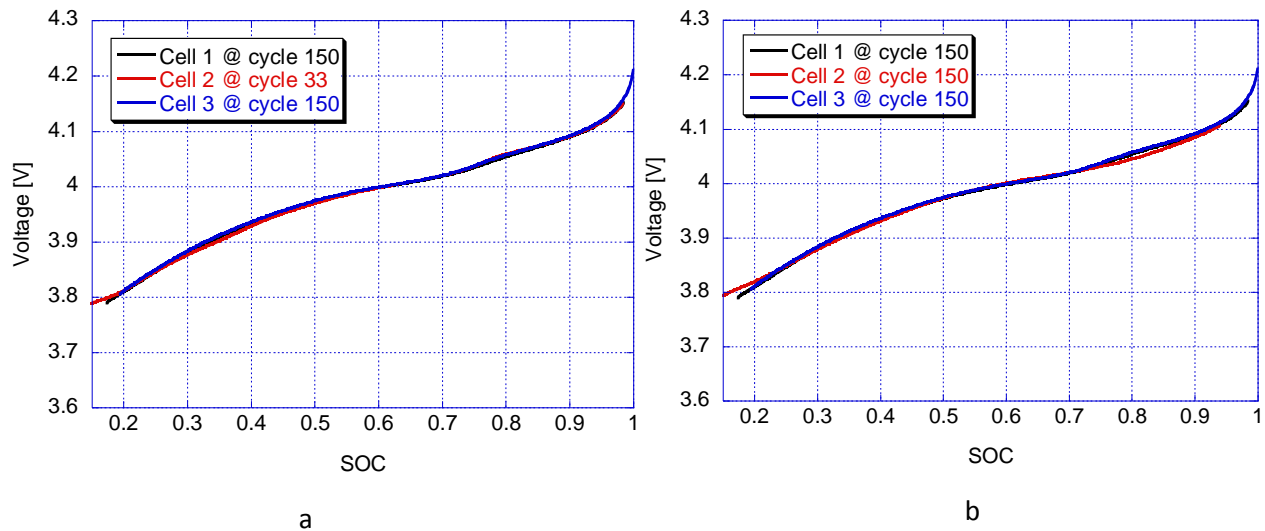


Figure 45 Comparison of ps-(OCV)=f(SOC) curves according to cell capacity rations evolution

The polarization resistances have not been considered in this analysis because the early under-discharge and under-charge phenomena due to the temperature imbalance led to SOC imbalance in the cells that made their calculation tricky.

5.3.1.4 Conclusion

Three spinel-based Li-ion cells with negligible variability on their intrinsic attributes have been placed into a string configuration and subjected to high current cycle aging. The spinel material being known to have poor performances at high temperature, one of the cells was put into an incubator at 60°C while the two others were at room temperature. As expected, the cell that was cycling at elevated temperature was found to be the limiting cell during cycle aging and was thus at the origin of the weaker pack performance (when compared to a single cell) and its fading. However, contrary to what is said in the literature about the degradation of the spinel material at high temperature it was found that it was not the main factor of the capacity decline. As a matter of fact, the higher capacity fade for the cell cycled at elevated temperature was explained to be due to a loss of lithium inventory that occurs at a faster rate than it is observed at 25°C as well as loss of graphite. These degradation mechanisms had

been reported by Ramadass^{46-48,50} and explicated by a repeated film formation over the surface of the anode during cycle aging which results in increase rate of lithium loss and creates a large reduction in the use of the negative electrode active material.

5.3.2 Ageing of commercial Graphite/composite [NMC+spinel] Li-ion cell in a string configuration with initial capacity variability and initial SOC imbalance

After the conditioning process, differences of capacity among cells of a same batch were pointed out and deserve attention when cells are put in a pack configuration. As a matter of fact, when used in a string configuration, the capacity of each cell will be the same during cycling since the same current is flowing through all of them. Therefore a cell with a lower capacity would be expected to become the limiting factor of the string by reaching the cutoff voltages earlier than the others, if it was originally charged to the same SOC as the others. In other words, the non-limiting cells would not use their full capacity and energy would just be wasted. In addition, as a side effect, the voltage ranges, and thus the SOC ranges, of each cell during cycling would follow a different evolution and lead to an increase of the imbalance among the cells in the string. That is the reason why, in an ideal case, all cells have to deliver the same capacity so the performance of the pack can be optimal. For highlighting this phenomenon on a 3-cell pack in a string configuration, the cell choice was made in order to have the greatest imbalance in term of maximum initial capacity. For this purpose, the discharge capacities at C/5, obtained in the conditioning cycles, were compared. Attention was paid to the resistance values, so there is almost no imbalance due to the polarization, Table 6

Polarization resistance (discharge)	Cell 1: 56.4 mΩ Cell 2: 56 mΩ Cell 3: 53.2 mΩ
Q_5	Cell 1: 1.9033 Ah Cell 2: 2.0048 Ah Cell 3: 1.9433 Ah
Q_R	Cell 1: 20.1 mAh/%SOC Cell 2: 21.0 mAh/%SOC Cell 3: 20.6 mAh/%SOC
SOC _{initial} when put in the pack	Cell 1 = 99.2% Cell 2 = Cell 3 = 96.6%

Table 6 INL cell selection for pack configuration (based on maximum capacity)

Cells are generally set to the same SOC before being placed in pack configurations, and this is usually performed on a voltage basis, i.e. the charging process is interrupted when the desired voltage is reached. Because of slight voltage measurement disparities on tester channels due to calibration issues, SOC imbalances with involuntary origin could be included and accelerate pack failures. To illustrate this phenomenon, one cell was a little more charged than the others when they were initially placed in the string. As a result, an extra imbalance on the initial SOC was added to the pack. One could think this is a very bothersome for drawing conclusions; however, it is relevant to the battery manufacturers that are doing cell selection for pack applications since they use the same testers and methods to compare their cells. The anticipated effects of such an imbalance should emphasize the ones of the capacity imbalance, which means: voltage and SOC ranges disparities during cycling.

5.3.2.1 Experimental

Three 1.9 Ah 18650 cells with [NMC+spinel] composite positive electrode from a 32-cell batch provided by INL were put in a string configuration. The string was then subsequently subjected to cycling at a 2C-rate in discharge regime while recharging with the protocol typically recommended by the manufacturer with a CC step at C/2 followed by a CV step at 12.6V (4.2*3) with C/25 cutoff at room temperature. Same tester and same facility as aging test previously described were used. 6-h rest period was allowed every 10 cycles to reduce test duration. RPTs were performed upon every 10 % of capacity loss with charge-discharge cycles at C/25 and C/2 respectively, a remnant capacity measurement after the C/2 discharge has been added. Auxiliary voltage channels with extra safety cutoff conditions have been included for safety reason. Also a 0.47 Ω 5 W resistor was placed in series in the circuit in order to monitor the current flowing through the pack. Before being included in the pack, each cell was charged separately on an Arbin HVBT 5560[®] system following a CC-CV manufacturer process.

5.3.2.2 Results

Figure 46(a) presents the evolution of capacity changes over the 2C-rate cycle aging regime (in circles) along with those determined in the RPTs by C/25 and C/2-rate discharges (squares and triangles respectively). The pack capacity decreases steadily up to about 650 cycles, and the rate capability remains intact. Beyond 650 cycles, the capacity loss accelerates and the rate capability worsens. During the first stage, the cell loses 0.6 mAh per cycle, which represent 3 % per 100 cycles. In the second stage of cycle aging, rate capability worsens and the fading accelerates (from -1 mAh to -3.7 mAh). Since the nominal capacity at C/2 is 1.90 Ah, the EOL is reached when the capacity falls below 1.52 Ah; thus the pack reaches its EOL after 715 cycles of aging.

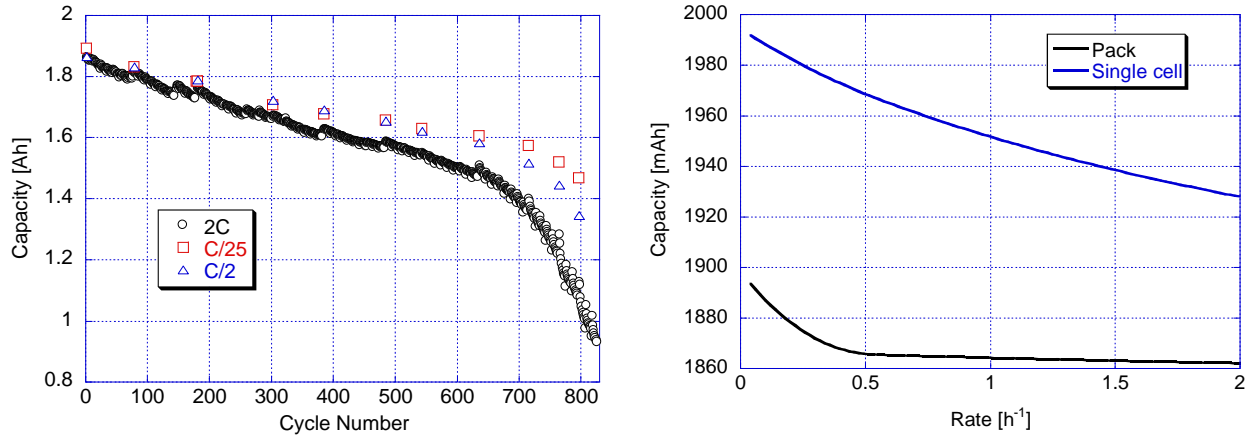


Figure 46 (a)Capacity variations as a function of cycle number measured during cycle aging and from reference performance tests using different C/n rates; (b) Peukert curves of single cell and pack

The fading phenomenon resembles the one observed on a single cell subjected to the same cycle aging¹³, Figure 47. The single cell failed earlier than the pack, after 500 cycles only. However we should note that the pack was subjected to lower C-rate discharges during its RPTs (i.e. C/25 and C/2 for the pack versus C/25, C/5, C/2, 1 C, 2C and 5C for the single cell). Furthermore, the cutoff voltages were also different: as the pack was cycling between 7.8-12.6 V during its RPTs, which is basically equivalent to 2.6-4.2 V per cell, the single cell RPTs used a charging protocol up to 4.25V. These higher rates as well as higher voltages may have caused irreversible damages to the single cell, which explain why it is failing 150 cycles earlier. Regarding the pack performance, as it was noticed during the previous degradation study on the Peukert curve, capacities are lower for the pack than they are for the single cell, Figure 46(b), which means that they are limited by the cell variability.

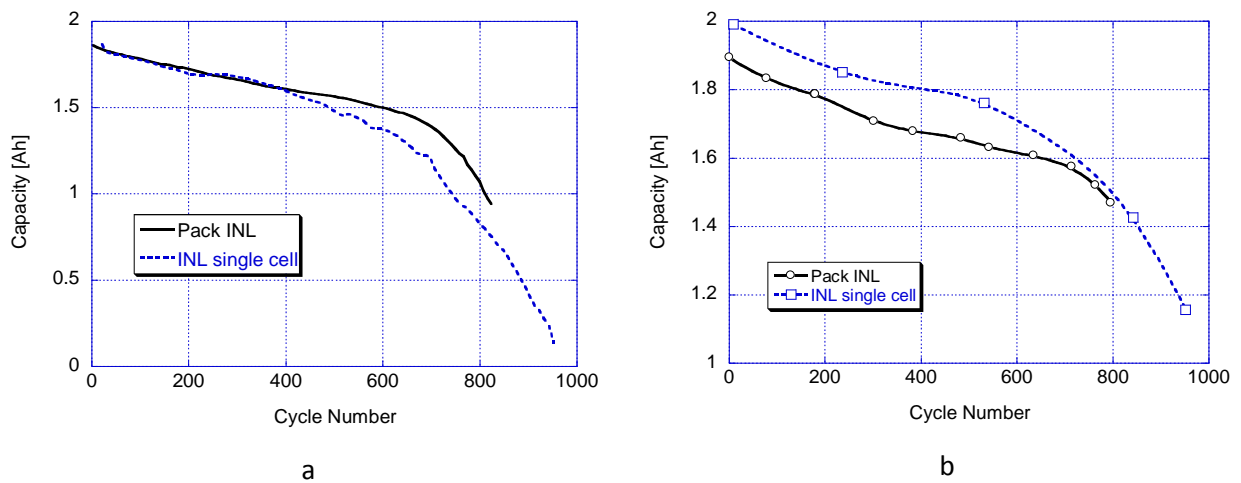


Figure 47 Capacity variation comparison between pack and single cell at (a) 2C, and (b) C/25

Figure 48(a) displays the evolution of the RPVs at the EOC and EOD for several rates over the cycle aging for the pack and the single cell. Again, results are similar and show same trends. The EOD RPVs and RCVs remain relatively stable for the first 650 cycles and they are rate dependent; after 650 cycles they begin to increase at considerable paces. The EOC RPVs and RCVs are constant for 650 cycles and start to decrease very slowly after that. These variations with rate and cycle number indicate that the states of the cells and their electrodes at the EOC and EOD are varying in a complex manner through cycle aging and need to be investigated further.

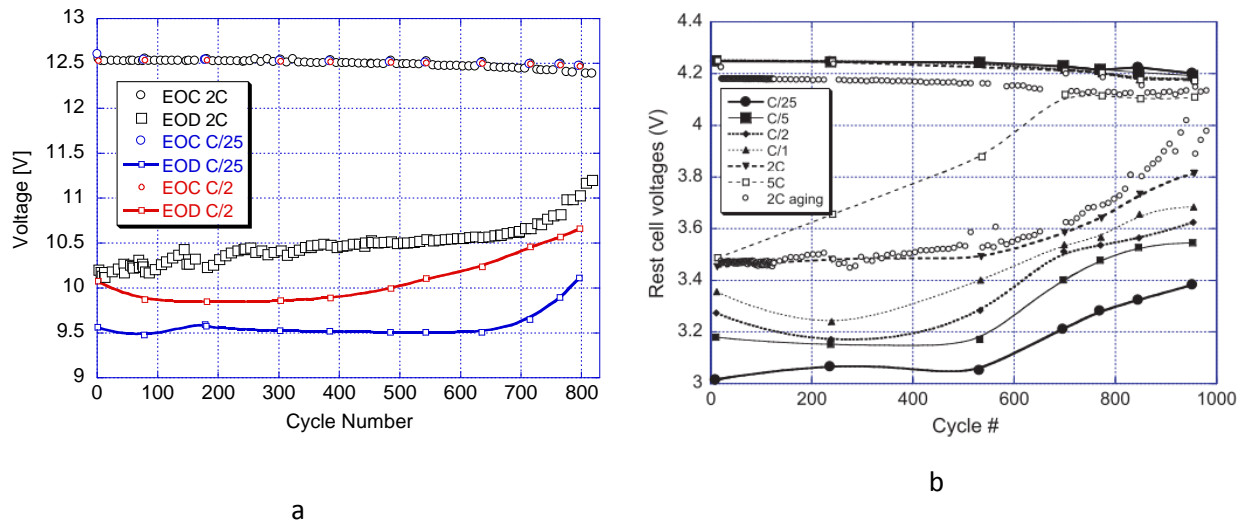


Figure 48 (a) Rest pack voltages (RPVs) versus cycle number as measured during the cycle aging and from RPTs at the BOD and EOD; (b) Relax cell voltages (RCVs) from the single cell study

The evolution of the pack ps-OCV=f(SOC) curves over cycle aging, Figure 49(a), emphasizes that the correspondence between OCV and SOC varies by the cycle aging, especially under 60 % SOC. If the wrong ps-OCV=f(SOC) curve is used, uncertainties larger than 10 % can be estimated on the SOC inference. Therefore, it is an absolute necessity to recalculate the ps-OCV=f(SOC) curves during cycling in order to determine accurate SOC. The same evolution had been shown on the single cell, Figure 49(b).

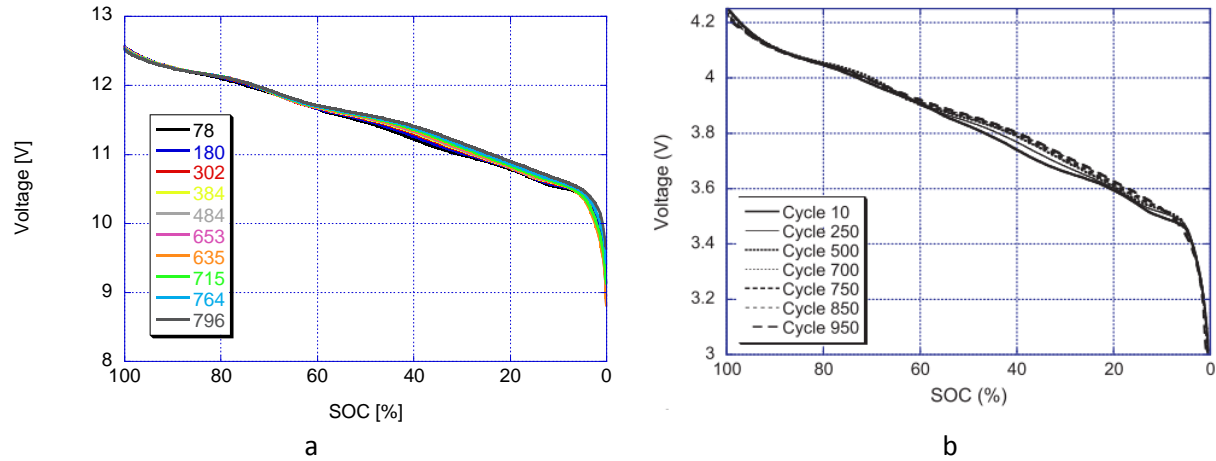


Figure 49 (a) The ps-OCV=f(SOC) curves as a function of cycle for (a) the pack and, (b) the single cell

Pack SOC_s determined from the evolving ps-OCV=f(SOC) curves calculated at each RPTs as well as the ones from the voltage average, the SOC average and the remnant capacity measurements are represented on Figure 50(a). At the EOD, all methods give the same SOC_s that are in agreement with the experimental ones (i.e. SOC_s determined from remnant capacities). However, at the EOC, the method using the pack ps-OCV=f(SOC) curves is the only one that provides SOC_s that are close to 100 %, all the other ones being approximately 5 % lower. Since the charging process was always performed following the manufacturer protocol with a CC-CV step and a 75 mA cutoff, the pack SOC at the EOC should be very close to 100 %. As a matter of fact, the CV step is equivalent to a CC step with very low C-rate in charge. Therefore, it can be claimed that the method using the pack ps-OCV=f(SOC) curves is the most accurate for pack SOC determination, as it was also already pointed out in the previous study. Consequently, only this method will be considered in the discussion. As for the EOD and EOC SOC evolutions during cycle aging, the EOD one increases slowly and steadily from 2% to 10% during approximately 650 cycles, and then starts to increase drastically to more than 30%; on the other hands, the EOC one is relatively constant. Figure 50(b) presents a comparison of the evolution of the capacity ration upon cycle aging based on the Δ SOC as inferred by the RPTs and RCVs from the evolving ps-OCV=f(SOC) curves and the capacity measured at each cycle for the pack and the single cell respectively. The pack capacity ration varies from 19 mAh%SOC⁻¹ at the beginning of life to 15 mAh%SOC⁻¹ after 800 cycles which represent a 21% decrease in the amount of materials involved in the cell reactions upon cycle aging. After 800 cycles the single cell capacity ration decreased of approximately 35 %. However, like explained already, differences in RPT procedures may have caused additional damages to the cell. In both cases the decrease follows the same trend with the capacity loss; thus, it is linear at first, and then it accelerates.

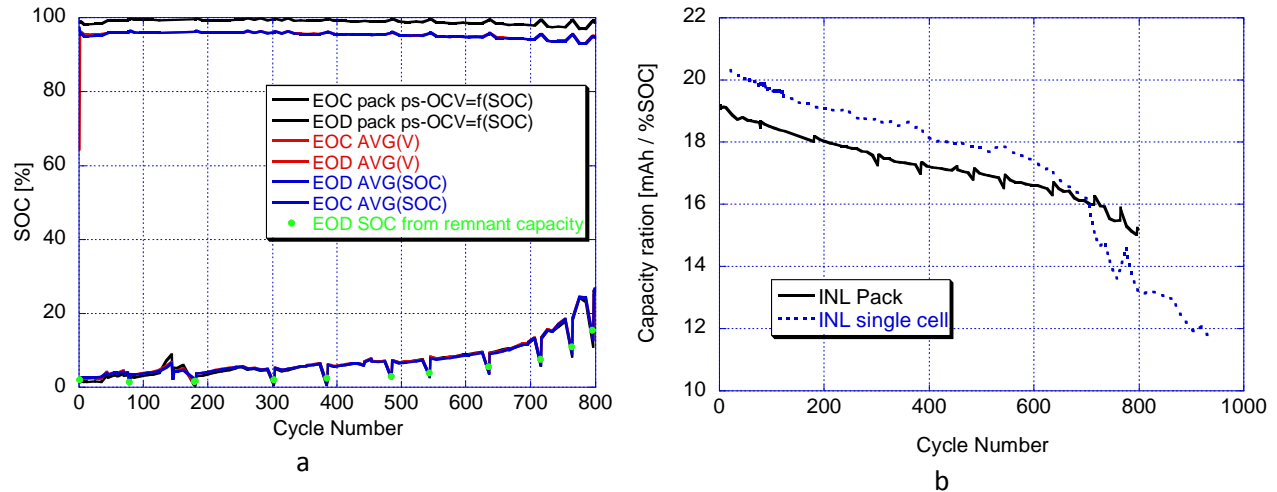


Figure 50 (a) Pack SOC evolution from floating pack ps-OCV=f(SOC) curves. (b) Comparison of capacity ration evolution between pack and single cell

5.3.2.3 Discussion

In order to pinpoint the causes of aging of the pack, the three cells placed in the string will now be studied separately by combining the differential capacity analysis and SOC tracking of the cells over cycle aging. Figure 51(a) presents the RCVs of each cell in the pack versus cycle number as measured during the cycle aging at the EOC and EOD. The first noticeable imbalance in the BOL is the higher voltage for the cell #1 at the EOC. As mentioned previously, this is easily explained by the fact that this specific cell was a little more charged than the others when it was placed in the string. Therefore its voltage range during cycling differed from the others and reached higher values at the EOC. What is interesting to point out is the tendency to equilibrate with the two other cells upon cycles. After 400 cycles, all cells in the string seemed to reach the same voltage after relaxation at the EOC. Regarding cell #2 and #3, they were always very similar and stable at the EOC. At the EOD, more variations are observed in the first 300 cycles. They are most likely due to the capacity disparity among the cells. However, like for the EOC, the RCVs of each cell converge towards the same value and then follow the exact same trend from cycle 350 to cycle 830. In Figure 51(b), all these RCV values are converted to SOCs by using the evolving ps-OCV=f(SOC) curves of each cell. In the beginning of life of the pack, the initial SOC imbalance is easily visible with 3% more on the cell #1 at the EOC. Like on the RCVs, SOCs of each cell tend to converge to identical values at the EOD as well as the EOC until 650 cycles approximately. Then a new imbalance is rising: cell #2, which initially had the greatest capacity, reaches lowest SOCs in charge and in discharge. Because the RCVs of each cell at the EOC and EOD after 300 cycles are very

similar, it explains why the pack-SOCs determined from the three different methods in Figure 50 are almost identical.

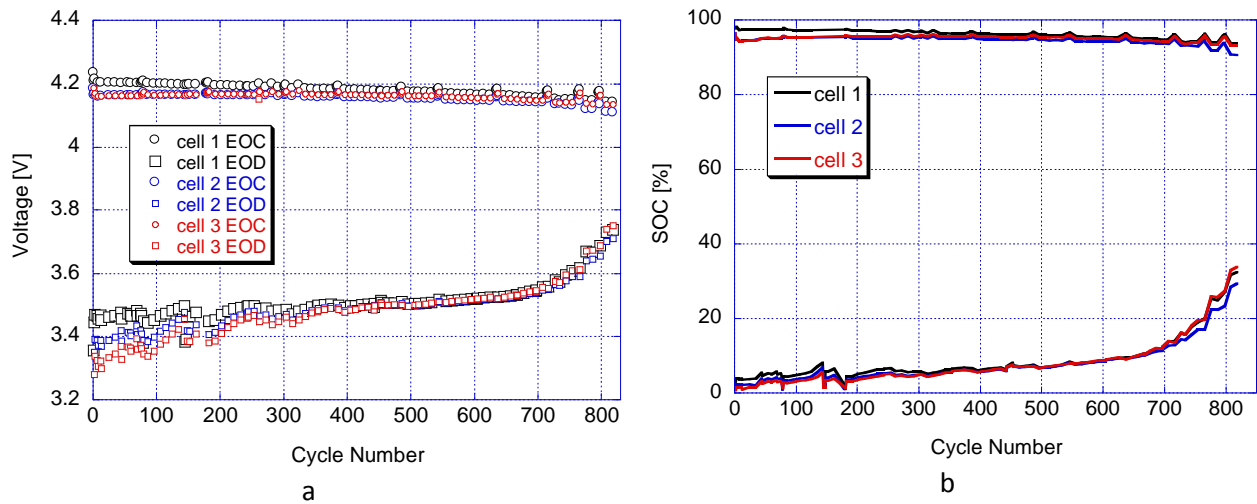


Figure 51 (a) RCVs of each cell in the pack versus cycle number as measured during the cycle aging at the beginning- and end-of-discharge. (b) Evolution of the end-of-charge and end-of-discharge SOC of each cell determined during cycle aging.

Figure 52(a) and (b) display a closer look at the EOC and EOD SOC. At the EOC, cell #2 always showed the lowest SOC and seemed to diverge from the two others during cycle aging. On the other hand, cell #1 that started with a higher SOC converged slowly to the cell #2. At the EOD, similar evolution is noted: cell #1 slowly tends to equilibrate with #3, while #2 starts diverging after 650 cycles. As we can judge, at the EOL, cell#1 is charged to only 91% SOC while cells #2 and #3 are almost at 94%. In discharge, cell #1 barely reaches 29% while #2 and #3 are above 34% of SOC.

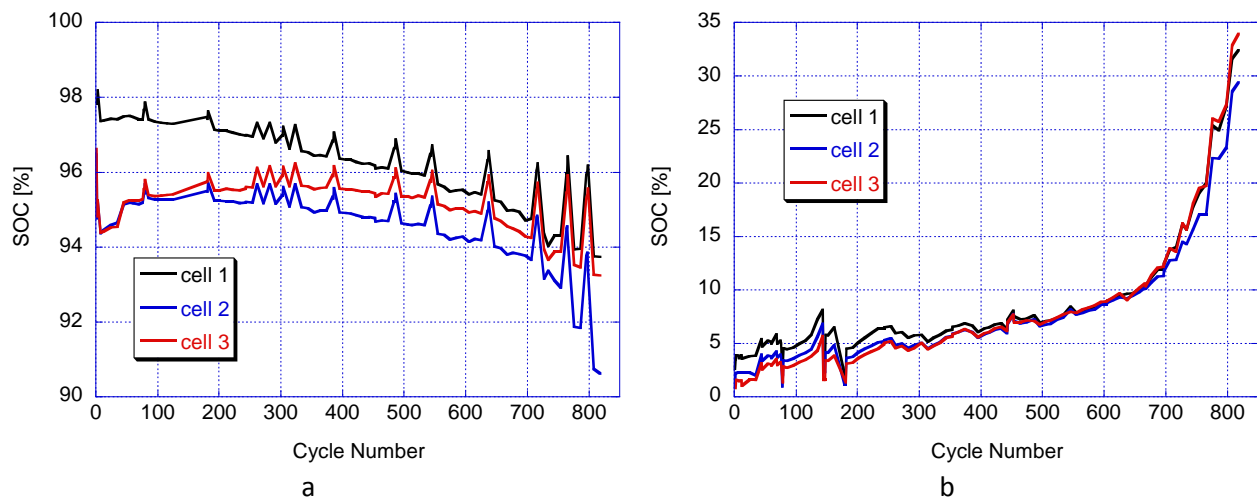


Figure 52 (a) End-of-charge SOC for each cell in the pack determined from the evolving ps-OCV=f(SOC) curves of each cell. (b) End-of-discharge SOC for each cell in the pack determined from the evolving ps-OCV=f(SOC) curves of each cell.

These differences in Δ SOC lead to variability among capacity rations since the capacity withdrawn is the same for each cell in the string. Therefore it can be claimed that active material is lost at different rate among the cells in the pack. As a matter of fact, after 420 cycles the capacity ration of cell #2 (blue curve), which was the highest since the beginning of life, quickly drops below the two others, showing a critical decline in the content of active material for cell #2, Figure 53.

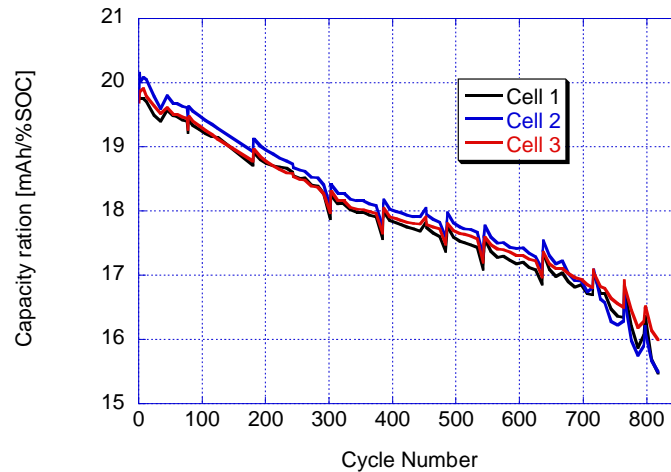


Figure 53 Evolution of capacity ration for each cell in the string calculated from the Δ SOCs given by the evolving ps-OCV=f(SOC) curves.

Since the voltages at the terminals of each cell in the pack were recorded, the IC curves of each cell can be analyzed. The C/25-rate discharges of each RPT for each cell are displayed on Figure 54. The unique features of the IC curve of this composite positive electrode as well as the degradation mechanisms of this kind of cell has already been discussed in the literature^{13,30}. The results of the study showed that the degradation occurred in two stages: a first one mainly related to loss of lithium inventory (from parasitic reaction to form SEI layer on the electrode surfaces²⁵), and a second one induced by loss of active materials in both electrodes^{2,13,32,41}. The cells in the pack seem to follow the same degradation. In fact, when comparing the IC curves of the cells that were aged in the pack to the single cell ones, the evolution of the peaks during cycle aging is the same. Unfortunately, from the C/25-rate discharge IC curves, no noticeable difference is observed between the 3 cells in the string. However, it is clear at this point that the cell #2 experienced a quicker degradation than that of the two other ones. Even though some peaks are showing lower intensities, on the last graphite peak for example, there is no obvious sign of fading before the cycle number 650 where this specific cell already started to degrade critically. One thing that can be noticed is the EOD cutoff voltage evolution: the IC curves of cell

#1 and #3 do not reach 0 Ah.V⁻¹ anymore after the cycle number 715, whereas cell #2 seems to completely finish its electrochemical reactions before reaching the cutoff condition.

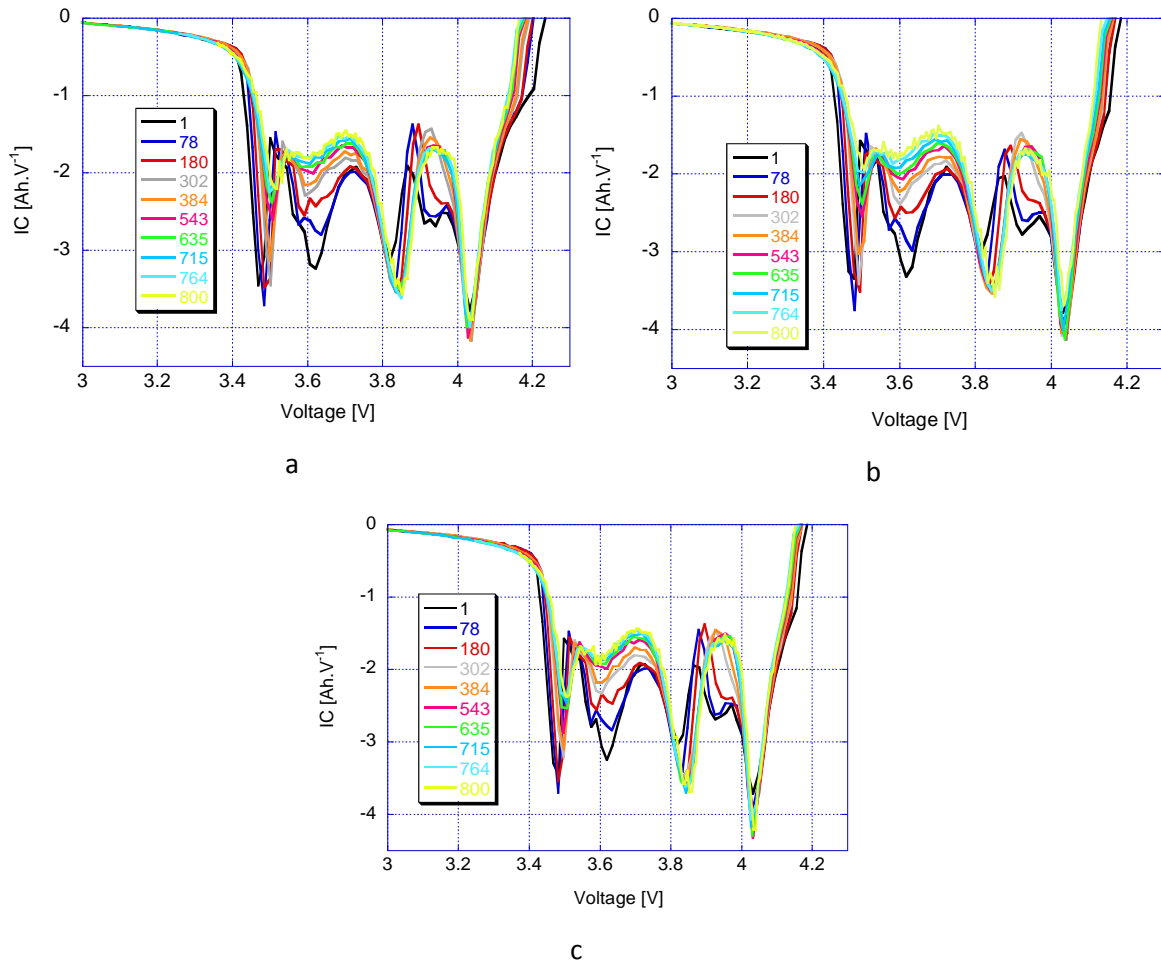


Figure 54 IC curves at C/25-rate for (a) cell #1, (b) cell #2, and (c) cell #3

Figure 55(a) presents the EOD voltages before relaxation for each cell during cycle aging. The first thing noticeable is that cell #2 reaches the safety cutoff ending the discharge steps earlier than expected after 759 cycles. The cutoff condition in discharge was supposed to stop the discharge when the string voltage reached 7.8 V (approximately 2.6 V per cell). Furthermore, a safety setting was imposed in order to avoid over-discharge. During the first 760 cycles the pack was discharged until the regular cutoff voltage. However, the fact that the cell #2 attains the safety limit earlier than the other cells changed the conditions and cell #1 and #3 became less and less discharged. Thus the pack voltage at the end of discharge increased from 7.8 V at cycle 760 to 8.4 V at cycle 840. What is interesting to notice is how stable used to be this cell during the 600 first cycles and how it started to reach lower and lower voltages in about 150 cycles. On the other hand, at the EOC, no cell reached the safety cutoff

voltage and the limit of 12.6 V was always achieved, Figure 55(b). Cell #2 always reached the lowest voltage until 700 cycles, most likely because of its greater initial capacity. However, the rapid drop in the discharge voltage induced an increase of its EOC voltage. Therefore, there is here another proof of the faster loss of capacity for the cell #2 compared to the others which could have been observed while monitoring the cell voltages.

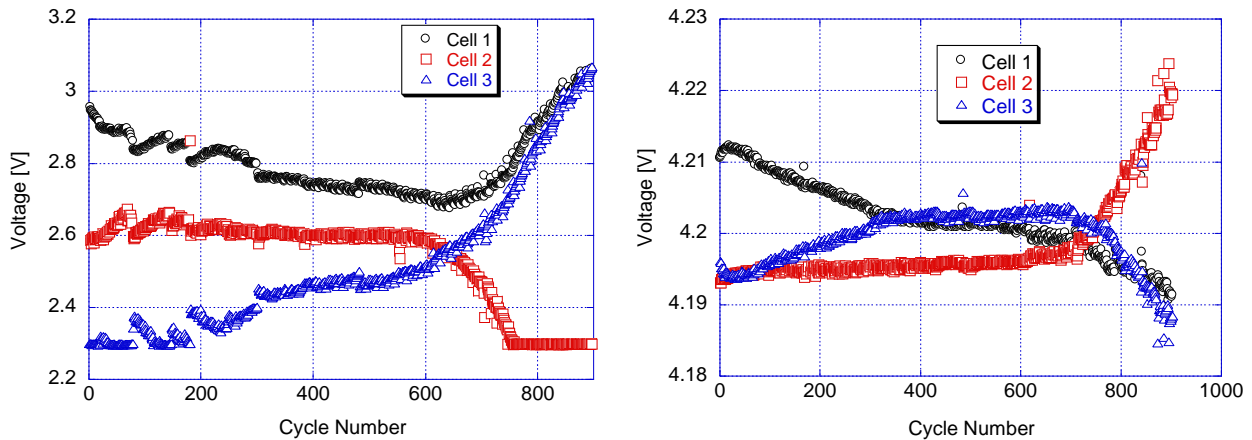


Figure 55 (a) EOD voltage before relaxation. (b) EOC voltage before CV step.

One of our first assumptions on the reasons for which cell #2 reached lower and lower voltages until the safety limit, was the increase of polarization resistance in discharge. Figure 56(a) displays the evolution of this polarization resistance calculated from the IR drop at C/25, C/2 and 2C-rates. Unfortunately, even though there is a clear increase of resistance for all the cells in discharge, cell #2 does not even present the greatest one and evolve linearly like the two other ones during cycle aging. The polarization resistance in charge has also been calculated and is shown on Figure 56 (b). In this case, cell #2 seems to increase more than the others, but no drastic change in its evolution would foresee or explain the causes of the rapid failure of cell #2. In charge and discharge, the augmentation of the polarization resistances is the same for all cells since all the rates are identical (i.e. lines are parallel).

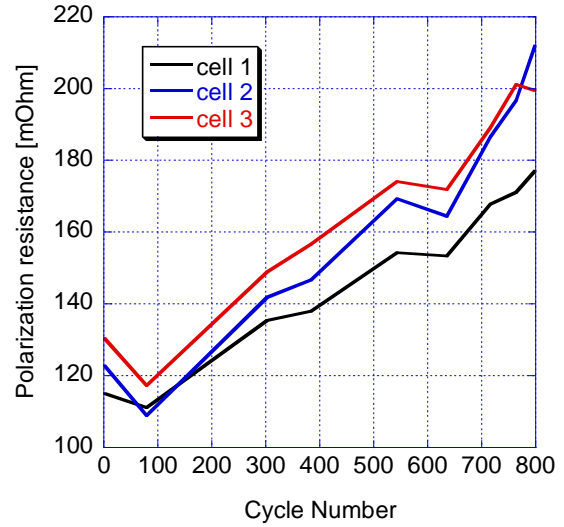
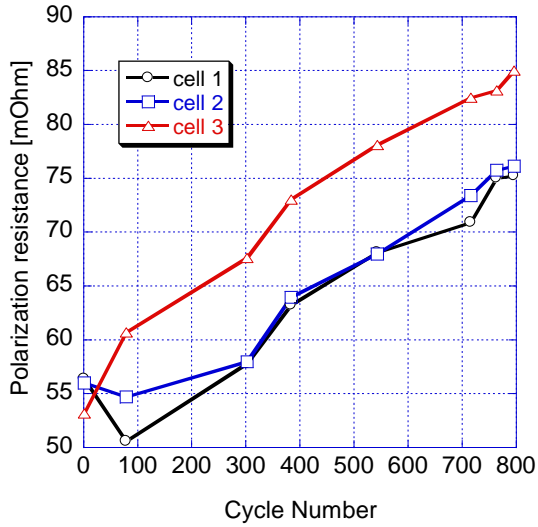
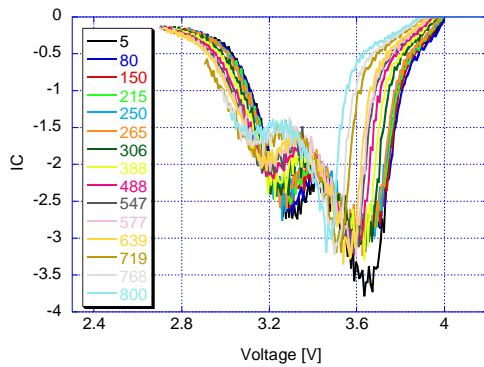
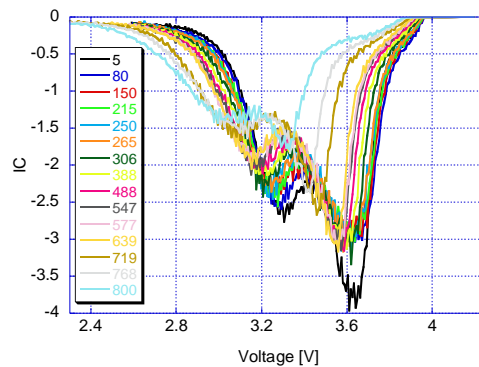


Figure 56 (a) Polarization resistance in discharge. (b) Polarization resistance in charge.

While investigating on how the cell #2 degraded earlier than cell #1 and #3, attention was paid to the IC curves of the 2C-rate discharges of the cycle aging. Figure 57 shows the evolution of these IC curves for each cell separately. As it can be seen on those curves and from the calculations made above, the voltage drop used for the polarization resistance is the same and evolve similarly for all cells. However, the big IC peak originally observed at 3.6 V has shifted to 3.3 V for the cell #2, whereas it moved only towards 3.5 V for cell #1 and #3. Therefore a new resistance value was calculated using the voltage drop of this exact same peak between the C/25 and 2C-rates for its computation. This resistance could not be noticed on the C/25-rate discharges because resistance effect are negligible and cannot be seen with such a low current (even C/2-rate discharge did not show a clear deviation of this peak). The results are plotted on Figure 58(a). Cell #1 and #3 are both increasing linearly but cell #2 present a rapid intensification after the cycle number 635.



a



b

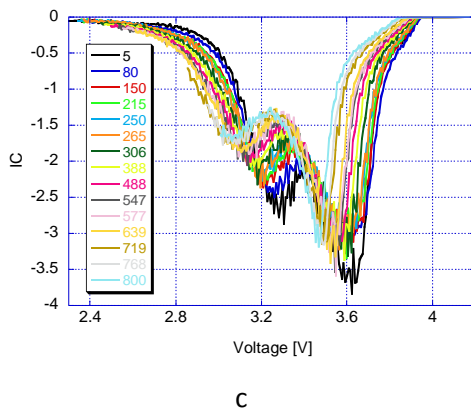


Figure 57 IC curves at C/2-rate for (a) cell #1, (b) cell #2, and (c) cell #3

From the literature¹³, it has been investigated that the first electrochemical reaction that takes place in this kind of cell chemistry is the solid solution on the NMC material. Therefore, it has been concluded that the first polarization resistance calculated from the voltage drop in discharge corresponds to the resistance of the NMC material. On the other hands, the peak which has been taken into account for the second resistance is purely related to the phase transformations occurring in the spinel material. Thus it has been associated to the resistance of the spinel material. The positive electrode being made out of two different materials, two resistances can be deciphered, one related to each material. Consequently, they will follow different evolution during cycle aging because of differences in degradation mechanisms and rates for the two materials.

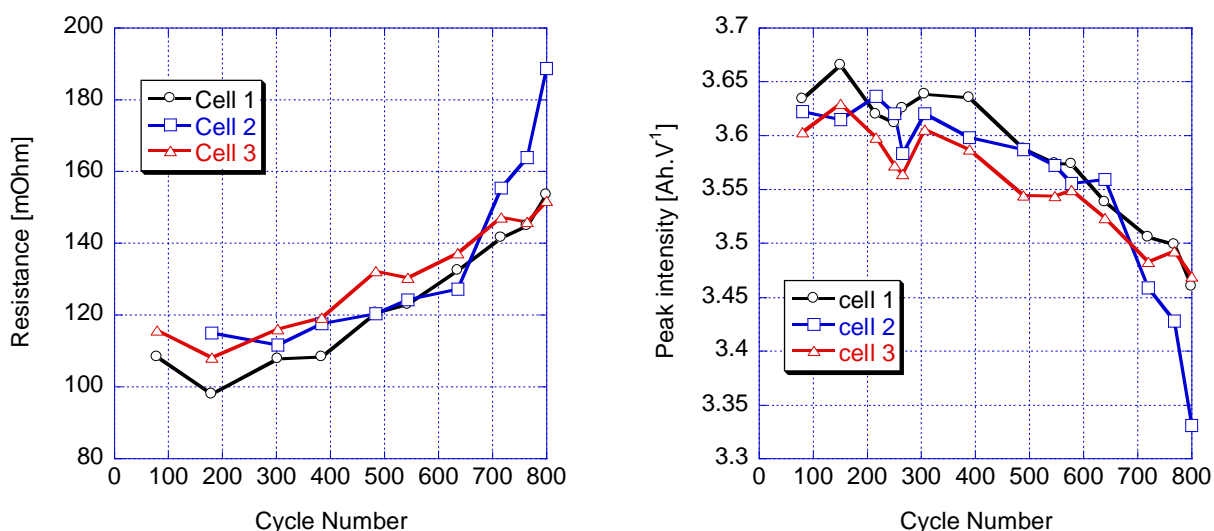


Figure 58 (a) Spinel Resistance. (b) Spinel peak intensity evolution.

Finally, the intensity of the IC peak associated to the spinel material has been examined, Figure 58(b). All the three cells follow the same decrease in peak intensity until the cell #2 starts to drop

drastically after 630 cycles, which emphasizes that this cell is degrading by losing active material (mostly spinel material in this case).

5.3.2.4 Conclusion

Three cells showing variability on their maximum capacity and on their initial SOC (added on a voluntary basis) have been placed into a string configuration and subjected to a 2C-rate cycle aging. The pack performance was affected by the cell imbalance; however, it was found that the initial disparities included in this string did not seem to be at the origin of the pack capacity fading. As a matter of fact, cell #2, which had the greatest capacity and would have been expected to be the strongest link in this string, was the first one to fail. After investigating the IC curves at different rate, the capacity ration evolution as well as the SOC and voltages before relaxation on the cells separately, it has been proved that its quicker degradation was mostly related to the spinel material of the composite positive electrode. This material was subjected to an increase of resistance as well as a higher loss percentage than that of the NMC material, which increased the local rate on the electrode and accelerated its failure. Therefore, it explains why it could not be seen on the RCVs. In fact, all cell voltages were matching at the EOC and EOD because, at the EOC, the RCVs give information on the NMC solid solution, whereas, at the EOD, RCVs give information on the graphite.

5.3.3 Ageing of commercial Graphite/NMC Li-ion cell in a string configuration with imbalance on polarization resistance

The aim of this test is to observe and understand the evolution of a 3-cell string, with imbalance on polarization resistance, subjected to cycle aging. When placed in a string configuration, cells with high resistance are expected to reach cutoff voltages sooner than cells with low resistance, resulting in an incomplete use of the capacity, and thus energy, of the other cells. Moreover, like it has been showed in the literature, the polarization resistance has a tendency to increase during cycle aging. Therefore, the imbalance within the pack would be intensified, leading to an earlier EOL for pack applications than that of single cell applications.

As noticed in the cell-to-cell variation study in chapter 3, NMC cells presented high disparities in their discharge polarization resistance, hence their selection for the purpose of this test. The three cells were chosen from their polarization resistance and capacity ration values in order to have the greatest disparity in term of resistance and the closest amount of active material (i.e. the same Q_R). Table 7 summarizes the initial conditions. The cell presenting the greatest initial polarization resistance was expected to be the limiting factor of the pack and thus the main actor of the degradation of this pack.

Polarization resistance (discharge)	Cell 1: 255.1 mΩ Cell 2: 149.7 mΩ Cell 3: 490.1 mΩ
Q ₅	Cell 1: 2.0122 Ah Cell 2: 1.9532 Ah Cell 3: 1.9871 Ah
Q _R	Cell 1: 21.7 mAh/%SOC Cell 2: 21.6 mAh/%SOC Cell 3: 21.6 mAh/%SOC

Table 7 IHR cell selection for pack configuration (based on polarization resistance)

5.3.3.1 Experimental

The three 1.95 Ah 18650 cells with NMC positive electrode from a 24-cell batch provided by Molicel® were put in a string configuration. The string was then subsequently subjected to cycling at a C/2-rate in discharge regime while recharging with the protocol recommended by the manufacturer with a CC step at C/2 followed by a CV step at 12.6V (4.2*3) with 40mA cutoff (using a Maccor 4300® system). 6-h rest period every 10 cycles were allowed and RPTs upon every 10% of capacity loss were performed. Each RPT contains charge-discharge cycles at C/25 and C/2, respectively. As for the two previous pack-aging tests, auxiliary voltage channels with extra safety cutoff conditions have been included and a 1.025 Ω 10 W resistor has been placed in series in the circuit in order to monitor the current flowing through the pack.

5.3.3.2 Results

The pack capacity evolutions at C/2 and C/25-rates are represented on Figure 59(a). Two stages in the capacity fading can be identified. The first one, from cycle #1 to cycle #420 approximately, is linear and rate independent with a loss of 3.6% per 100 cycles. The second one, after 420 cycles, shows an acceleration of the fading up to 14% at C/25 and 25% at C/2, as well as a rate capability that deteriorates. Those two fading stages are also easily observed on RPV evolution and more particularly at the EOD, Figure 59(b). Both C/2 and C/25 RPVs at the EOD show a flat and constant behavior for the first 420 cycles and a rapid increase afterward. At the EOC no particular phenomenon is detected, except a small decrease that seems to start after 400 cycles. Concerning the EOL of the pack, if the same conditions as the single cells are considered (i.e. EOL reached when the capacity equals 80 % of the initial one), it is reached after 470 cycles.

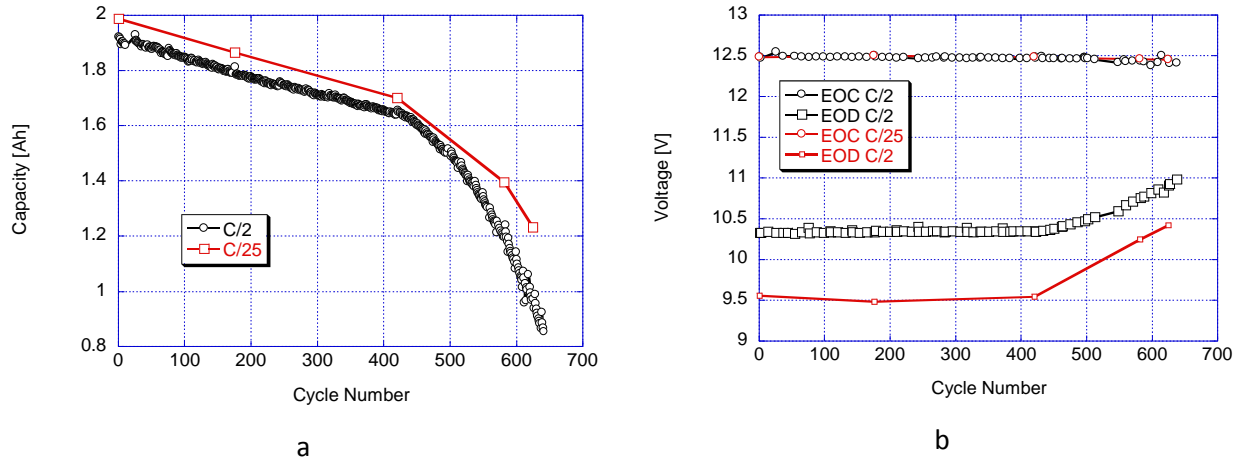


Figure 59 (a) Capacity variations as a function of cycle number measured during cycle aging and from reference performance tests using C/25-rates. (b) Rest pack voltages (RPVs) versus cycle number as measured during the cycle aging and from RPTs at the BOD and EOD.

In term of performance, the pack capacity is inferior to the single cell capacity at all C-rates, as shown by the Peukert curves in Figure 60(a). Consequently, the pack performance is limited by the cell variability. If all cells were ideal, the two curves would be superimposed. Regarding degradation, the capacity fading phenomena is similar to the one monitored on a single cell under the same aging conditions, Figure 60(b). As a matter of fact, the two stages as well as the bending point mentioned before can also be distinguished with comparable slopes and cycle number. Hence, the pack degradation does not seem to be directly related to the intrinsic disparity originally input.

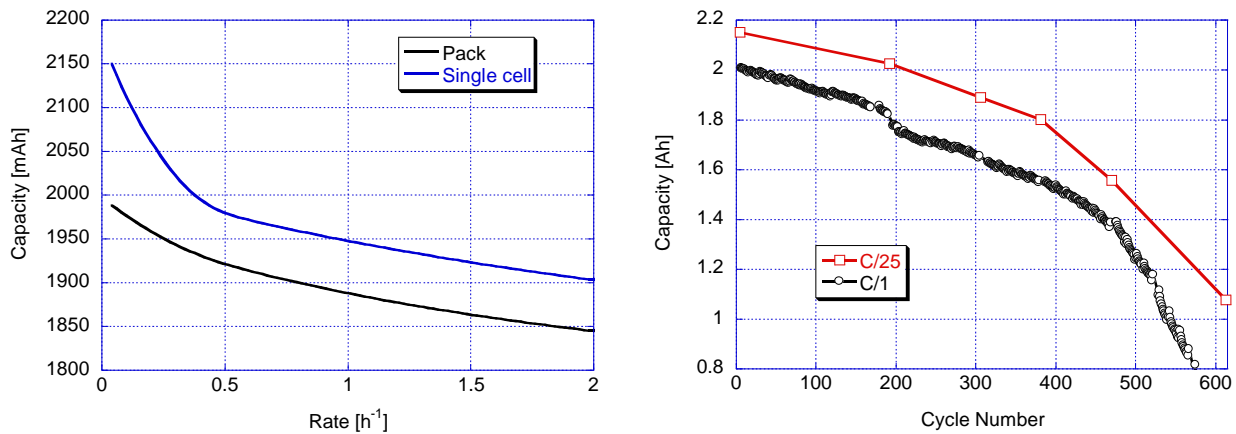


Figure 60 (a) Peukert curves of single cell and pack; (b) Capacity evolution as a function of cycle number for single cell cycling at identical conditions

Since the pack was subjected to C/25-rate cycles at cycles 1, 175, 420, 500 and 580, ps-OCV=f(SOC) curves have been recalculated and used for SOC determination during cycle aging. Figure 61 displays the evolution of these curves. During the first stage of the degradation they were all really

similar (black, red and blue curves), whereas they began to deviate in the second stage (green, light blue and yellow curves). Uncertainties up to 20 % SOC can be inferred if the wrong ps-OCV=f(SOC) curve is used. On the other hand, one of the advantages of this deviation is that the plateaus related to the phase transformations tend to disappear to give a “more linear” ps-OCV=f(SOC) curve that enhance the accuracy of the SOC estimation, as explained in chapter 4. The pack SOCs determined during cycle aging are plotted on Figure 61(b) according to three different methods (i.e. pack ps-OCV=f(SOC), voltage average and SOC average). Contrary to the RPVs, they do not show drastic changes at cycle number 420 but seem constant until 500 cycles. Then they start to evolve towards lower SOCs at the EOC, -2 %, and higher SOCs at the EOD, +22 %. Interestingly, the SOC at the EOD was always greater than 7 %. The method #1, using the pack ps-OCV=f(SOC) curves gives SOC that are ~2 % greater at the EOC than that of the others. Regarding the EOD, different trends are observed depending on which method is used after 500 cycles. Since no remnant capacities were measured during the RPTs, the method providing the most accurate SOCs could not be identified explicitly. However, the results from chapter 4 as well as the other pack degradation studies presented previously allowed maintaining that the method using pack ps-OCV=f(SOC) curves is the one giving the best SOC tracking for the pack no matter what cell chemistry, cell variability or aging conditions are considered.

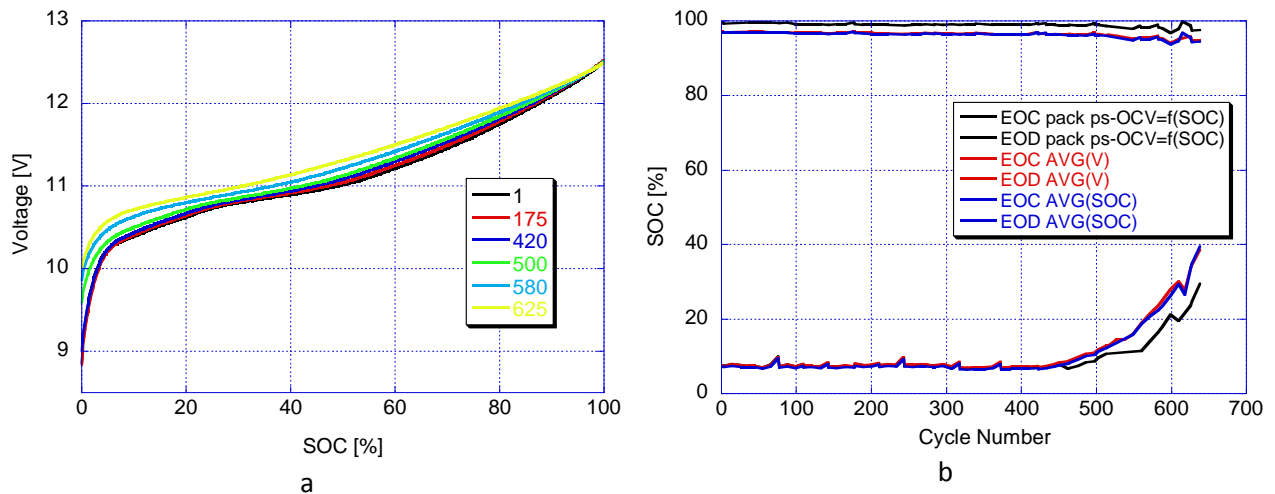


Figure 61 (a) Pack evolving ps-OCV=f(SOC) curves. (b) Pack SOCs from the evolving ps-OCV=f(SOC) curves determined with 3 different methods

As a result of the quick change in the SOC ranges, Δ SOCs, as well as pack capacity, the pack capacity ration is also subjected to a rapid drop between 400 and 500 cycles. During the stage one, the loss was approximately -3.75 % per 100 cycles, and accelerated to -14 % per 100 cycles in the second stage of degradation. These values being similar to the ones of the capacity fading, our first guess for the

main reason of the capacity decline would be the loss of involved active material. In order to decipher the actual reason of the pack degradation, cells are studied separately in the discussion.

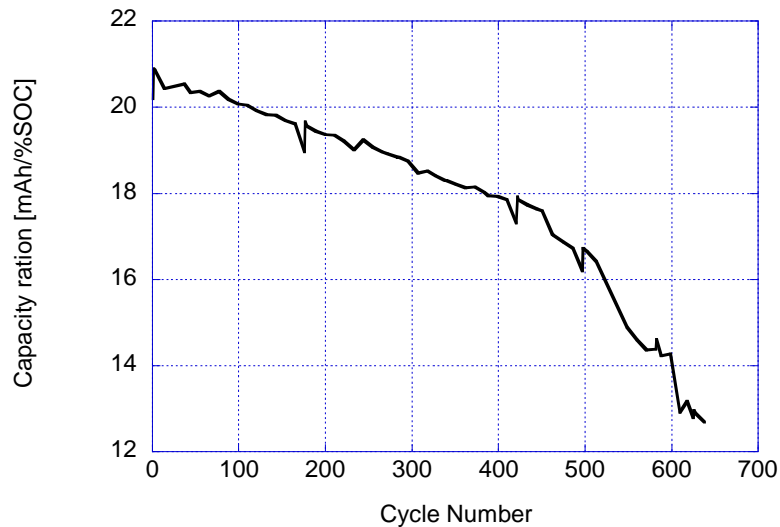


Figure 62 Pack capacity ration evolution during C/2-rate cycle aging

5.3.3.3 Discussion

Along with the relax pack voltages, relax cell voltages are really consistent during the first stage of degradation (i.e. 420 first cycles) and display variations in the second stage, Figure 63(a). The first noteworthy phenomenon in this figure is how the cell #2 diverges from the others in the last part of the cycle aging. As a matter of fact, this cell starts to reach lower and lower voltages at the EOC, -120 mV in 200 cycles, leading to a rise of the others of 50 mV. At the EOD, all cells begin to increase after 420 cycles, cell #1 and #3 seem really similar and steady in their evolution although cell #2 deviates following a nonlinear trend. These changes are accentuated when voltages are converted to SOCs using the evolving ps-OCV=f(SOC) curves of each cell, Figure 63(b). Cell #2 looks like it is getting more and more discharge with SOCs of 25% at the EOD, whereas cells #1 and #3 reach only 45%. As a consequence, cell #2 cannot reach SOC values greater than 90% at the EOC when the others seem to be able to reach higher SOCs than they had at the beginning of the cycle aging.

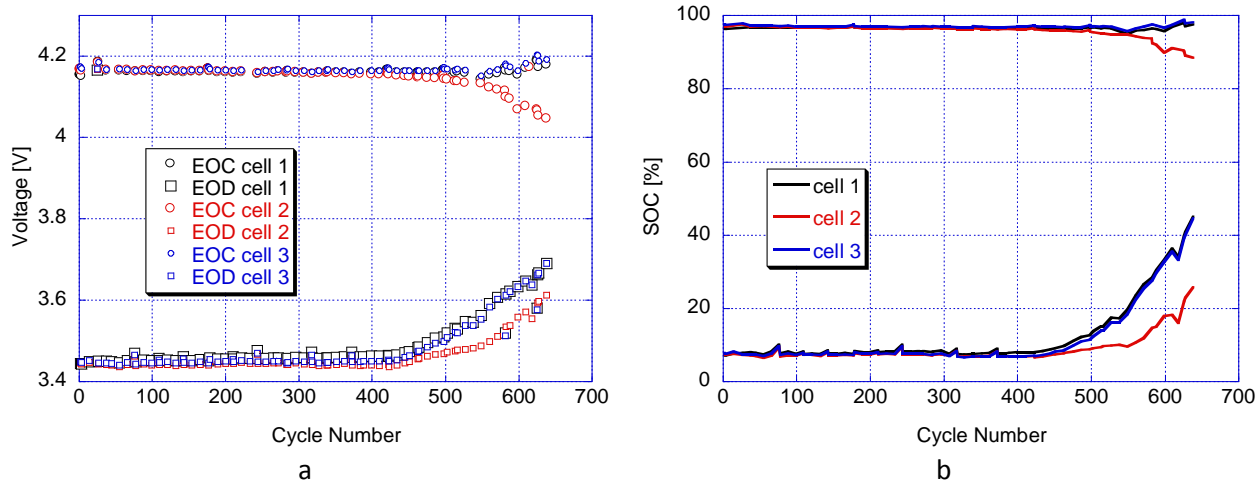


Figure 63 (a) Relax cell voltages (RCVs) of each cell in the pack versus cycle number as measured during the cycle aging at the beginning- and end-of-discharge. (b) Evolution of the end-of-charge and end-of-discharge SOC of each cell determined during cycle aging.

Cell #1 and #3 oscillating between 45% and 98% SOC after 600 cycles, they use only 53% of their SOC range. Cell #2 goes from 25% to 90% and thus uses 65% of its SOC range. The capacity withdrawn at each cycle being the same for all cell within the string, the evolution of capacity ratios shown on Figure 64 is easily explained. Therefore it can be claimed that cell #2 lost a lot of active material (both electrode active material and Li^+ ions) comparing to the others that kept on decreasing slowly and steadily²⁵. The rapid drop of capacity ration after 400 cycles was immediately perceived in the pack performance, reinforcing our assumption saying that the limiting cell drives the pack to its EOL, even though the other cells still show good rate capability and capacity.

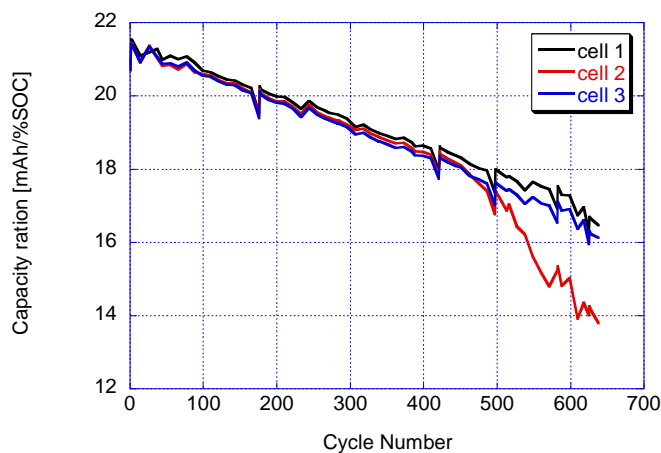


Figure 64 Capacity ration evolution per cell in IHR pack with initial imbalance base on the polarization resistance

In order to quantify the loss of material noticed on the capacity ration evolutions, peak intensities of IC curves were studied. As we can judge on Figure 65 representing the C/25-rate discharge during cycle aging for each cell, the cell #2 shows a different degradation. First of all its main IC peak around 3.6 V, related to the phase transformation of the NMC material of the positive electrode, decreases continuously while the other cells show a slower aging process. In addition, the last (below 3.5 V) peaks of each cell seem to be affected. However, after 420 cycles, cell #1 and #3 are experiencing under discharge, most likely due to the earlier cutoff voltage reached because of the accelerated fading of the cell #2 performances.

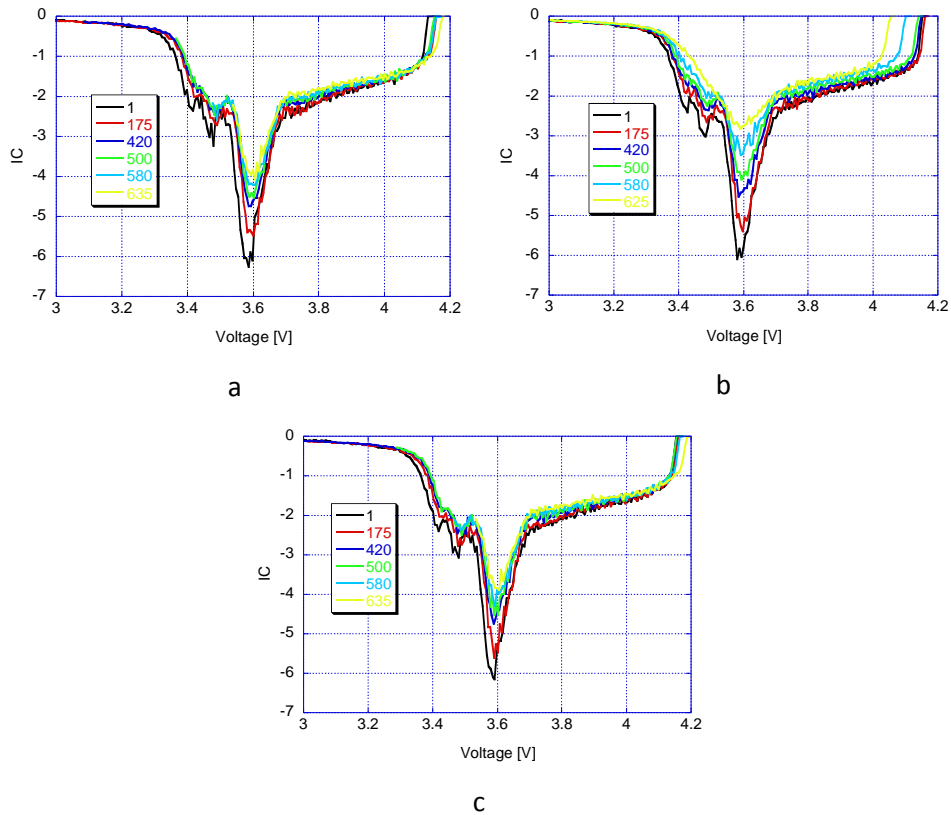


Figure 65 IC curves at C/25-rate in discharge for (a) cell #1, (b) cell #2, and (c) cell #3

Figure 66(a) highlights the cutoff conditions in discharge before the relaxation periods. As noticed on the IC curves, cell #2 does reach the safety cutoff conditions after 420 cycles, stopping the discharge step sooner than expected. As a drawback, cell #1 and #3 are getting less and less discharged and the EOD pack voltage rises from 8.1 V (~2.7 V per cell) to 9.4 V at the end of the test. Two cells were thus not going to SOCs lower than 45%, losing about the same amount in term of energy for the pack. Unfortunately, these early cutoff do not allow us to say much about the state of the negative electrode (i.e. graphite) of cells #1 and #3 since its evolution is monitored at BOC on IC charge curves. In charge,

no cells ever reached the safety limit. Most likely because the electrochemical reaction ends on a long solid solution that slowly raises the voltage, whereas there is a rapid drop of voltage at the EOD. Concerning the loss of involved active material on the positive electrode, Figure 66(b) emphasizes how two cells seem really consistent while the other one started to follow a different trend that shows faster deterioration of its electrodes. Quantitatively, about 25 % more have been lost for cell #2 than that of the others.

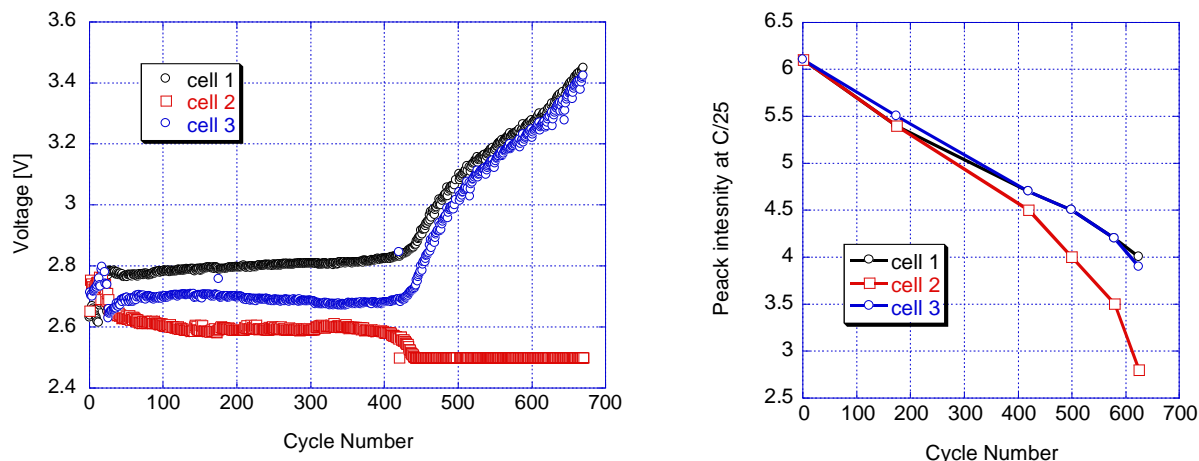


Figure 66 (a) Cell voltage at the end of discharge before relaxation per cell. (b) NMC peak intensity evolution per cell.

The loss of active material determined so far is important but does not explain such a rapid drop in the performance of the cell #2. After more investigations, an interesting behavior has been noticed on the IC curves of the C/2-rate charges, Figure 67. When cell #1 and #3 IC curves show a similar behavior at the EOD, going slowly back to less than $2 \text{ Ah}\cdot\text{V}^{-1}$, strange peaks above 4 V are showing up for cell #2. Since they do not correspond to any of the electrochemical reactions that are supposed to occur in this kind of cell chemistry, they have been associated to the phenomenon of lithium plating. The intercalation / de-intercalation of lithium into graphite occurs at an electrochemical potential close to that of Li^+/Li and is one of the main advantages of using graphite as anode materials. On the other hand, if the surface potential of the graphite is forced to sufficiently low potentials, Li^+ ions may form metallic lithium at the surface instead of the intended intercalation. This process is not fully reversible as dissolution of lithium may form other compounds rather than Li^+ ions, which could explain the rapid degradation of the cell #2⁴². The negative electrode showing a limited kinetics as well as an increase of polarization resistance does not accept the Li-ions as fast as it did in the initial state and metallic lithium starts to plate at the surface of the electrode, increasing the loss of lithium inventory, as well as the loss

of active material, and thus explaining the important degradation noticed on cell #2 compared to the others.

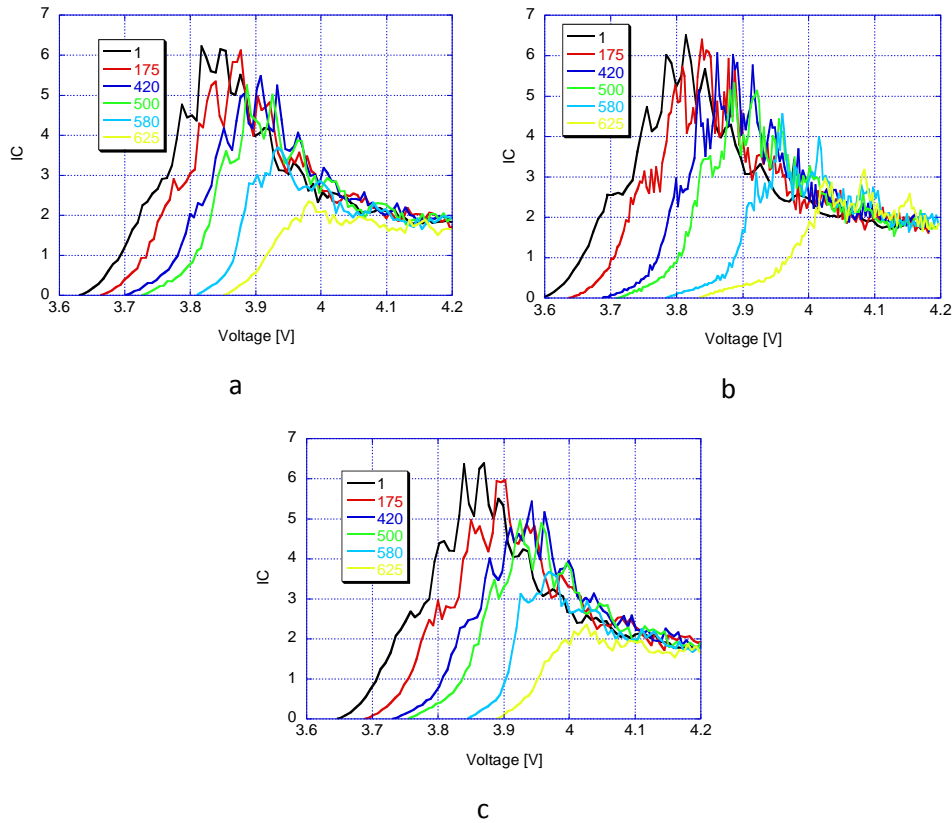


Figure 67 IC curves at C/2-rate in charge for (a) cell #1, (b) cell #2, and (c) cell #3

5.3.3.4 Conclusion

Three high energy cells with pure NMC positive electrode showing variability on their initial polarization resistance have been placed into a string configuration and subjected to a C/2-rate cycle aging. After a constant linear decrease of the capacity during 420 cycles, the pack quickly failed and reached its EOL at 470 cycles. However, it was found that the initial disparity included in this string did not seem to be at the origin of the rapid pack failure. In fact, cell #2 that had the lowest resistance appeared to be the major actor of the fading. Nevertheless, by looking at the initial conditions, this cell also presented the lowest capacity at C/5-rate. Therefore, its lower capacity may have been a larger source of imbalance in the string. After careful analysis of the various charge and discharge IC curves at different rates, it was established that its rapid failure was due to a quick loss of graphite accompanied with formation of metallic lithium at the negative electrode surface instead of the expected Li⁺ ions intercalation. This phenomenon occurs when the graphite is forced to reach low potentials and could

thus be explained by the lowest capacity of the cell #2 compared with that of the others that pushed the cell to attain critical voltages and SOCs.

5.4 Conclusions on pack degradation

All sources of variability among cells from different manufacturing choices and processes on one hand, and within the cells of a same batch on the other hand, have been described and taken into account for cell selection for pack applications in this chapter.

The studies of three 3-cell strings' performance and aging behavior with three different sources of imbalance (temperature, OCV matching, and resistance respectively) were discussed with vigorous data analysis using techniques, such as incremental capacity analysis, as functions of battery selection and SOC tracking. We found that the SOC and SOH of multi-cell strings can be determined by the rationalization of battery behavior. The process explained how the limiting cell is identified and how such cell affects performance of the multi-cell configurations. The trends of the aging processes are comparable to the single cell aging results. Some insights derived from the test results of the 3-cell strings are intriguing, and sometimes, contrary to our intuition. For instance, in the two last cases where the cells were chosen from their intrinsic attributes according to their resistance value on one hand and the maximum initial capacity on the other hand, the limiting cell was not the one that was expected to fail in the hypothesis.

Our approach in systematically understanding multi-cell behavior by correct SOC determination is very effective in deriving better characterization and model techniques to describe battery degradation phenomena and extend the knowledge from cells to strings and eventually an entire battery system.

6 Conclusion and future directions

In this thesis, a universal state-of-charge (SOC) determination method for both Li-ion single cell and battery pack is introduced, tested and validated. Results confirm that the method allows pack SOC estimation at all disregarding Li-ion cell chemistry used, aging scenario, or cell variability (i.e. intrinsic, extrinsic or by cell selection).

The SOC definition used by the United States Advanced Battery Consortium, is intended for engineering purpose, which is empirical. Without a clear state function definition for SOC that could be validated properly, such a definition is vague and difficult to use, especially through degradation (Figure 68). In this work, a thermodynamic-based understanding has been established, contrary to the conventional empirical capacity-based approach. The results show that when the battery is fully equilibrated, its state function is well defined; thus, the thermodynamic properties related to the content of exchangeable Li^+ ions in the electrode materials provide a universal correspondence in open-circuit-voltage (OCV) versus SOC. Using this methodology the SOC of a battery can be properly determined and validated. This OCV-SOC correspondence follows with the capacity loss during aging (i.e. the evolution of the amount of exchangeable Li^+ ions), thus the determination of SOC remains feasible with degradation. Hence, reliable information on how much energy is left in the battery can always be displayed to the user, as illustrated on Figure 69.

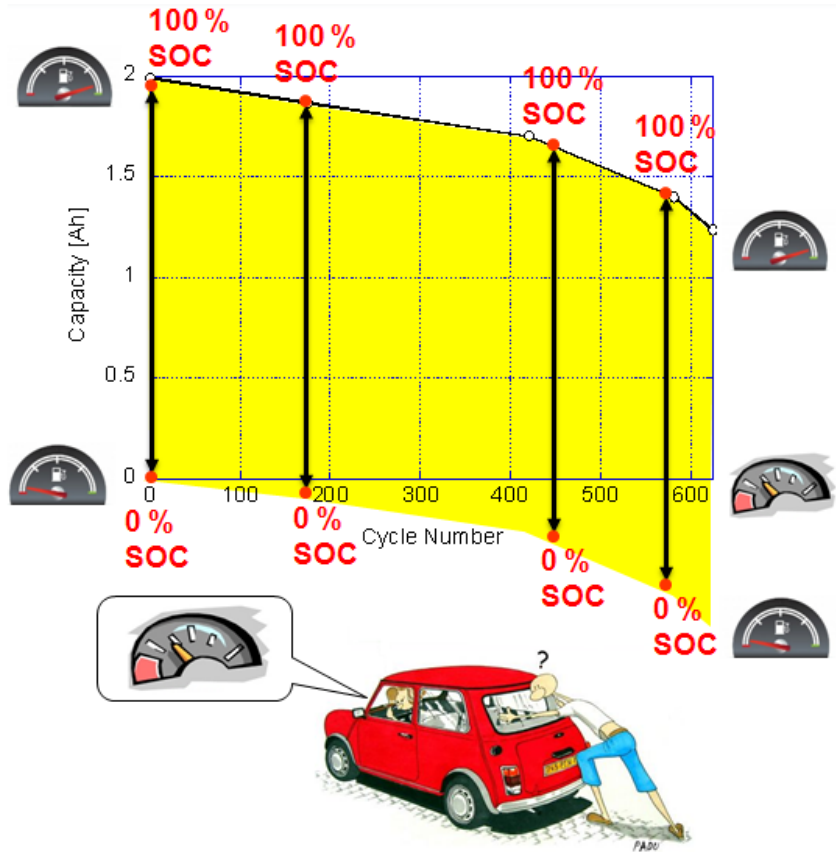


Figure 68 USABC SOC definition limitation: capacity loss not considered

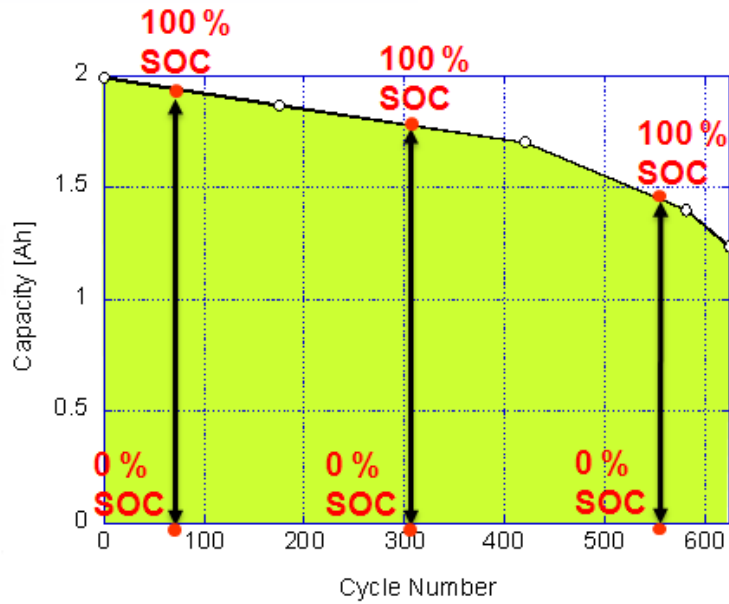


Figure 69 SOC gauge evolution during cycle aging

Regarding the pack SOC determination, five methods using the $ps-OCV=f(SOC)$ correspondence have been investigated. The best method is experimentally validated using three configurations with 3-cell strings of different types of Li-ion chemistry. All of them led to the same conclusion: the pack state-of-charge is most accurately determined when using the evolving pack $ps-OCV=f(SOC)$ curves no matter what cell variability presents.

In this work, the effects of two of the intrinsic attributes, disparities in the cell resistance and capacity, as well as two of the extrinsic disparities in the initial SOC and ambient temperature, are studied. Three 3-cell strings were aged at different conditions following their performance claimed in the manufacturer specs in order to study the performance evolution of the strings under cycle aging. In all cases the pack performance is limited by some aspects of the cell variability. However, criterions made in the cell selection as anticipated to be limiting factor in the pack degradation is followed not consistent with the test results in all cases. Although the pack degradation was always due to the performance fading of one of the cells, it did not always follow the hypothesis. The interrelationship among the three cells in the string may not be as trivial as we originally considered. The impact from such interrelationship on string performance needs to be evaluated in details in the future.

A combination of proper single cell SOC tracking using the $ps-OCV=f(SOC)$ evolution and incremental capacity analysis was used for string aging studies. Major degradation mechanisms were successfully determined for each 3-cell string aging study. This knowledge will assist future research at HNEI to find better ways to select cells for pack application in order improve pack performances, minimize pack degradation and maximize battery life.

7 Appendix

7.1 Li-ion cell chemistries

7.1.1 Material properties and atomic structures

The following Table 8 summarizes the several cell chemistries described. The main difference between these different materials lies in their atomic structure and their ability to intercalate and de-intercalate Li^+ ions during successive charges and discharges. Table 9 compiles those different crystal structures.

Chemical name	Material	Short form	Specific capacity (mAh/g)	Notes	Applications	Cell reference
Lithium Cobalt Oxide	LiCoO_2	LCO (Li-cobalt)	130	High capacity, low rate capability	Cell phone, laptop, camera	PWZ
Lithium Manganese Oxide	LiMn_2O_4	spinel	120-140	Most safe, lower capability but high power and long life	Power tools, e-bikes, EV, medical, hobbyist	IMR
Lithium Nickel Manganese Cobalt Oxide	LiNiMnCoO_2	NMC	160-170	High capacity, low rate capability		IHR
Lithium Iron Phosphate	LiFePO_4	LFP	170	High capacity, high rate capability		PWZ

Table 8 Cell chemistry properties and applications

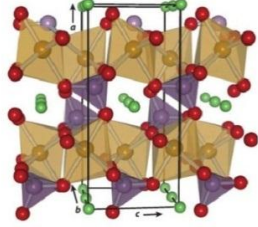
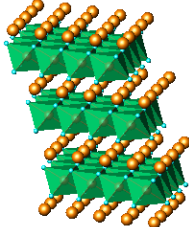
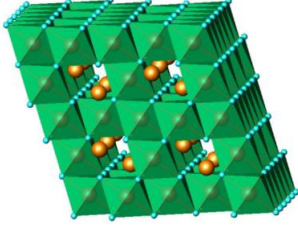
Electrode material	1-D tunnel structure of LFP	2-D layered structure of LCO or NMC	3-D structure of LMO
Crystal structure			

Table 9 Positive electrode crystal structures

7.1.2 Atomic structures and capacity of Li-ion cells

These different atomic structures confer to the electrodes different properties. One which is particularly of importance for battery is the capacity. The capacity of an insertion compound is limited by the concentration of Li^+ ion that can be inserted reversibly in the host¹⁰. In chapter 1, we explained how it is obtained from the formation reactions that occur at each electrode.

Their performance and theoretical capacity can thus be calculated and compared:

- The LiCoO_2 is driven by the following reaction when charged, Equation (8):



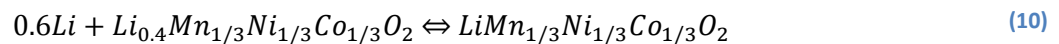
Using the definition of the maximum theoretical specific capacity presented in Chapter 1.2.1, its

capacity is found to be $Q_{\text{Li}_{0.4}\text{CoO}_2} = \frac{F}{Wt_{\text{Li}_{0.4}\text{CoO}_2}} \times 0.6 = 171\text{Ah} / \text{kg}$

- The spinel, which is driven by Equation (9) has a theoretical specific capacity of $Q_{\text{Mn}_2\text{O}_4} = 154\text{Ah} / \text{kg}$.



- And, finally, the NMC, with the following insertion reaction, Equation (10) has a theoretical specific capacity of $Q_{\text{Li}_{0.4}\text{Mn}_{1/3}\text{Ni}_{1/3}\text{Co}_{1/3}\text{O}_2} = 173\text{Ah} / \text{kg}$



As expected by the theoretical calculation and found in the literature¹² we have the following ordering for the 3 studied chemistries of Li-ion battery, Equation (11):

$$Q_{LiMn_2O_4} < Q_{LiCoO_2} < Q_{LiMn_{1/3}Ni_{1/3}Co_{1/3}O_2} \quad (11)$$

In most cases Li-ion batteries that are based on lithium-insertion compounds as cathodes are limited by the capacities of the cathode material¹⁰. In order to maximize the capacity, two different approaches could be envisaged: either the number of Li⁺ ion exchanged has to be increased, and/or, a compound with a very low molecular weight should be considered. At this point it is easy to understand the aim of composite electrodes in order to increase this capacity. However, the capacity itself does not determine the performance of the battery. The next paragraphs focus on how to quantify those performances.

7.1.3 Experimental illustration of performances of diverse Li-ion chemistries using ps-OCV=f(SOC) curve

It has been proved that the SOC is a thermodynamic property defined by the lithium content in each electrode. Consequently, the ps-OCV=f(SOC) curve must be the same for all the Li-ion cells sharing the same chemistry, by means of same electrode composition, same ratio of negative over positive electrode (i.e. electrode loading) and same amount of Li⁺ ion. In fact, two Li-ion cells having the same characteristics mentioned previously but in different proportions, will be defined with the same ps-OCV=f(SOC) curve. On the other hands, two Li-ion cells having different electrode composition or disparities in negative over positive electrode ratio or different amount of Li ion will present different capacities, performance and ps-OCV vs. SOC curves.

The next three figures illustrate some of these differences by showing:

- The difference in ps-OCV=f(SOC) curve between two different electrochemical cells: one is the Nickel Zinc battery and the other one a LIB, Figure 70.
- The difference in ps-OCV=f(SOC) curve due to the use of different material for the positive electrode, Figure 71.
- The difference in ps-OCV=f(SOC) curve due to a different ratio of amount of negative over positive electrode (NE/PE ratio), Figure 72.

These curves are used as the signature of the cells and most of the information that can be drawn from battery testing will be extracted from them. A comparison of diverse Li-ion cell chemistries will

emphasize the importance of understanding these $ps\text{-OCV}=f(\text{SOC})$ curves as well as other parameters that deserve attention such as capacity ration and Peukert coefficient.

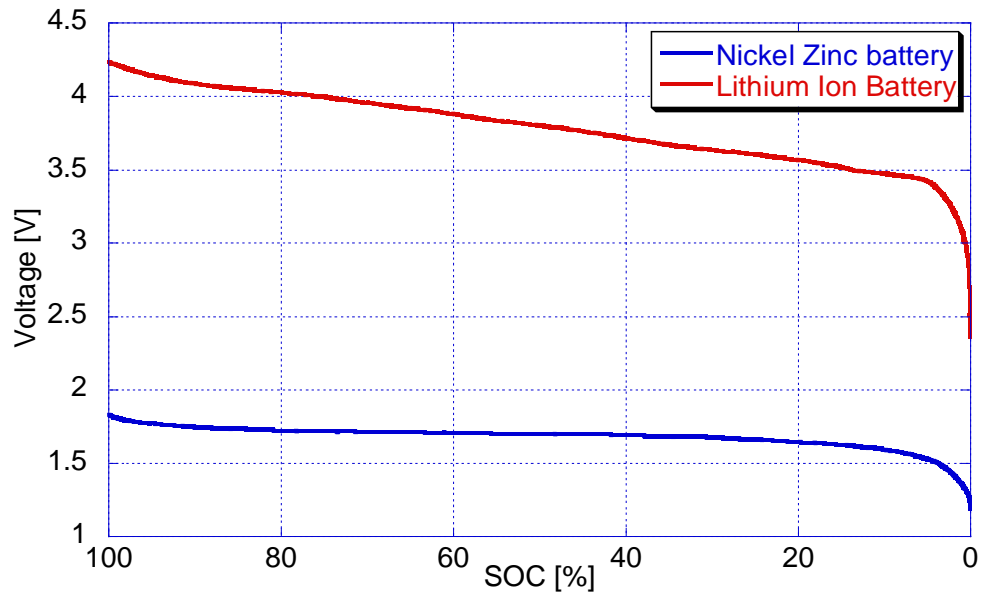


Figure 70 Comparison of $ps\text{-OCV}=f(\text{SOC})$ curve for two different chemistries (Nickel Zinc and Li-ion)

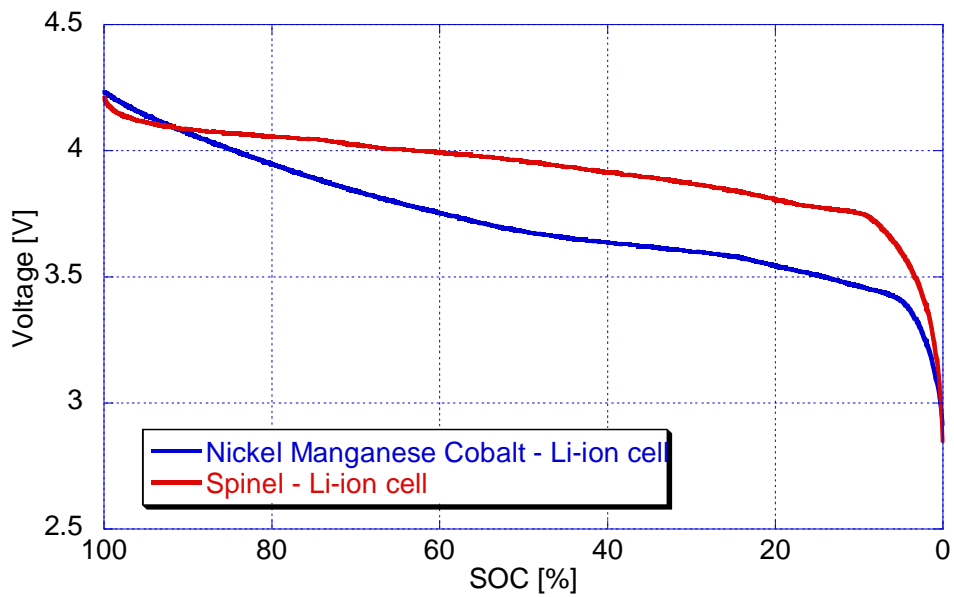


Figure 71 Comparison of $ps\text{-OCV}=f(\text{SOC})$ curve of two Li-ion cells with different positive electrode materials

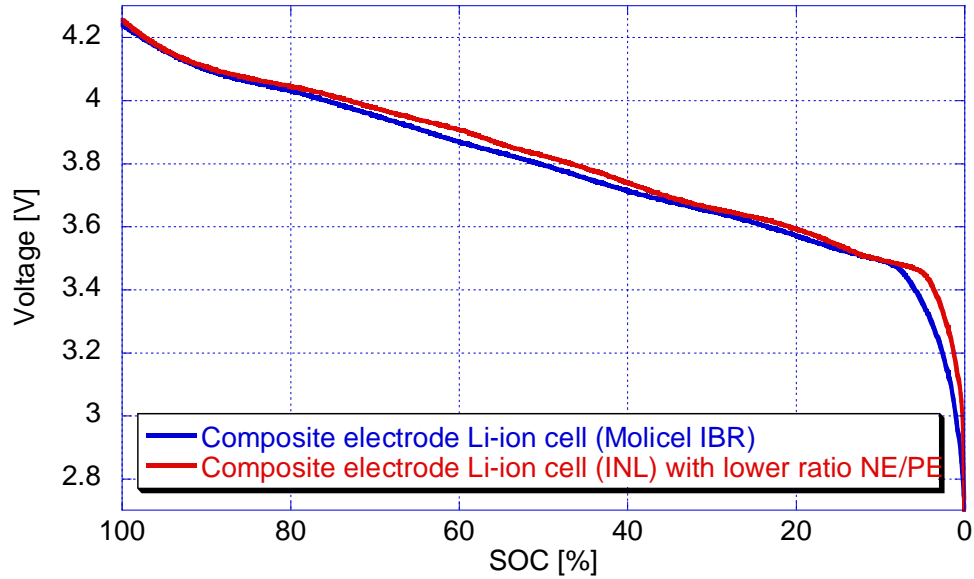


Figure 72 Comparison of ps-OCV=f(SOC) curve for two Li-ion cell with different NE/PE ratio

7.1.4 Li-ion cells studied in thesis work

	IHR (NMC)	IBR (NMC+spinel)	IMR (spinel)	INL (NMC+spinel)
Typical Capacity	1950mAh	1500mAh	1200mAh	1900mAh
Nominal Voltage	3.6V	3.6V	3.8V	3.7V
Charge Voltage	4.2V ±0.05V	4.2V ±0.05V	4.2V ±0.05V	4.2V ±0.075V
Charge Current	Less than 2.0A	Less than 6.5A	Less than 2.0A	Less than 5.0A
Discharge Current (Max.)	4.0A	25A	20A	5.7A
Discharge Cutoff Voltage	3.0V	2.0V	2.5V	2.7V
Weight	45.0g	45.0g	45.0g	43.0g
Operating Temperature	-20°C to 60°C	-20°C to 60°C	-20°C to 60°C	-20°C to 60°C
Weight Energy Density	160 Wh/kg	129 Wh/kg	101 Wh/kg	163 Wh/kg
Volume Energy Density	415 Wh/l	326 Wh/l	286 Wh/l	421 Wh/l

Table 10 Manufacturer specs of studied cells

7.2 Origins of cell variability

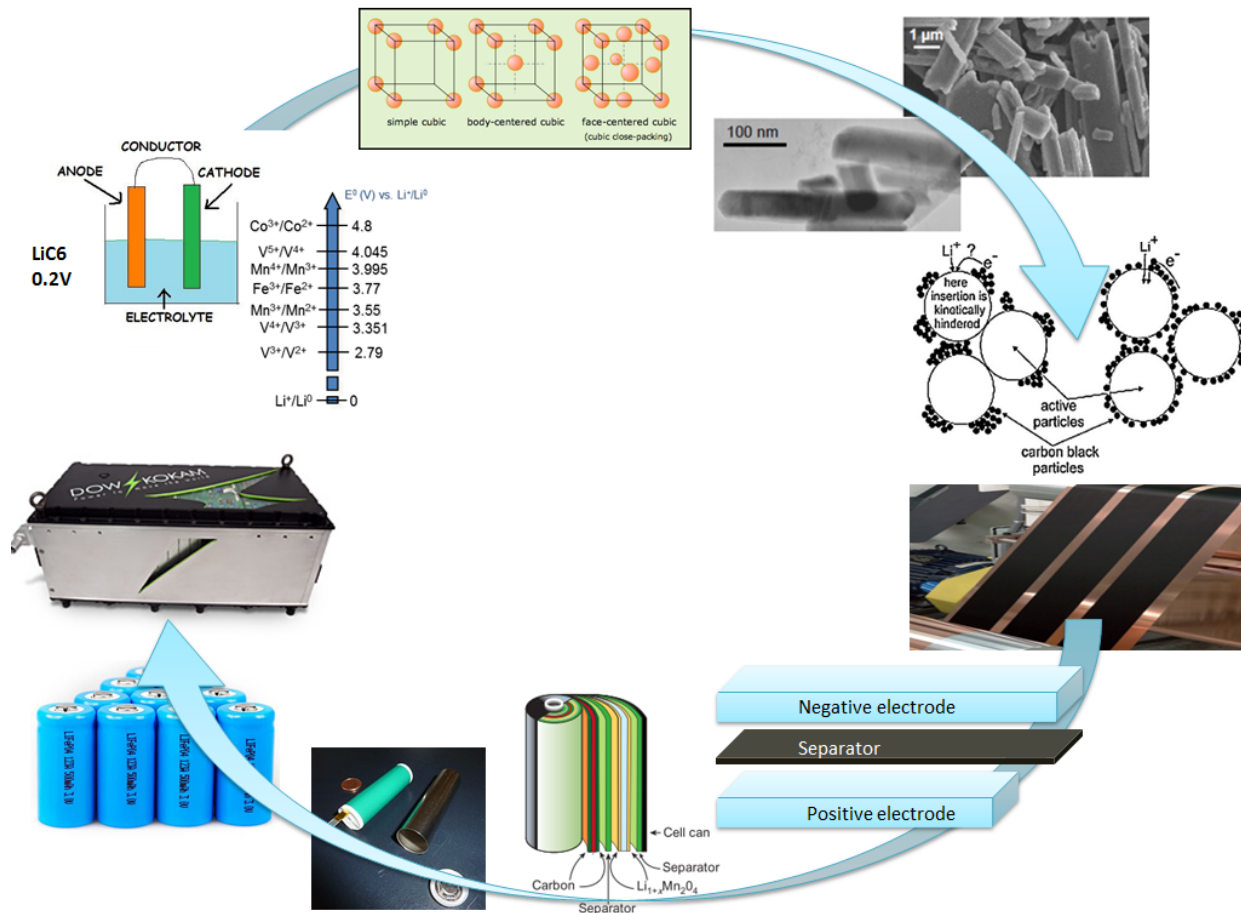


Figure 73 From redox couples to battery packs

7.2.1 Influence of redox couples

The first factor that deserves attention when dealing with batteries is the electromotive force of the cell as it directly refers to the voltage generated by the battery and thus, the chemical components involved. In LIBs technology, the possibility to use different transition metals offers a lot of diverse combinations in order to have the highest potential as possible. The most common redox couples that have been used over the past 20 years are referenced in Figure 74^{5,6}. It is very important to keep in mind that the ones with the highest potential might not give the best performance since materials come with different density and do not react similarly over aging or under temperature constraints.

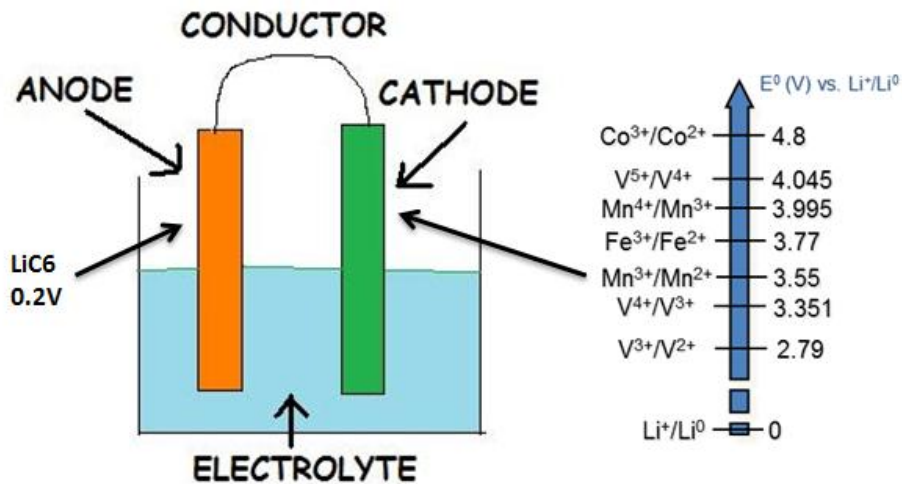


Figure 74 Diverse redox couples used in Li-ion batteries

7.2.2 Influence of crystal structure of active material

The electromotive force of the cell may come from the redox couples that come into play but the evolution of the voltage during charges and discharges will depend on the active material itself. LIBs use insertion active materials and those come with different crystallographic structures that will go through diverse changes during lithium insertion and de-insertion resulting in different electrode potentials. Figure 75 shows a comparison of how the voltage evolves by inserting Li^+ ion in two different structures using the same active material (i.e. Cobalt): the available capacity is the same but one electrode material seems to work at a higher potential than the other with 4.75 V for LiCoPO_4 and 4.2 V for LiCoO_2 .

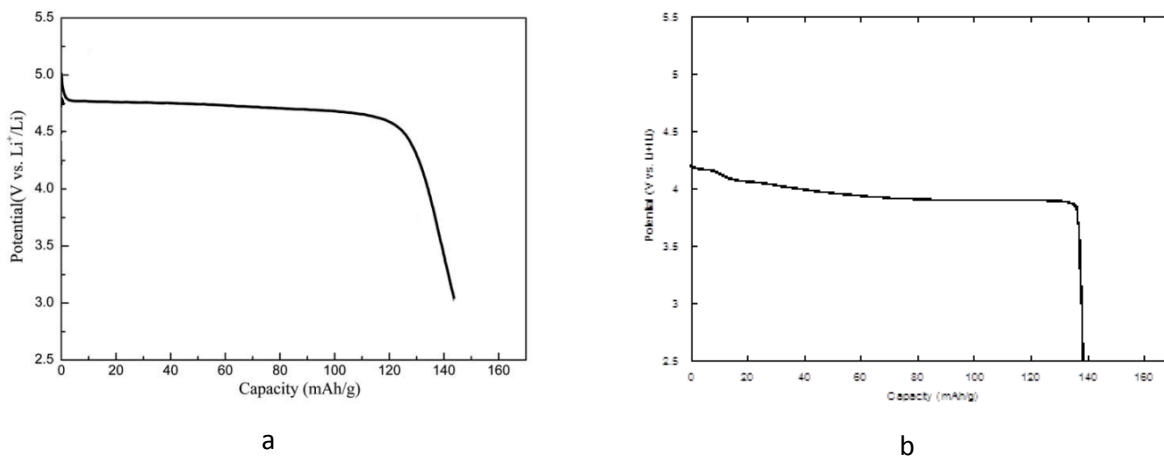


Figure 75 Potential vs. capacity of lithium insertion in a) LiCoPO_4 and b) LiCoO_2

7.2.3 Influence of synthesis conditions of active materials

In the literature, great importance is also attached to the influence of the synthesis conditions on the electrochemical behavior of the active materials. For instance, in his PhD work⁵¹, M. Dubarry showcased a comparison of a vanadium oxide active material prepared with different grain morphology and firing temperature. It has been proved that a material prepared at 350°C (noted SG350) had a high initial capacity, Figure 76, a but a weak cycle life with a rapid loss of capacity due to small grain size, Figure 76c, whereas the same material prepared at 650°C with bigger grain had a good cycle life but a low capacity, because of a too important increase of grain volume. An optimum was found when firing temperature was 580°C (SG580). In that case the capacity during cycling was stable because of a good size and shape of the grains, Figure 76b.

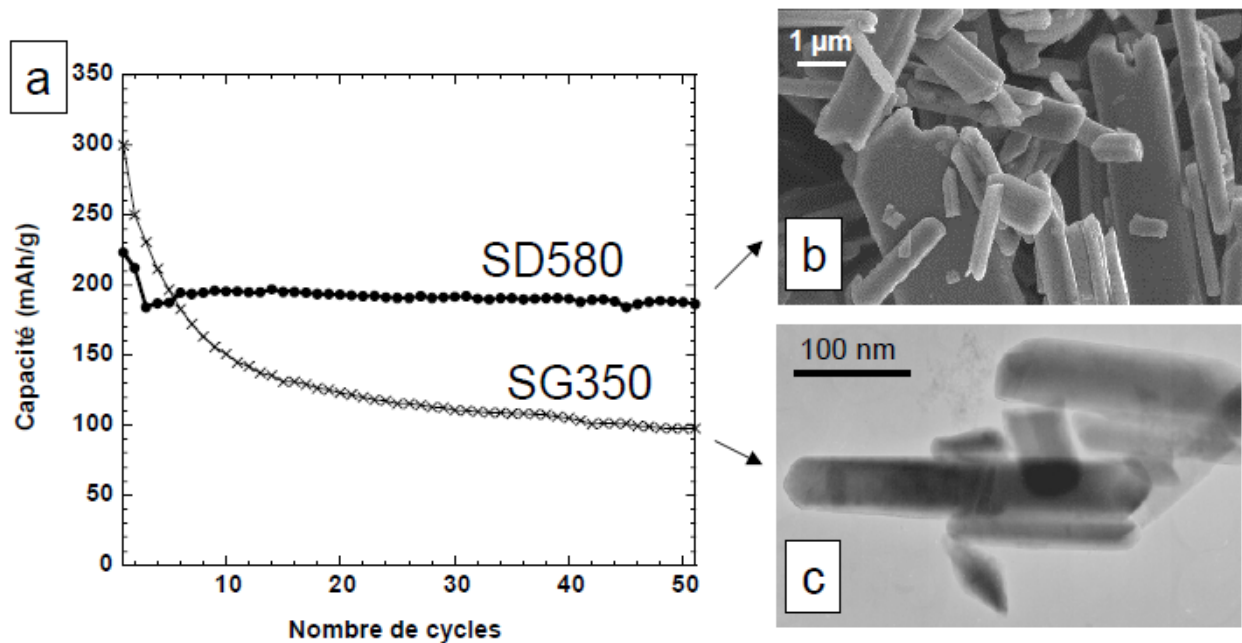


Figure 76 Capacity evolution for a vanadium oxide active material obtained from different synthesis processes

7.2.4 Influence of the electrode architecture

Putting a lot of effort into seeking for new structures of active materials and optimizing existing ones are not the only improvements that can be made on the electrodes of rechargeable batteries since these active materials cannot function by themselves as electrodes. As a matter of fact, an electrode is a very complex medium that needs to transport the ions and the electrons from the electrolyte/electrode and current collector/electrode interfaces, respectively, to the surface of the active material grains in which they will be intercalated. In LIBs, these mediums (or composite electrodes) are a mixture of the

active material, an electronic conducting agent (often carbon black), and a non-electroactive polymeric binder^{52,53}. The carbon black additive ensures the electronic percolation within the composite electrode and the binder gives its mechanical strength to the electrode. As for the transport of ions, the porous composite electrode is impregnated by the liquid electrolyte. As says B. Lestriez, “it appears obvious that the morphology within the composite architecture has an influence on the electrode performance”⁵³. Figure 77 emphasizes the influence of the carbon black distribution within the electrode. If the electronic percolation does not encircle uniformly the active material grains, the insertion of Li^+ ions will be hindered and the electrode performance as well. This also has a direct impact on the specific capacity of the electrode.

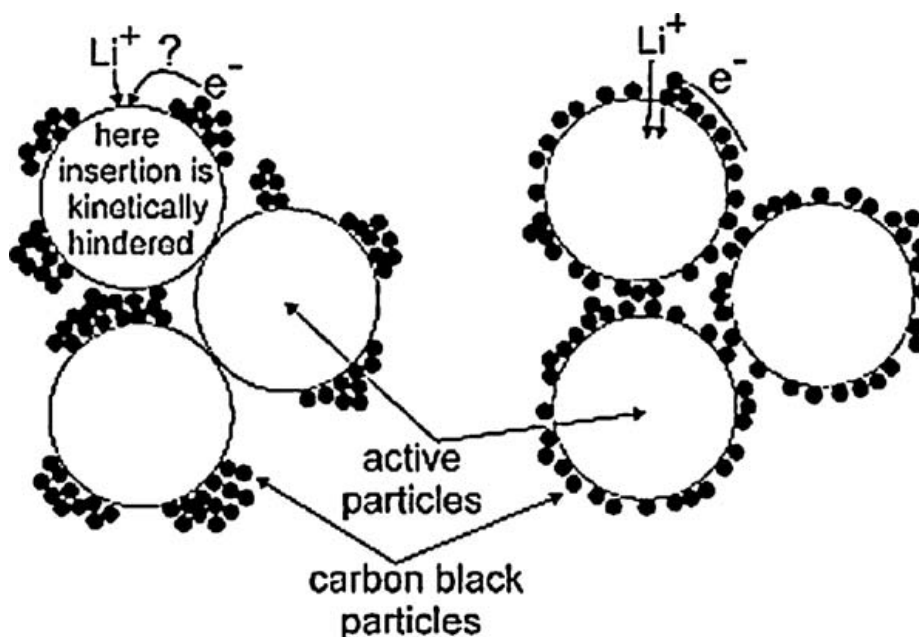


Figure 77 Schematic drawing indicating the impact of carbon black distribution on the kinetics of Li^+ /electron electrochemical insertion into active material⁵⁴

7.2.5 Influence of electrode processing

The carbon black distribution issue raised in the previous paragraph is on the rise during a manufacturing process of electrodes performed by tape casting, Figure 78. Through this process, the metal oxide active material is mixed with the carbon black and the binders by using a solvent before being settled on the current collector band (which is then cut to make a battery batch). If the mix is not homogeneous, the electrode slurry will show a concentration gradient which will be, after settling, at the origin of the variability between cells. In fact electrodes made from the beginning of the tape might have different performance than that made from the end of the tape in term of rate capability. The

influence of the volatile solvent concentration during mixing of the composite components has been studied by E. Ligneel and its effect on discharge capacity showed a strong impact⁵⁵, Figure 79. For concentration below the optimal one, the mechanical energy available for mixing is insufficient to overcome viscosity forces and to reach a good dispersion of the constituents in the bulk of the electrodes. On the other hand, for concentration above the optimal one, settling of the active material and carbon black particles in the low viscosity suspensions can create concentration gradient. In these two cases the electrochemical performance is degraded⁵⁶.

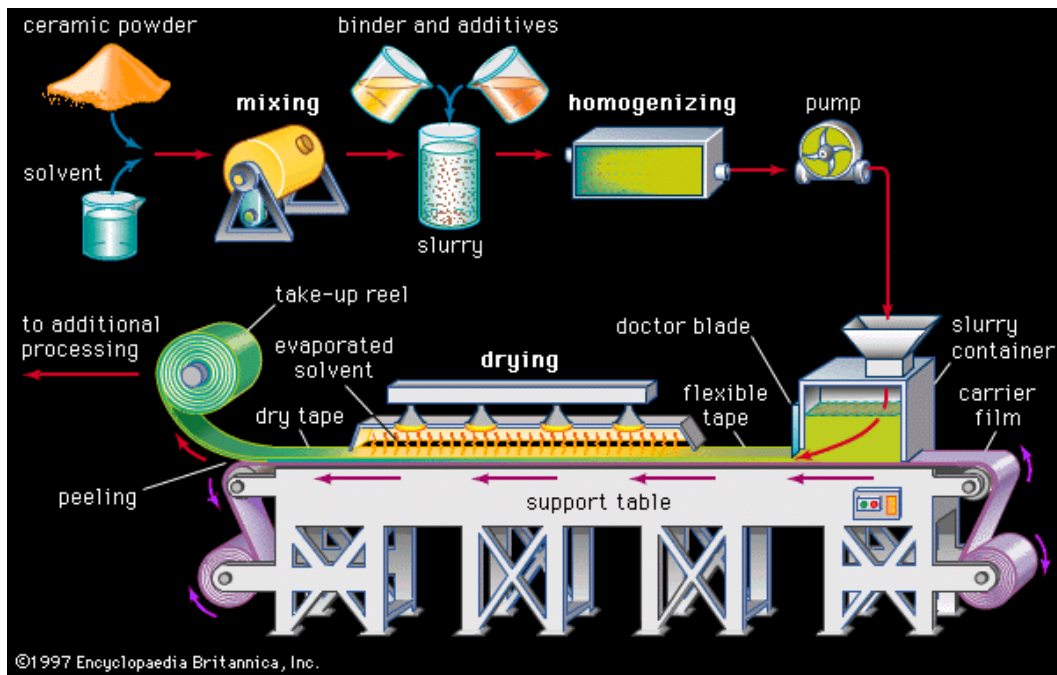


Figure 78 Tape casting process

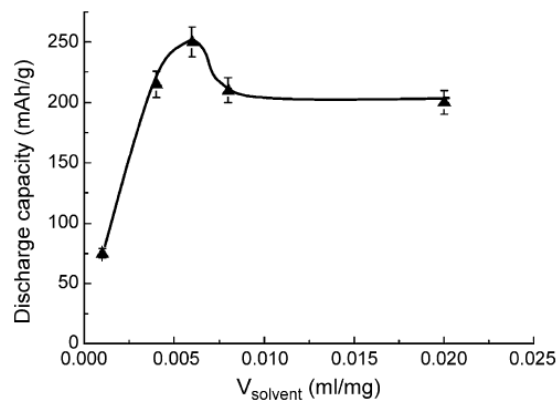


Figure 79 Evolution of the discharge capacity with the solvent concentration expressed in mL/mg of dried material⁵⁶

7.2.6 Electrode loading

Positive and negative electrodes are made following the same processes since they both need ionic and electronic wiring to the active material grains. Therefore all the issues on performance previously presented for one are similar for the other. However, cathodes and anodes offer different characteristics in term of diffusion velocity, resistance and mechanical strength. For example, it is known that graphite has a greater resistance than that of the positive electrode active material which emphasizes the fact that lithium diffusion is slower in the anode. It is actually the reason why charging rates are usually much lower than discharging rates for most LIBs (because Li^+ ions are inserted in the graphitic anode when charging). This remark becomes very important when designing batteries for high power or high energy applications. As a matter of fact, graphite being slower than the positive electrode active material for lithium diffusion, high power cell will use more graphite than high energy cells in order to increase the reaction surface at the negative electrode. In other word, the electrode loading, which is defined as the amount of negative over positive electrode ratio (NE/PE ratio), will be greater for high power batteries than it will be for high energy batteries. As a drawback, its specific capacity will be lower. Figure 80 displays a comparison of two cells sharing the same shape factor (i.e. 20650 size casing) and using the same LiFePO_4 active material with a different electrode loading. One presents a much higher capacity and will be used for high energy applications whereas the other one will be used for high power applications.

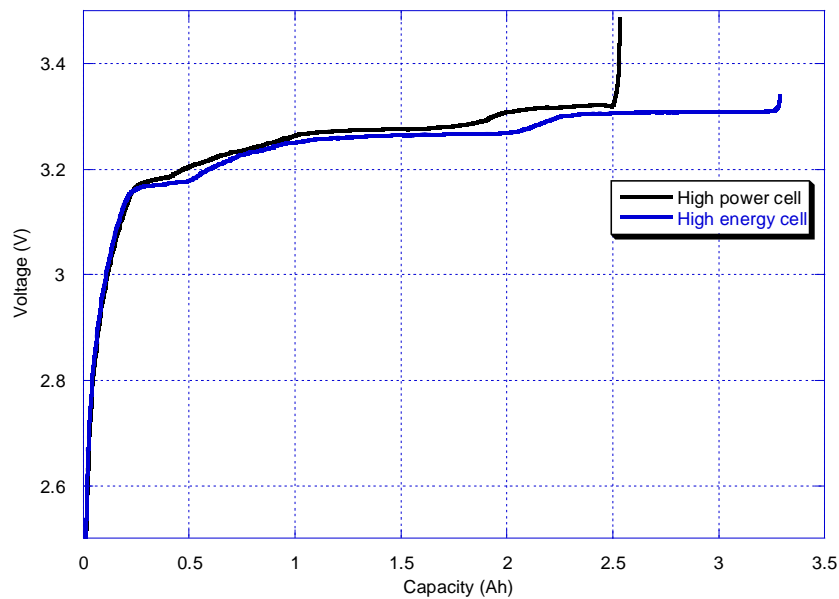


Figure 80 Comparison of two cells using same active material but different electrode loading

7.2.7 Electrode separator

One component of the batteries that has not been mentioned yet and has a strong impact on the cell performance is the separator. It is a porous sheet placed between the positive and negative electrode that is permeable to ionic flow. Its primary function is to prevent physical contact between electrodes of opposite polarity. In LIBs two layers of separators are sandwiched between positive and negative electrodes and then wound together in cylindrical configurations, Figure 81. A number of criteria must then be considered when selecting a separator for a particular battery. They include the following: electronic insulator, minimal electrolyte resistance, chemical resistance to electrolyte, uniform in thickness and, sufficient physical strength to handle electrode volume changes during insertion-de-insertion processes. The order of importance of these various characteristics varies, depending on the application. For instance, the thicker the separator, the greater the mechanical strength and the lower the probability of punctures during cell assembly but the smaller the amount of active materials that can be placed in the can. On the other hand, the thinner separators take up less space and permit the use of longer electrodes which increase both capacity and, by increasing the interfacial area, rate capability⁵⁷. Furthermore, the thinnest also makes it a low resistance separator. Therefore, a compromise in requirements for the separator must be made to optimize performance, cost and safety.

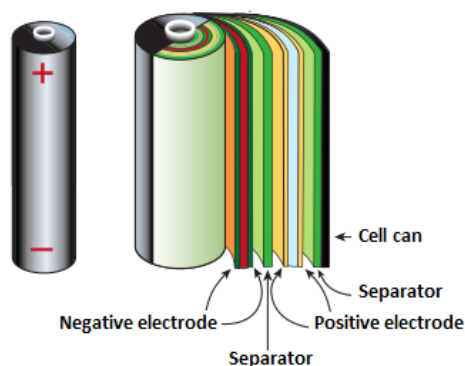


Figure 81 Cylindrical cell components

7.2.8 Influence of casings

Battery casings, or battery housings, are the shells encasing the functional battery parts and chemicals. There are four main cell type configurations for LIBs: coin, cylindrical, prismatic and flat casings. Since sizes are standards in most cases, the amount and length of electrodes that can be input in the casing will determine the maximum capacity of the cell. Obviously the weight of the casing will also show variations and involve more variability on cell 'specific capacity.

7.2.9 Importance of formation cycle

LIBs are built discharged with all the lithium in the positive electrode. During the first charge which is more often called formation cycle, a very important film is formed at the surface of the graphite negative electrode. It is named as a Solid Electrolyte Interphase (or SEI layer) and it is essential to the longevity of the battery because it prevents further reaction with the electrolyte. Its formation contributes to irreversible capacity because it consumes Li^+ ions^{14,25}. Therefore, the way this is realized after electrode manufacturing could affect the performance of the battery. The use of LTO as an anode offers a big advantage compared to graphite since no SEI layer is formed. Therefore, the irreversible capacity is low. As a drawback the operating voltage of LTO is 1.5V vs. Li, which is greater than that of graphite with $\sim 0.2-0.05\text{V}$ vs. Li (very close to that of the Li^+/Li^0 redox couple) which leads to a lower voltage of the electrochemical cell.

7.3 Cell variability

7.3.1 Amount of material involved and capacity ration

From the RCVs at different time steps t_1 and t_2 of a charge or a discharge, a ΔSOC can be deciphered for any given rate. It represents the range of SOC used from t_1 to t_2 , as illustrated in Equation (12).

$$\Delta SOC = SOC(t_1) - SOC(t_2) \quad (12)$$

By dividing the capacity used between these two time steps by the corresponding ΔSOC , a term referred as “capacity ration”, noted Q_R , can be determined, Equation (13). It depicts the capacity associated with each percent of SOC and its unit is Amps-hour per percent of SOC ($Ah.\% SOC^{-1}$).

$$Q_R = \frac{C_{t_1-t_2}}{\Delta SOC} \quad (13)$$

Reciprocally, if the maximum range of SOC, ΔSOC_{MAX} , obtained from the RCVs at the beginning-of-discharge (BOD) and at the end-of-discharge (EOD) after relaxation, and Q_R are known, the maximum capacity, Q_{MAX} , that the cell is able to offer can be defined as shown in Equation (14).

$$Q_{MAX} = Q_R \times \Delta SOC_{MAX} \quad (14)$$

Therefore, it can be claimed that the maximum capacity can be inferred from the capacity ration only since ΔSOC is just a matter of normalized capacity. Being related to the cell capacity, Q_R is thus proportional to the amount of material involved in the electrochemical reactions and its knowledge enables the quantification of the content of Li^+ ions and electrode active materials (also referred as primary and secondary active materials respectively) within the cell. Like the cell capacity, the capacity ration will decrease during aging as the cell degrades since some active material will become inactive and some Li^+ ions will be consumed in adjacent reactions; some examples of its evolution will be shown in chapter 5.

The advantage of this intrinsic attribute to the cell is its rate independency. In fact, its value can be calculated from any rate and the choice of the rate to obtain its value with the best accuracy will depend on the current range of the battery tester used. Table 11 summarizes the averaged values obtained from low rate discharges as well as the standards deviation for the four types of Li-ion cells studied. Figure 82 displays the distribution of capacity ration, calculated from the C/2-rate cycle, among the different chemistry batches.

Cell	IMR	IHR	IBR	INL
Average (mAh/%SOC)	11.37	21.60	15.12	20.06
Standard deviation (%)	0.75	0.6	0.63	0.4

Table 11 Capacity ration averages and standards deviation

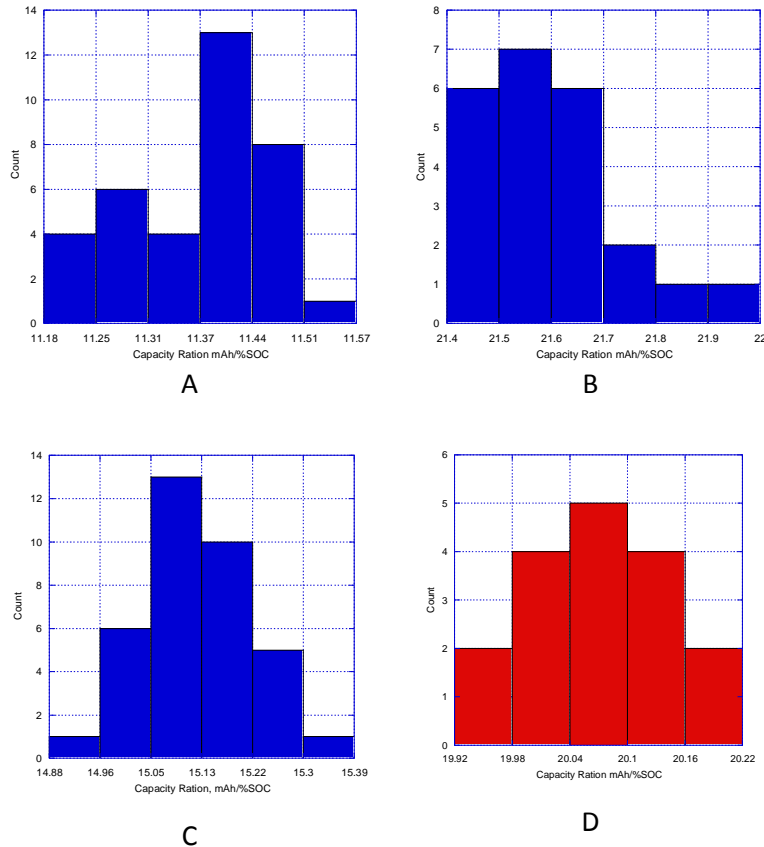


Figure 82 Capacity ration distribution for (A) IMR, (B) IHR, (C) IBR, (D) INL

As expected, high energy cells have a higher capacity ration than high power cells. In fact, IHR and INL cells have a Q_R greater than $20 \text{ mAh.\%SOC}^{-1}$; whereas IBR and IMR are respectively 15.12 and $11.37 \text{ mAh.\%SOC}^{-1}$. An interesting comparison to point out here is between INL and IBR cells: they both have the same size and use a composite positive electrode made out of lithium manganese and nickel manganese cobalt oxide but they show different Q_R values. A previous study on INL cells allowed determining the ratio between the two materials used in the positive electrode: the electrode composition have thus been estimated to comprise $2/3$ of $\text{LiMn}_{2/3}\text{Ni}_{1/3}\text{Co}_{1/2}\text{O}_2$ and $1/3$ of LiMn_2O_4 based on

the capacity of electrochemical reactions³⁰. The IBR cell being a high power cell and thus showing a lower capacity than the INL cell, plus the facts that $\text{LiMn}_{1/3}\text{Ni}_{1/3}\text{Co}_{1/3}\text{O}_2$ being a high energy material and LiMn_2O_4 a high power material allow us to draw the following conclusion: IBR cells contain more spinel material in the positive electrode than INL cells and less $\text{LiMn}_{1/3}\text{Ni}_{1/3}\text{Co}_{1/3}\text{O}_2$. However, since they do not use the same graphitic negative electrode, the exact ratio in the IBR cells cannot be deciphered without looking at the incremental capacity curves³⁰.

The very low disparity in capacity ration among the cells allows maintaining that they are well manufactured and, thus, good for battery pack applications. In fact, less than 0.8% of standard deviation shows that they have a very similar loading of active material in their electrodes. Another study made on a lot of one hundred AAA size 300 mAh LiCoO_2 Li-ion cells purchased from a commercial vendor has been performed previously and showed a poor manufacturing with a wide spread of more than 1.5% in capacity ration; which made these cells difficult to handle in pack configurations³⁶.

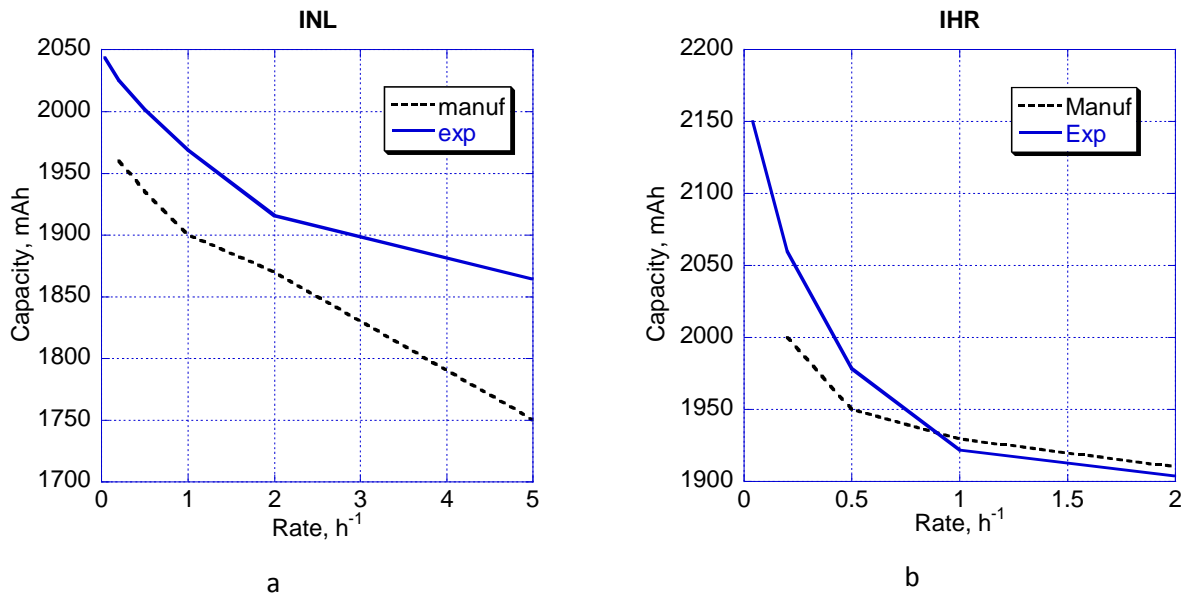
7.3.2 Rate capability and Peukert coefficient

The rate capability of a cell is a measure of its ability to deliver the same capacity in a defined potential window irrespective of the C-rate used to cycle the cell. The C-rate is the unit by which charge and discharge times are scaled. A battery rated at 1 Ah provides 1 A for one hour if discharged at 1C. The same battery discharged at 0.5C provides 500 mA for two-hours. Thus, 1C is often referred as a one-hour discharge; a 0.5C or C/2 would be two hour, and C/25 a 25 hour discharge. When the cell impedance increases, cutoff potentials are reached sooner and there would be a decline in the rate capability of the cell. So, any change in the current dependence of the polarization effects in the cell is expected to show up as a change in the slope of the rate capability³². A good technique to characterize the rate capability is to use the Peukert representation. It depicts the discharge capacity as a function of the C-rate. Knowing the application (i.e. high power or high energy) as well as the C-rate usage range specific to that proper application, a comparison of different Li-ion battery chemistries can be performed in order to select the most appropriate type of cell. For example, the INL and IHR cells using different positive electrode materials but having similar capacities, 1.9 Ah and 1.95 Ah respectively, and supposed to be cycled with the same C-rate usage range according to their manufacturer specs, a comparison of the two rate capabilities appears necessary so as to make a selection for a given application. Table 12 summarizes the capacities of both cells from the manufacturer specs sheet as well as the ones obtained experimentally.

C-rate	Q _{IHR} Manuf.	Q _{IHR} Exp.	Q _{INL} Manuf.	Q _{INL} Exp.
C/25	-	2150.12	-	2043.99
C/5	2000	2059.8	1960	2025.23
C/2	1950	1978.69	1935	2001.89
C	1930	1922.18	1900	1968.84
2C	1910	1903.3	1870	1915.49
5C	-	-	1750	1864.12

Table 12 Manufacturer and experimental discharge capacities of IHR and INL cells

The experimental data were acquired using an Arbin BT 2043[®] system with Arbin Universal cell holders[®]. Results are shown in Figure 83. For both cells, experimental capacities were found to be greater or equal to the manufacturer ones as we can judge on Figure 83(a) and (b). An interesting fact to note is that when the manufacturer Peukert curves are plotted on the same graph, IHR cells seem better than INL cells since they have higher capacities at all rates, Figure 83(c). However, when the experimental Peukert curves are plotted on the same graph, it appears that INL cells have higher capacities than IHR cells for rates greater than C/3, Figure 83(d).



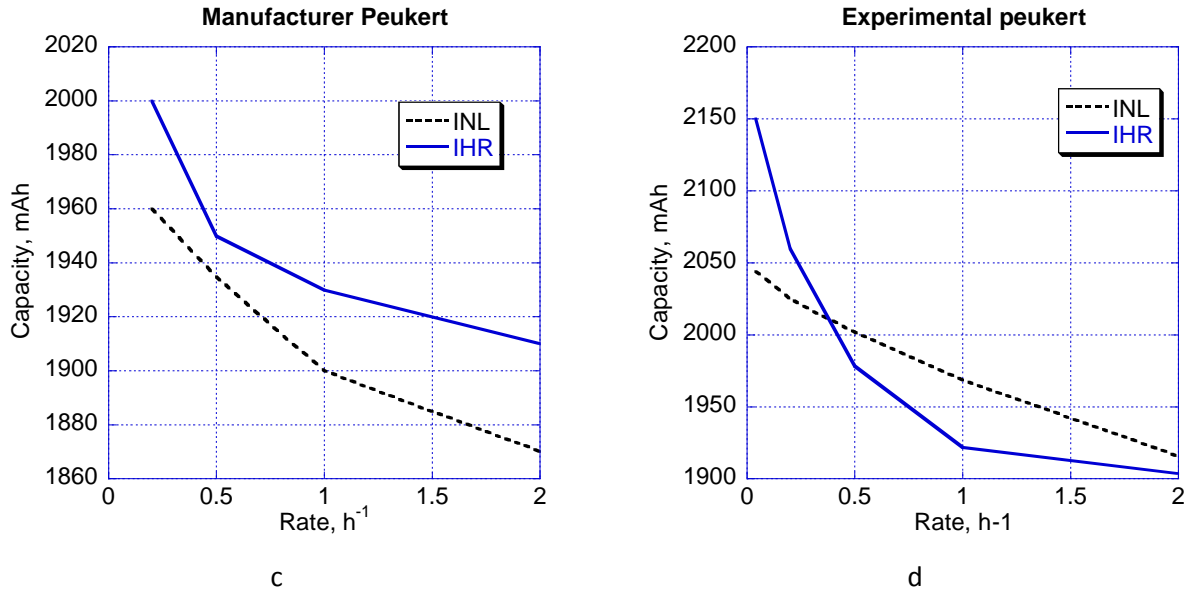


Figure 83 Peukert curves of (a) INL cell, (b) IHR cell, (c) IHR and INL manufacturer specs, and (d) IHR and INL experimental data

The advantages of the composite electrode are highly emphasized here: INL cells, including spinel material (i.e. high power material) in its positive electrode, show higher performances at higher rates than that of IHR; on the other hands results are pretty good at low rates for high energy applications thanks to the NMC material (i.e. high energy material).

The IBR and IMR cells being both high power cells, their comparison is not straightforward. As a matter of fact they present C-rate usage ranges that are much wider than that of INL and IHR cells. Their Peukert curves are shown on Figure 84. Here the experimental capacities are lower than the ones given by the manufacturer.

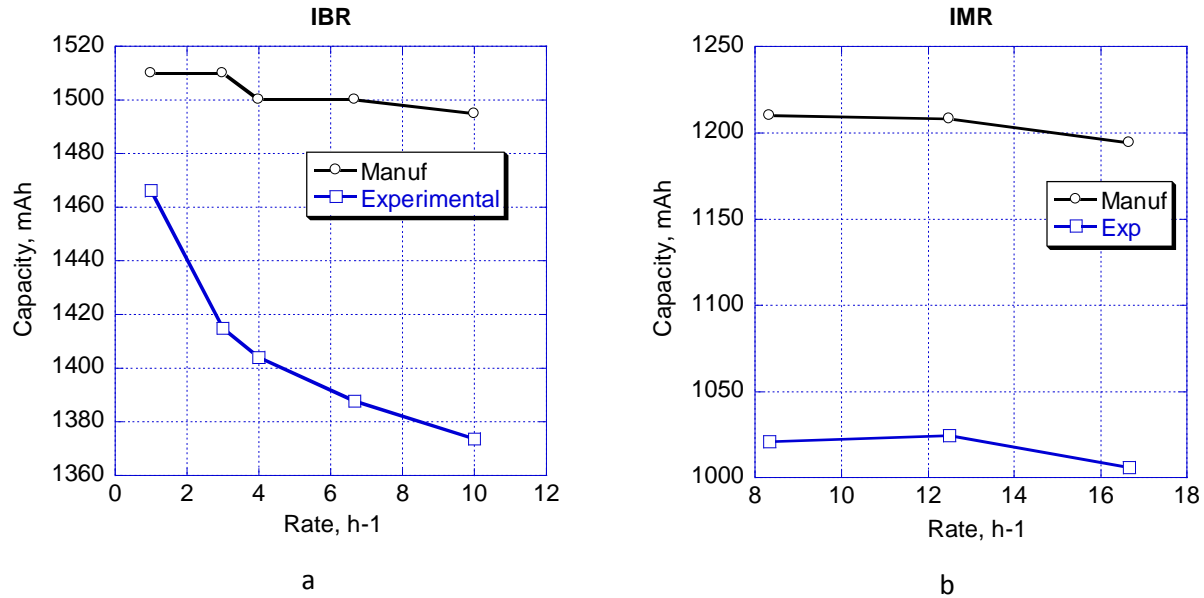


Figure 84 Peukert curves of (a) IBR cells and, (b) IMR cells

The rate capability of a cell is then characterized with the Peukert coefficient which is deciphered from a mathematical law describing an exponential relationship between the discharge current and the delivered capacity over a specified range of discharge currents, Equation (15).

$$Q = I^{Pk} \times t \quad (15)$$

Q is the delivered capacity (Ah), Pk is the Peukert coefficient (dimensionless), I the discharge current (A) and t the time to discharge the battery (h). The closer this coefficient is to unity, the better the cell to acting as an 'ideal cell' in its C-rate usage range. In this case, the Peukert curve would thus be a straight line. From the experimental data presented above that were obtained during the characterization tests, the Peukert coefficient of each of the four cells studied were deciphered. They are recapitulated in Table 13.

Cell type	Peukert coefficient
IHR	1.02
INL	1.02
IBR	1.005
IMR	1.002

Table 13 Peukert coefficient of studied cells

Since the cells were submitted to only two different rates during their conditioning cycles, the ratio Q_5/Q_2 was calculated instead of the Peukert coefficient (Pk). In fact, the latter cannot be obtained from only two points. However, the same conclusions can be drawn from it as it is illustrated in the following mathematical reasoning:

$$\frac{Q_5}{Q_2} = \left(\frac{I_5}{I_2} \right)^{Pk} \frac{t_5}{t_2}$$

$$\frac{Q_5}{Q_2} = \left(\frac{Q_{nom} \times C/5}{Q_{nom} \times C/2} \right)^{Pk} \frac{t_5}{t_2}$$

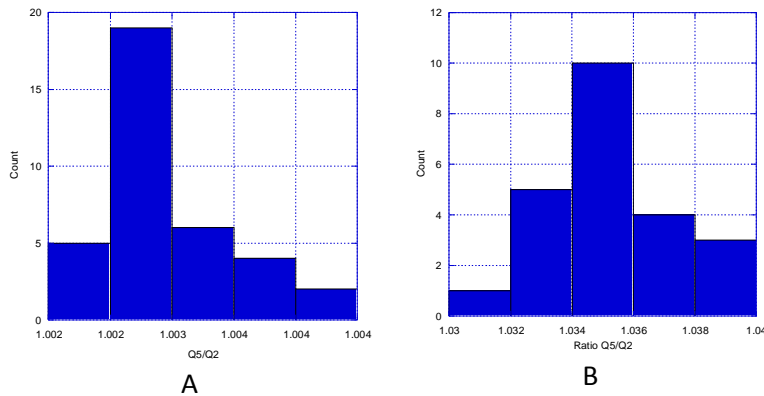
$$\frac{Q_5}{Q_2} = \left(\frac{2}{5} \right)^{Pk} \frac{t_5}{t_2}$$

which can also be approximated by:

$$\frac{Q_5}{Q_2} \approx \left(\frac{2}{5} \right)^{Pk} \frac{5}{2}$$

$$\frac{Q_5}{Q_2} \approx \left(\frac{2}{5} \right)^{Pk-1}$$

P_k tending to one makes the difference P_k-1 tending to 0 and the ratio Q_5/Q_2 tending to one as well. Thus it proves that the same information can be withdrawn from the ratio without calculating the Peukert coefficient.



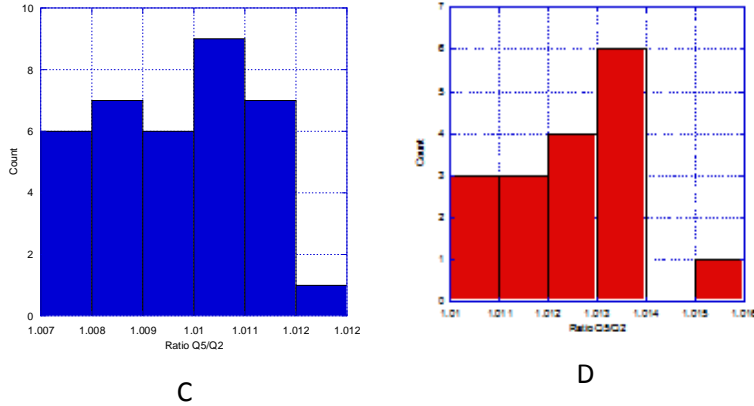


Figure 85 Q5/Q2 ratio distribution for (A) IMR, (B) IHR, (C) IBR and (D) INL cells

Cell	IMR	IHR	IBR	INL
Average	1.003	1.035	1.001	1.0125
Standard deviation (%)	0.05	0.2	0.13	0.14

Table 14 Q5/Q2 ratio averages and standard deviation

From the Peukert's law, if the exponent constant was equal to one, the delivered capacity would be independent of the current. It would also mean that the whole capacity of the battery would be available at every rate. From the results of the conditioning cycles, the Peukert coefficient of the IMR cells appears to be the lowest one with 1.003 with the lowest spread of about 0.05 %, which is not surprising since it is a high power cell that can handle very high current (and thus its capacities at C/2 and C/5 are about the same). On the other hand the INL and IHR cells are high energy cells. Thus they are more sensitive to rate differences and show a higher Q_5/Q_2 ratio with a larger spread. Like the capacity ration, the Peukert coefficient and its spread give information on the cell and its chemistry. In fact, just looking at the Molicel® results, i.e. IMR, IHR and IBR cells, we can decipher which one has been made for high power or high energy applications:

- IMR uses pure spinel as positive electrode which is a high power material and has a Peukert coefficient very close to one with almost no spread;
- IHR is a high energy cell using a high energy material, it has a high capacity and the greater Peukert coefficient with the largest spread;
- IBR, using composite electrodes, are between the two others in term of energy/power usage.

7.3.3 Resistance variations

The last parameter to analyze in the cell-to-cell variations study is the polarization resistance. In a pack, a cell with a higher resistance will reach the cut off voltages in charge or discharge faster than the other and thus will lead to an increase of the imbalance among the cell, accelerating the degradation process of the pack. In fact if the same current I is going through two batteries A and B in a series configuration that have R_A and R_B as their resistances with R_A greater than R_B , the Ohm's law says that $U_A=R_A \times I$ is greater than $U_B=R_B \times I$.

Figure 86 shows the cell voltage (in circles) immediate after polarization (i.e. due to the current-induced drop) corresponding to the onset of the first incremental capacity peak at $C/2$ and $C/5$ rates. These onsets and the rates allow us to determine the polarization resistance as express in Equation (16):

$$R = \frac{V_{C/5} - V_{C/2}}{I_{C/5} - I_{C/2}} \quad (16)$$

If more than two rates are available in the database, the voltage immediate after inducing current can be plotted according to the current. The curve obtained should follow a linear dependence with the polarization resistance as the slope. Obviously, the more points are used, the more accurate is the resistance value. However, it has been proved that using only the two conditioning rates allow deriving the resistance with less than 4% error³⁶.

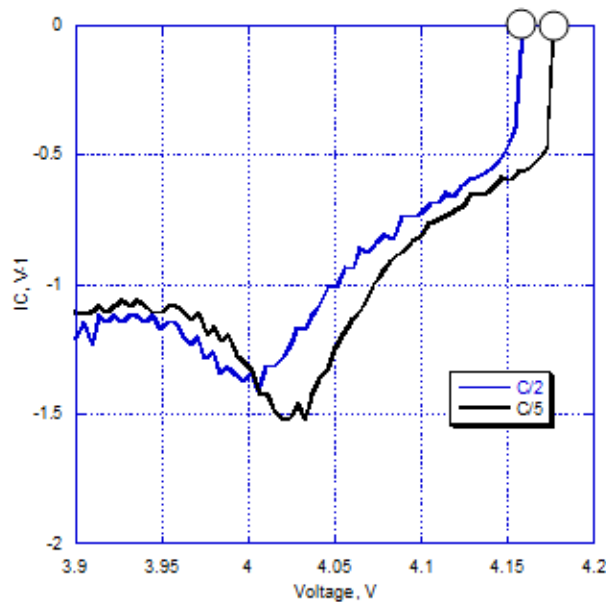


Figure 86 Incremental capacity curve used for polarization resistance calculation

Figure 87 and Table 5 display distributions and information on the polarization resistance calculated from the current induced drop between two different rates. IHR cells show much higher values with a broader spread. After investigation, it has been found that it must be due to the homemade racks used during the conditioning cycles. In fact, these same racks showed huge resistance values comparing to the ones used on the other tester for the exact same kind of tests (i.e. same kind of battery doing the same protocol). For the next test, some Arbin Universal Battery Holders® with very low resistance have been used.

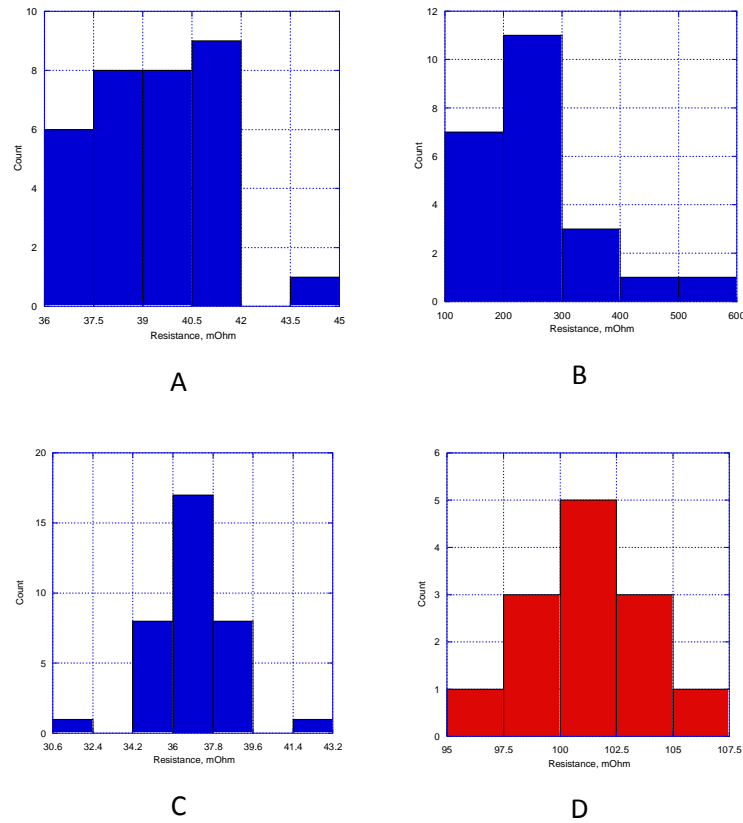


Figure 87 Resistance distribution for (A) IMR, (B) IHR, (C) IBR, (D) INL

Cell	IMR	IHR	IBR	INL
Average (mΩ)	39.4	261.8	37	102.9
Standard deviation (%)	4.6	40	4.8	6

Table 15 Resistance averages and standards deviation

7.4 Methods for determining the SOC in Li-ion batteries

7.4.1 Accuracy of the ps-OCV=f(SOC) curves

GITT and PITT methods being time consuming, different approaches are used experimentally to determine ps-OCV=f(SOC) curves. As mentioned previously, sufficiently low rate cycles (C/25 or lower) can be used. The next paragraphs document a comparison of these techniques on a 1.9 Ah 18650 lithium-ion cell using a BioLogic VMP3 tester. Results on their duration and accuracy are then discussed.

7.4.1.1 GITT test protocol

The first step in the procedure is to charge the battery using a constant current (CC) step at C/2 followed by a constant voltage (CV) step at 4.275 V until the terminating current drops below C/200. The cut-off voltage in charge is a little bit higher than the one specified in the manufacturer's specs in order to reach a fully charge state. Then the battery is discharge at C/20 (i.e. 95mA) for 12 minutes with 4-h rest period between each discharge until a relatively low voltage of 2.3 V. The cell is finally recharged using the same process, C/20 and 4-h rest periods, until 4.275 V. Figure 88 illustrates the voltage profile obtained after the full GITT cycle. Thus a sufficiently accurate curve of one hundred points for the charge and the discharge will be taken into account to obtain the ps-OCV=f(SOC) curve. Only the relaxed cell voltages are taken into account in the linear interpolation for calculating the ps-OCV=f(SOC) curve. Then an average of the charge and discharge relax cell voltage curves within the same voltage range is performed.

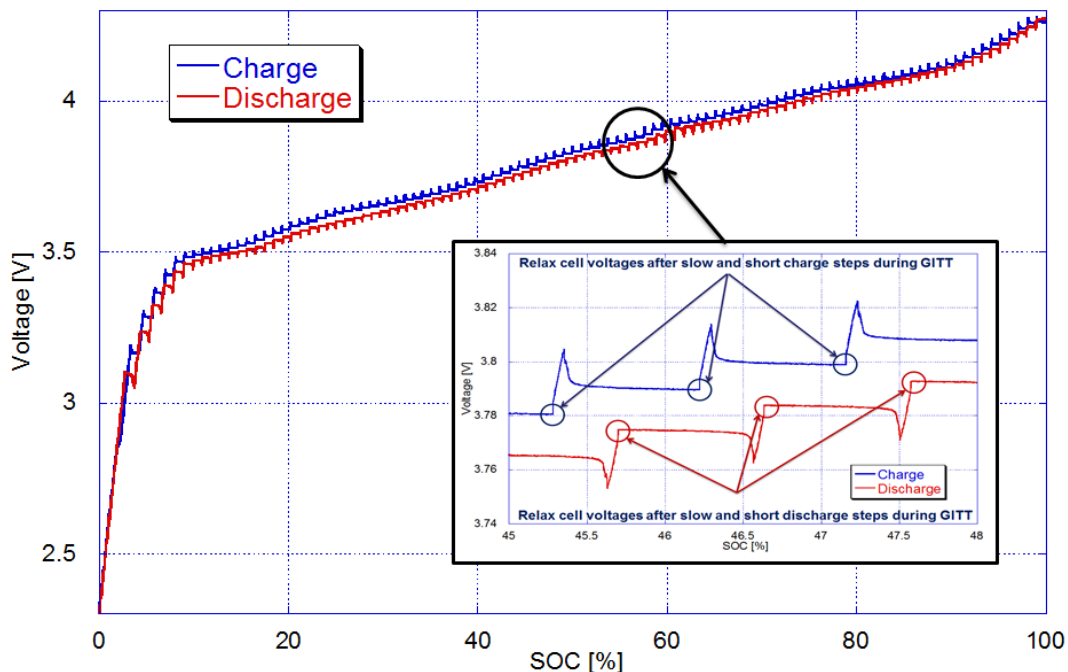


Figure 88 GITT cycle with zoom on relax cell voltages used for ps-OCV=f(SOC) curve

7.4.1.2 C/25-rate test protocol

A C/25-rate cycle on an extended voltage range can also be used to obtain the ps-OCV=f(SOC) curve derived by averaging the voltage between its charge and its discharge branches. At this rate, the effect of the resistance can be neglected, as it is seen on Figure 89 which shows the difference in voltage between C/2 and C/25-rate charge and discharge curves. Thus it can be assumed that each electrode is at an equilibrium state at each step. Lowering the rate would obviously reduce the resistance effect between the charge and discharge curves. However the duration of the test would be increased.

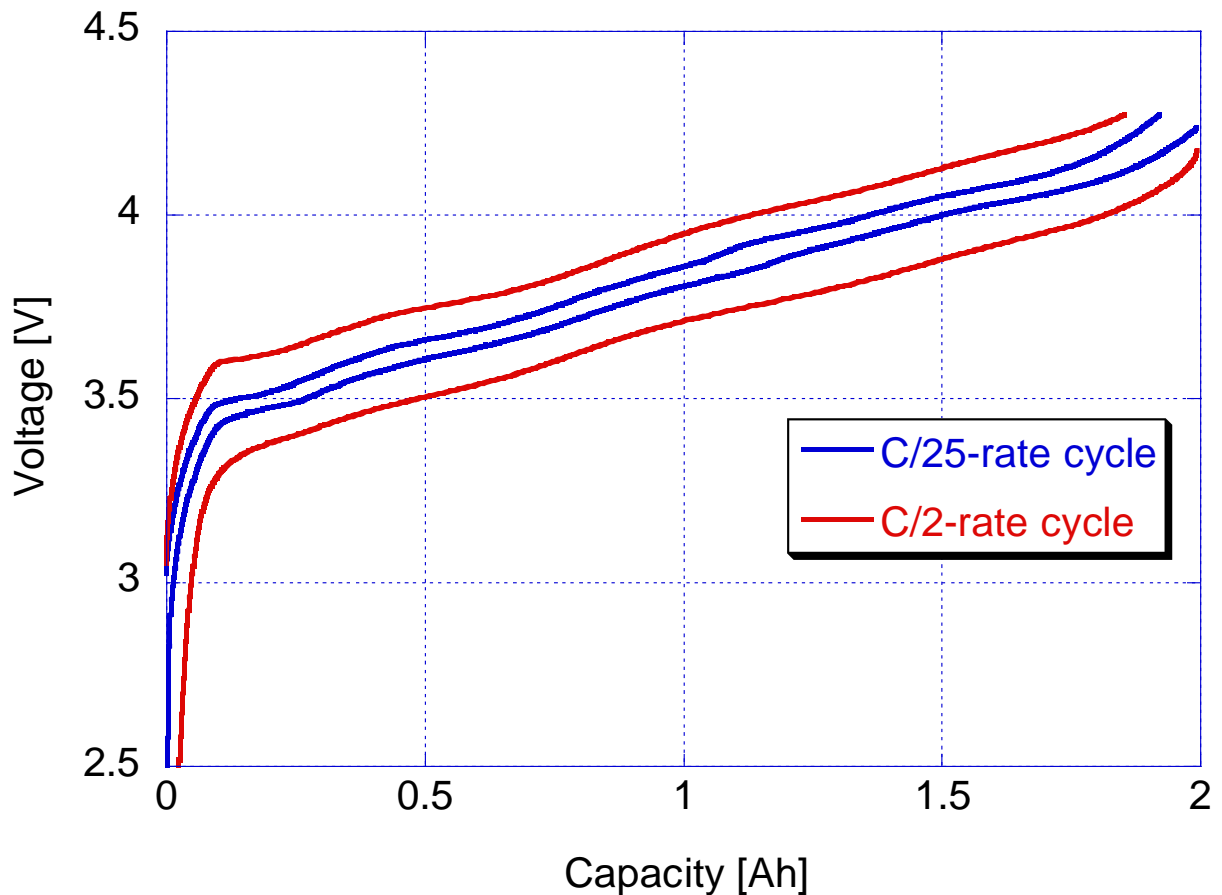


Figure 89 C/25 and C/2 rate cycles

7.4.1.3 Comparison

When the two ps-OCV=f(SOC) curves obtained from the described methods are plotted on the same figure, they appear similar, as we can judge on Figure 90. There might be some small voltage differences of the order of magnitude of the μV but that does not even correspond to more than 0.5 % when converted to SOC. In term of duration of testing time, the GITT took approximately 35 days whereas the C/25-rate cycle last only 3 days. Thus, the first conclusion that can be drawn is that the GITT

is way too long and does not give more accuracy than a C/25-rate cycle for SOC determination from the $ps-OCV=f(SOC)$ curve. Furthermore the GITT requires more computational work since a linear interpolation has to be realized from the retained relax voltage points. Thereafter, SOC's will be determined by reporting the RCVs on the $ps-OCV=f(SOC)$ curve obtained by averaging the C/25-rate cycle charge and discharge curves.

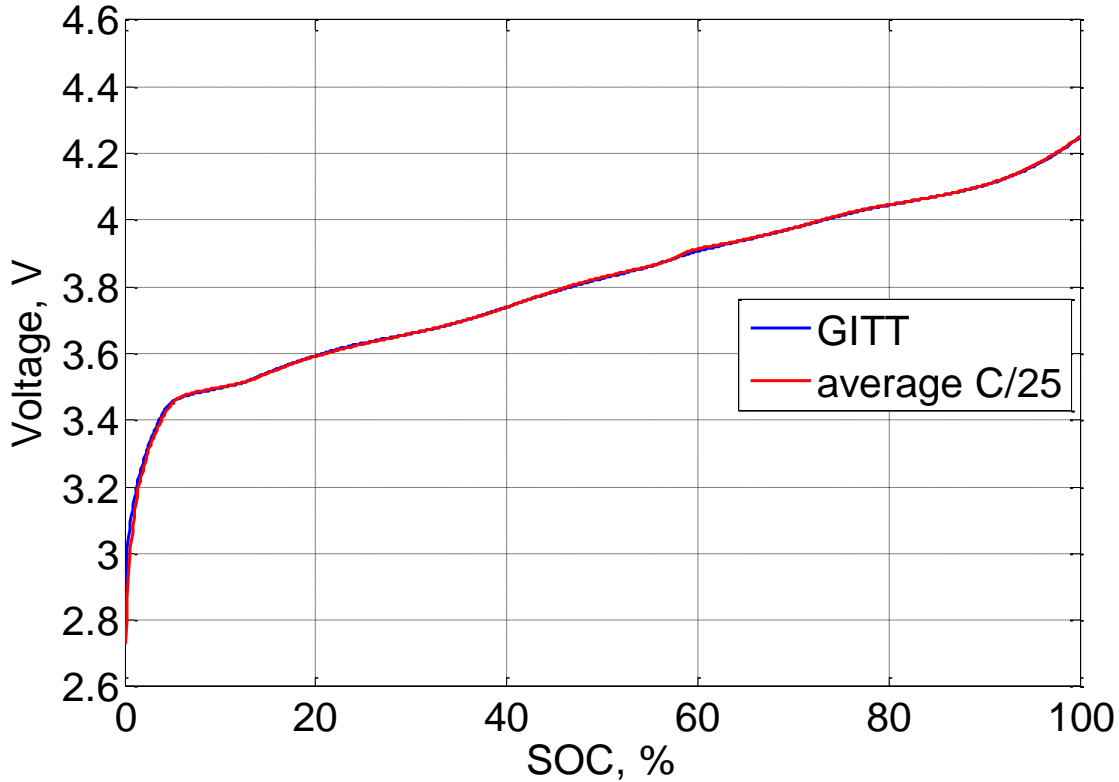


Figure 90 Comparison of OCV vs. SOC curves obtained from GITT and C/25-rate cycle

7.4.2 Techniques to derive model for SOC estimation

Different techniques based on the two previous methods exist to derivate models to help determining the SOC of a Li-ion cell. This part presents a selection of these techniques.

7.4.2.1 Artificial neural network

An Artificial Neural Network (ANN) is an information processing paradigm that is inspired by neuron operation in biological systems, as a simple imitation of human brain. ANNs, like people, learn from examples. It is configured for a specific application, such as pattern recognition or data classification, through a learning process. Due to its simplicity in handling data from, and structure of complex, or even unknown system, ANN has become one of the most widely used methods in complex

system modeling. In fact, it is like a black box approach that needs training data, Figure 91. The larger is the training database the more effective the network will be.

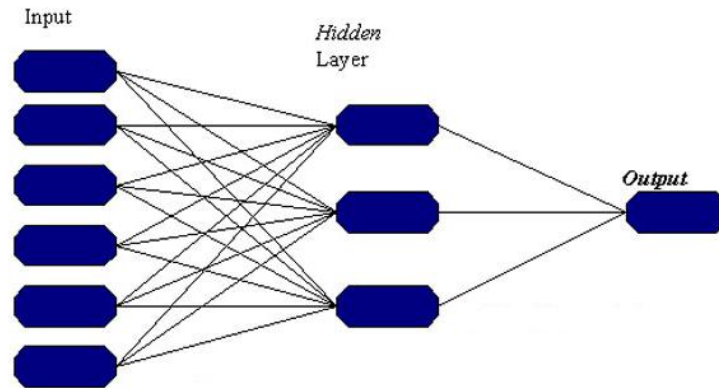


Figure 91 Artificial Neural Network

A typical simple neural network consists of three layers: an input layer, a hidden layer and an output layer. Depending on the specific needs, such as number of inputs and outputs, the number of nodes within different layers can be defined, for convenience or out of necessity. The lines connecting each pair of nodes are denoted as weights, which are literally mapping functions from one space to another²⁶.

Neural network techniques are useful in estimating battery performance which depends on quantifying the effect of numerous parameters (e.g. voltage level, temperature, discharge rate, age of the cell, etc), especially when most of which cannot be defined with mathematical precision^{58,59}. Algorithms are refined with the help of experience gained from the performance of other similar batteries⁹, they can be utilized without knowledge of the cell as long as the net training data is available. However, most of the erected traditional ANN based SOC determination models are offline, which cannot predict a cell's SOC in real time, and the data collection for accurate results takes ages⁵⁹.

7.4.2.2 Impedance spectroscopy and equivalent circuit model

This technique measures the impedance of a system over a range of frequencies. During the cell charge/discharge cycles the composition of the active chemicals in the cell changes as the chemicals are converted between the charged and discharged states; and this will be reflected in changes to the cell impedance. Analyzing the frequency response, Figure 92a, of the system allows finding out internal parameters value, such as capacitance and resistances, Figure 92b. Then an equivalent circuit for SOC estimate can be developed, Figure 93. The resistance R1 represents the resistance induced by the casing

and the wires; the two RC circuits are the electrodes, where C2 and C3 show the positive and negative electrode responses.

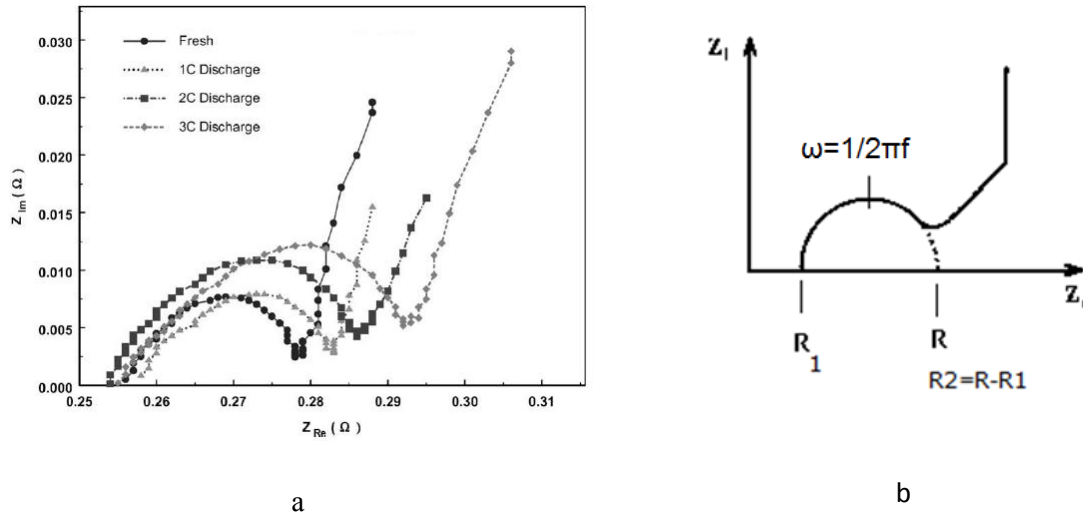


Figure 92 Nyquist plot obtained with impedance spectroscopy frequency response, (a) and parameters identification (b)

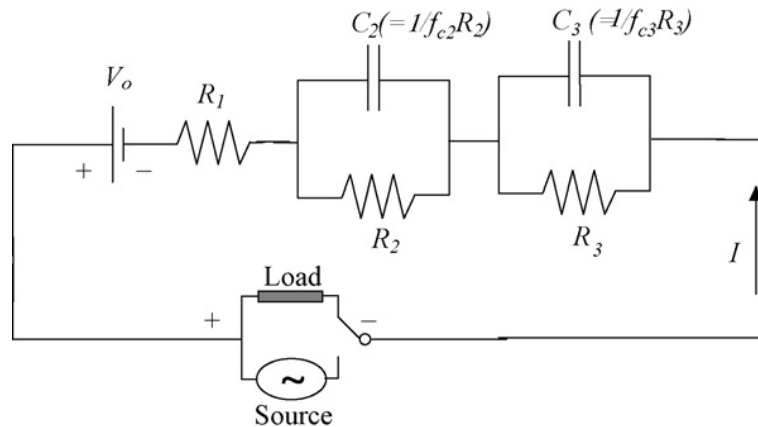


Figure 93 Li-ion battery equivalent circuit model

Measurements of cell internal impedance can also be used to determine SOC. Moreover, they can also reveal kinetics of active materials and provide implication SOH estimation if performed during cell aging. However they are not widely used due to difficulties in measuring the impedance while the cell is active as well as difficulties in interpreting the data since the impedance is also extremely temperature dependent⁹. Furthermore, the frequency response depends on the SOC level, which means that the measurement should be done on the whole SOC range.

7.4.2.3 Kalman filters

Kalman filtering is a technology for dynamic state system estimation which is used for producing estimates from the true values of measurements, Figure 94. It is based on a set of recursive equations that are repeatedly evaluated as the system operates.

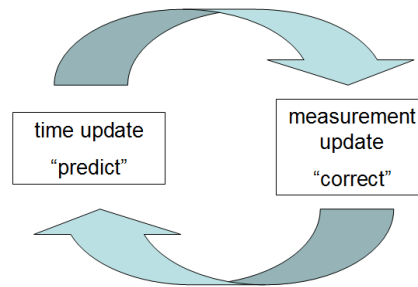


Figure 94 Principle of Kalman filter

Kalman filters (KF) are commonly used in many fields like: target tracking, global positioning, dynamic system control, navigation and communication. Although the KF algorithm is very efficient for linear dynamical systems, it is very limited for non-linear systems, and state transitions and measurements are rarely linear in practice. However, another version called the extended Kalman filter (EKF) allows applying the standard linear KF methodology to a linearization of the true nonlinear system. By using partial derivatives and Taylor series expansion, EKF linearizes the “Predict” and “Update” functions for current estimates. Additionally, the EKF has the advantages of the use of probability, which is the best way to estimate the highly non-linear internal states of systems like LIBs^{28,60-63}.

Models for SOC estimation of LIBs that are employed with KF are usually composed of two state transition equations: SOC and voltage; and one measurement: the OCV at the terminal of the cell. The SOC model is derived from the Coulomb Counting method, and is thus capacity based. On the other hand, the voltage model comes from the application of the Kirchhoff’s laws on the equivalent circuit model^{64,65}.

With the KF, a dynamic SOC inference can be provided, and uncertainty lower than 1% could be claimed^{9,66,67}. In addition, the algorithm gives indications on the error bound of the estimate with the help of state uncertainty matrices, which offer extra information on voltage plateaus for example. Also, the more measurements we have the more control on the model we can enjoy (i.e. current and capacity

models could be added to the state transition system). However, one of the biggest drawbacks is the need of a very accurate model of the LIB as well as the difficulty to determine the initial parameters.

7.4.2.4 Fuzzy logic

Fuzzy logic is a form of logic that deals with approximate rather than fixed data. In fact data may be categorized in two different ways: ‘crisp’ or ‘fuzzy’. Crisp sets categorize data with certainty, e.g., a temperature of 30°C. On the other hand fuzzy data is uncertain, e.g., the temperature is ‘warm’. This linguistic descriptor ‘warm’ can cover a range of temperatures and the degree to which a crisp data point falls into the fuzzy set of “warm” is indicated by a fit value (fuzzy unit) between zero and one. Ranges are defined by membership functions. The degree to which an element of the temperature set belongs to the fuzzy subset ‘warm’ is indicated by a quantity referred to as its ‘degree of membership’. Figure 95 illustrates an example of three subsets, defined by their membership functions, ‘cold’, ‘warm’, and ‘hot’. The concept can thus be easily adapted to the SOC of a battery between the three states ‘charged’, ‘half charged’ and ‘discharged’.

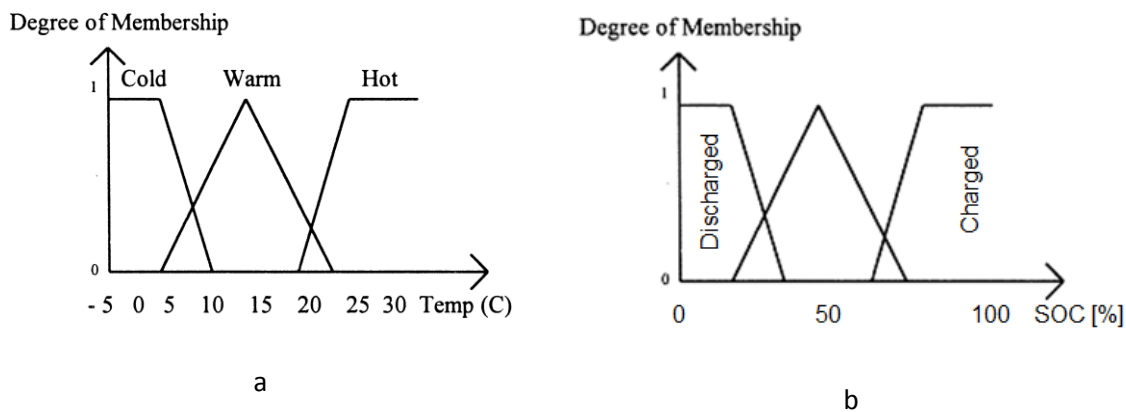


Figure 95 Membership functions for (a) temperature and (b) SOC

The process of determining the fit values of the real-valued data is referred to as ‘fuzzification’ of the data. A fuzzy system is illustrated in Figure 96 in which both the inputs and outputs are crisp sets (real-values). The fuzzy system has four conceptual components: a rule base describing the relationship between input and output variables, a database that defines the membership functions for the input and output variables, a reasoning mechanism that performs the inference procedure, and a defuzzification block which transforms the fuzzy output sets to a crisp (real-valued) output. The rules relating the input and the output variables are written in an ‘if . . . then’ linguistic format such as ‘if temperature is hot and discharge rate is high then output is low’.

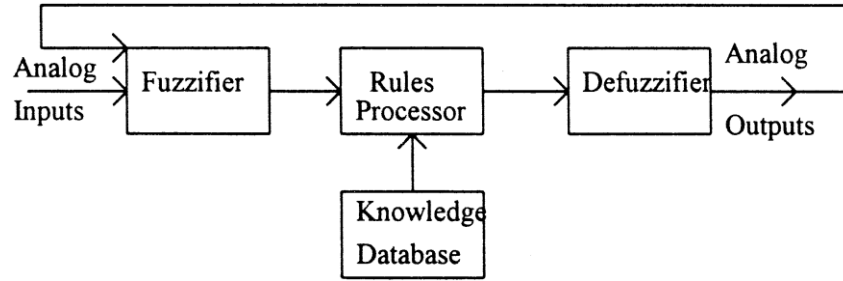


Figure 96 A complete fuzzy inference system

From this understanding, fuzzy logic is a powerful tool for non-linear systems and noisy data without the need of accurate mathematical model. Thus it seems great to handle complicated relationship between operating conditions and battery SOC. The biggest issue in this method is the membership functions and rule sets because they have to be described by an expert or generated by an ANN⁶⁸.

7.4.3 Summary

All the methods and techniques to determine SOC presented previously have advantages and drawbacks. They are all summarized in the following tables.

7.4.3.1 Methods

Method	Advantages	Drawbacks
<i>Coulomb Counting</i>	<ul style="list-style-type: none"> ▪ Online ▪ Easy to implement ▪ Accurate if good reference point is available 	<ul style="list-style-type: none"> ▪ Use of nominal capacity ▪ Require accurate current measurement ▪ Cost intensive for accurate current measurement ▪ Needs regular re-calibration points ▪ Difficult to calibrate ▪ Accumulative error ▪ Do not accommodate capacity fade
<i>Open Circuit Voltage</i>	<ul style="list-style-type: none"> ▪ Online ▪ Cheap 	<ul style="list-style-type: none"> ▪ Not usable during dynamic operation

	<ul style="list-style-type: none"> ▪ More direct inference than the coulomb counting ▪ More accurate measurement from voltage than current 	<ul style="list-style-type: none"> ▪ Needs long rest times ▪ Accuracy issues on voltage “plateaus”
--	--	--

7.4.3.2 Techniques

Technique	Advantages	Drawbacks
<i>Artificial Neural Network</i>	<ul style="list-style-type: none"> ▪ Do not need knowledge of the internal structure ▪ “Black box” approach ▪ Simplicity in algorithm development 	<ul style="list-style-type: none"> ▪ Needs data of similar batteries ▪ Accuracy depends on the training data ▪ Offline
<i>Impedance Spectroscopy & Equivalent Circuit Model</i>	<ul style="list-style-type: none"> ▪ Gives info on active materials within the cell ▪ May provide implication for SOH estimation¹⁷ 	<ul style="list-style-type: none"> ▪ Difficult to measure impedance while cell is active ▪ Very temperature sensitive ▪ Difficult to correlate impedance with SOC (esp. with aging)
<i>Kalman Filter</i>	<ul style="list-style-type: none"> ▪ Online ▪ Can handle dynamic situation for real-time estimate ▪ Indication of the error bound on the estimate (state uncertainty matrix) 	<ul style="list-style-type: none"> ▪ Needs substantial computing capacity and power ▪ Needs a suitable Li-ion battery model ▪ Difficulty in determining initial parameters ▪ Reference drifting over aging
<i>Fuzzy Logic</i>	<ul style="list-style-type: none"> ▪ Method amenable to determining battery condition regardless of which techniques of measuring is employed ▪ Can handle complicated 	<ul style="list-style-type: none"> ▪ Difficult to develop membership functions and rules (must be described by an expert or may be generated by ANNs)

	<p>relationship between operating conditions and SOC</p> <ul style="list-style-type: none"> ▪ Good for nonlinear model ▪ Do not need explicit mathematical models ▪ Hardware requirements are minimized ▪ Good for nonlinear system ▪ Do not need explicit mathematical models 	
--	---	--

7.4.3.3 Conclusions on methods and techniques to derive SOC estimation model

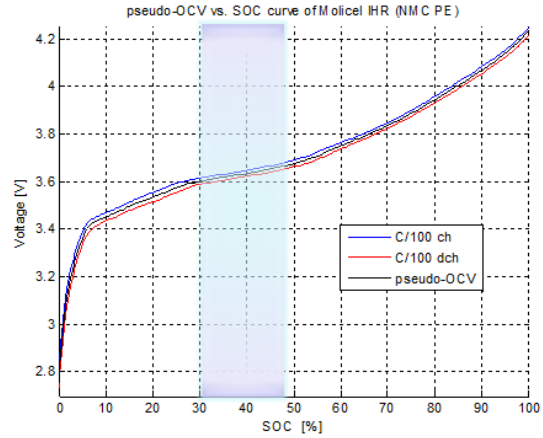
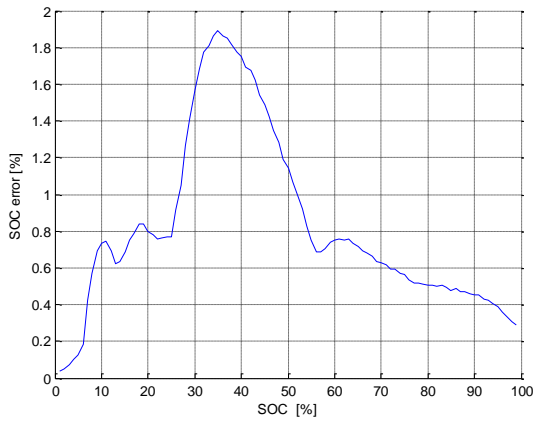
This chapter has presented a short overview of the existing methods and techniques for evaluation of SOC with special emphasis on LIBs. There is unfortunately no single best method since they all come with their merits and drawbacks:

- The most used technique at this time for all system is ampere hour counting because it is the most direct and easily implemented method.
- The determination of SOC by the means of impedance spectroscopy is still subject to debate because of its temperature sensitivity and the difficulty of its online implementation.
- The new promising methods for dynamic SOC estimate are the Kalman filter (that gives perspective for high dynamic usage), the artificial neural networks (with training data) and the fuzzy logic.
- Finally, the most accurate method and the one that is mostly going to be used in this thesis work is the open circuit voltage even though it works only and only if the cell reaches or is close to an equilibrium state^{69,70}. In other words, only relax cell voltages (RCV) will be considered for SOC determination, which means that the Li-ion cell has to relax for a long enough period that allows reaching a thermodynamic equilibrium and, thus, stable electrode potentials. Consequently, SOC determination will thereafter implicitly signify t-SOC determination.

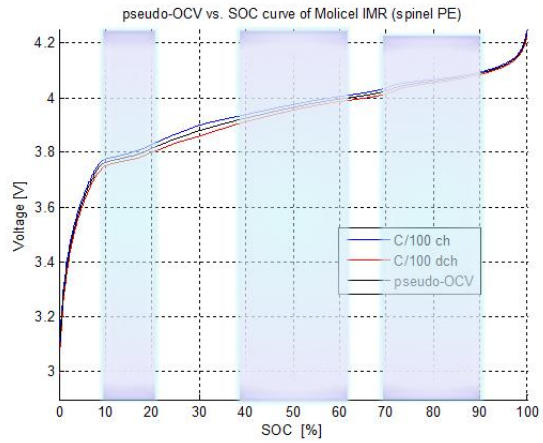
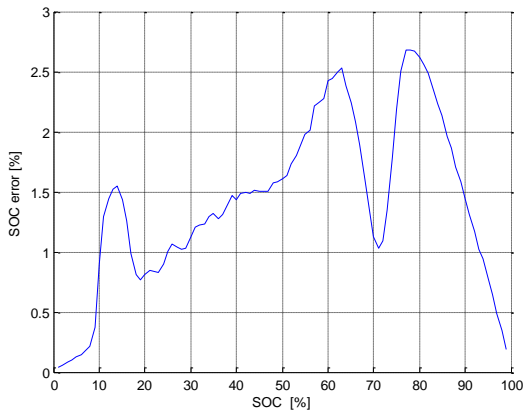
7.4.4 Uncertainty of SOC estimation using ps-OCV=f(SOC) curves for pack and single cell

This part summarizes the uncertainty on the SOC estimation for each Li-ion cell chemistry introduced in chapter 1 as well as the uncertainty zones on the ps-OCV=f(SOC) curves with a voltage measurement of ± 3 mV accuracy.

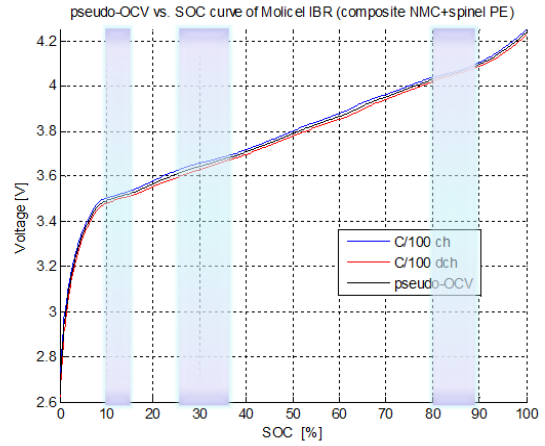
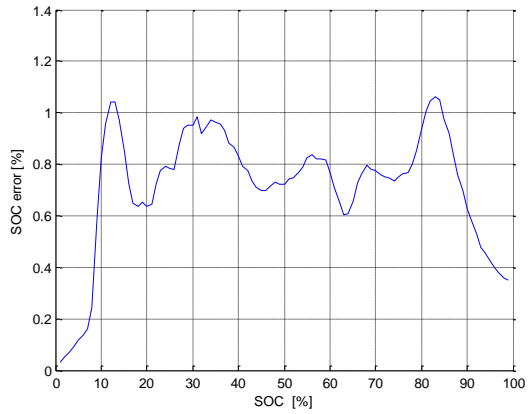
7.4.4.1 NMC PE (IHR)



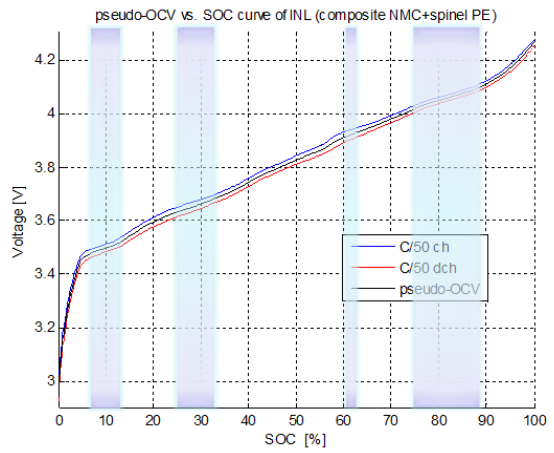
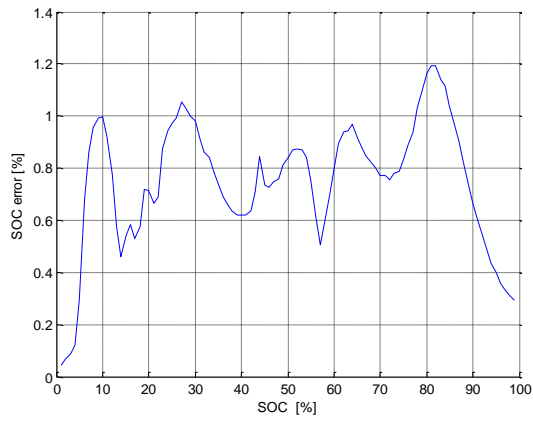
7.4.4.2 Spinel PE (IMR)



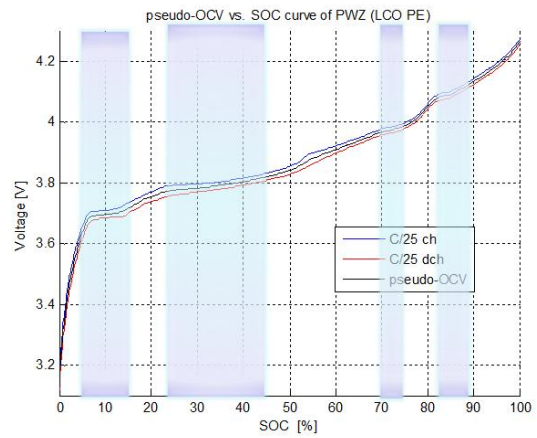
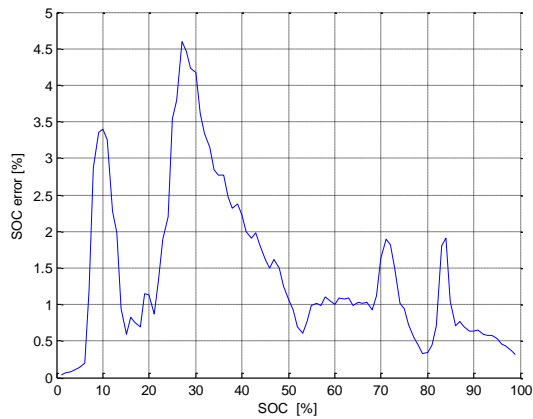
7.4.4.3 NMC+spinel PE (IBR)



7.4.4.4 NMC+spinel PE (INL)



7.4.4.5 LCO PE



7.5 Pack SOC

7.5.1 Summary of the 5 pack SOC methods

The two following tables provide a summary of the equivalent system to each pack-SOC estimation method, Table 16, as well as their merits and drawbacks, Table 17.

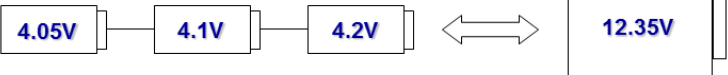


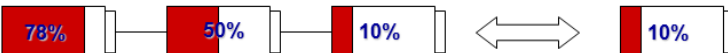

Method	Equivalent system	
Pack pseudo-OCV		
Average single cell RCVs		
Average single cell SOCs		
Single cell Min		
Single cell Max		

Table 16 Equivalent system to each pack-SOC estimation method

Method	Advantages	Drawbacks
Pack pseudo-OCV	<ul style="list-style-type: none"> • Direct inference of SOC from pack voltage • Really shows pack degradation 	<ul style="list-style-type: none"> • Need ps-OCV=f(SOC) curves during aging
Average single cell RCVs	<ul style="list-style-type: none"> • Pack is considered as a single cell 	<ul style="list-style-type: none"> • Imbalance of cells within pack not taken into account • Degradation of all cells assumed to be the same
Average single cell SOCs	<ul style="list-style-type: none"> • Pack is considered as a single cell • SOC imbalance can be detected 	<ul style="list-style-type: none"> • Imbalance of cells within pack not taken into account • SOC has to be calculated for each cell
Single cell Min	<ul style="list-style-type: none"> • Pack is considered as a single cell 	<ul style="list-style-type: none"> • Pack limited to limiting factor
Single cell Max	<ul style="list-style-type: none"> • Pack is considered as a single cell 	<ul style="list-style-type: none"> • Pack is considered as a single cell

Table 17 Advantages and drawbacks summary

7.5.2 SOC results per method

The resistance in the circuit allows checking the exact current going through the battery pack by measuring its voltage and using the Ohm's law. Since a high power channel was used for these tests (0-15 V and 15 A) for voltage requirements, the low current asked for C/25-rate cycles as well as remnant capacity at C/25 (~75 mA) were not very accurate and gave wrong capacities that had to be corrected, Table 18. The initial maximum discharge capacity of the pack at C/25 was found to be 1.8882 Ah after correction; this value will be taken as the maximum capacity that the pack can deliver.

Rate	Capacity given by Maccor tester (Ah)	Corrected capacity (Ah)
C/25	1.7903	1.8882
Remnant capacity of C/5	0.0663	0.0681
Remnant capacity of C/2	0.1068	0.1267
Remnant capacity of C	0.1189	0.1404
Remnant capacity of 3/2C	0.1398	0.1432
Remnant capacity of 2C	0.1330	0.1569
Remnant capacity of 5/2C (5A)	0.1925	0.1976

Table 18 C/25 capacity correction using the resistance in the circuit

7.5.2.1 SOC results method #1: Packs $ps-OCV=f(SOC)$ curve

With this first method, the pack is considered as a single cell. Therefore, the C/25-rate cycles performed initially and during the test allow to calculate the $ps-OCV=f(SOC)$ curves; and the relax pack voltages (RPVs) of the subsequent discharge rates allow to decipher the SOC as well as the SOC range of the pack. Since this pack has not been subjected to many cycles, all its $ps-OCV=f(SOC)$ curves are identical. Figure 97 shows the initial one.

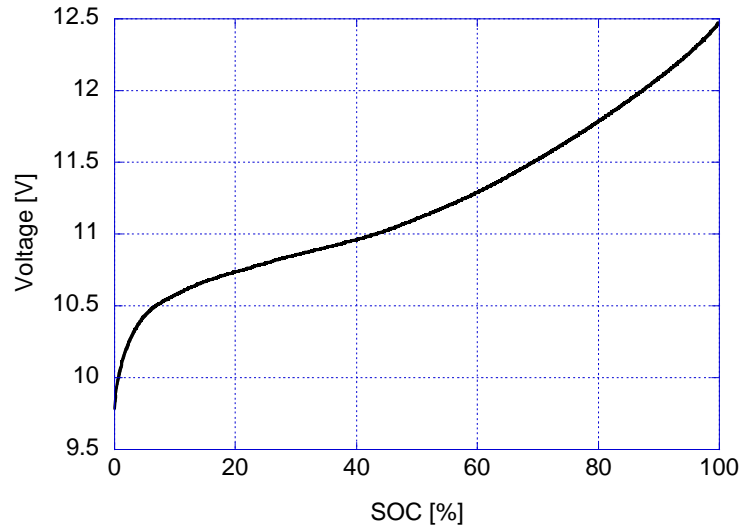


Figure 97 ps-OCV=f(SOC) curve of IHR pack

Table 19 summarizes the SOC_s at the EOC and EOD for all rates, both after relaxation, according to the pack ps-OCV=f(SOC) curve.

Rate	Capacity (Ah)	EOC-OCV (V)	EOC SOC (%)	EOD-OCV (V)	EOD SOC (%)
C/5	1.7684	12.4363	99.2883	10.3001	3.4631
C/2	1.7487	12.4470	99.1993	10.4630	6.1985
C	1.7362	12.4488	99.2365	10.4779	6.6530
3/2C	1.6835	12.4248	99.2726	10.520	8.2383
2C	1.7092	12.4198	98.6268	10.5081	7.7818
5/2C	1.6475	12.4333	99.2276	10.5793	11.1023

Table 19 EOC and EOD SOC_s from method #1

7.5.2.2 SOC results method #2: RPV/3 and single cell ps-OCV=f(SOC) curve

Here the pack is treated as a single cell. This involves doing the three following assumptions:

- All the cells are identical to the NSC,
- All cells were at the exact same SOC when put in the string,
- Cells are degrading on the exact same way and at the same rate.

Therefore, the pack voltage is divided by 3 and the ps-OCV=f(SOC) curve of the NMC is used for SOC determination (calculated during the initial characterization. The SOC_s inferred are sum up in Table 20.

Rate	Capacity (Ah)	EOC-OCV (V)	EOC SOC (%)	EOD-OCV (V)	EOD SOC (%)
C/5	1.7684	4.1454	95.18	3.4334	6.51
C/2	1.7487	4.149	95.41	3.4877	12.52
C	1.7362	4.1496	95.45	3.4926	13.05
3/2C	1.6835	4.1416	94.93	3.5067	14.66
2C	1.7092	4.1399	94.82	3.5027	14.19
5/2C	1.6475	4.144	95.09	3.5009	13.96

Table 20 EOC and EOD SOC from method #2

7.5.2.3 SOC results method #3: Average SOC

In this method, each cell is treated separately using its own RCVs and the ps-OCV=f(SOC) curve of the single cell (like in method #2); the 3 SOC are then averaged to give the pack SOC. Voltages of each cells are recorded by auxiliary voltage channels. Table 21 summarizes the SOC of each cell at each rate and shows the SOC average retained for the method #3.

rate	EOC-OCV (V)	EOC SOC (%)	EOC Pack SOC (average)	EOD-OCV (V)	EOD SOC (%)	EOD Pack SOC (average)
C/5	4.2238	99.47	94.60	3.5128	15.45	10.90
	4.2020	98.43		3.5064	14.63	
	4.0199	85.89		3.2888	2.63	
C/2	4.2236	99.46	94.80	3.5318	18.07	13.66
	4.2116	98.90		3.5300	17.83	
	4.0218	86.05		3.4093	5.08	
C	4.2243	99.49	94.85	3.5343	18.40	14.05
	4.2127	98.96		3.5326	18.19	
	4.0222	86.09		3.4193	5.56	
3/2C	4.2233	99.45	94.38	3.5496	20.41	15.52
	4.1938	98.01		3.5391	19.02	
	4.0172	85.68		3.4402	7.12	
2C	4.2129	98.97	94.30	3.5421	19.43	15.06
	4.2024	98.45		3.5408	19.25	
	4.0146	85.47		3.4334	6.51	
5/2C	4.2222	99.40	94.56	3.5644	22.27	17.90
	4.2022	98.44		3.5595	21.64	
	4.0192	85.84		3.4632	9.79	

Table 21 EOC and EOD SOC from method #3

7.5.2.4 SOC results method #4: Minimum SOC

In this method cells are treated separately like in method #3 but it is now believed that the pack is driven by the cell that shows the minimum SOC. In our case, it is the cell #3, in red in Table 22.

rate	EOC-OCV (V)	EOC SOC (%)	EOD-OCV (V)	EOD SOC (%)
C/5	4.2238	99.47	3.5128	15.45
	4.2020	98.43	3.5064	14.63
	4.0199	85.89	3.2888	2.63
C/2	4.2236	99.46	3.5318	18.07
	4.2116	98.90	3.5300	17.83
	4.0218	86.05	3.4093	5.08
C	4.2243	99.49	3.5343	18.40
	4.2127	98.96	3.5326	18.19
	4.0222	86.09	3.4193	5.56
3/2C	4.2233	99.45	3.5496	20.41
	4.1938	98.01	3.5391	19.02
	4.0172	85.68	3.4402	7.12
2C	4.2129	98.97	3.5421	19.43
	4.2024	98.45	3.5408	19.25
	4.0146	85.47	3.4334	6.51
5/2C	4.2222	99.40	3.5644	22.27
	4.2022	98.44	3.5595	21.64
	4.0192	85.84	3.4632	9.79

Table 22 EOC and EOD SOC from method #4

7.5.2.5 SOC results method #5: Maximum SOC

In this method cells are treated separately like in method #3 but it is now believed that the pack is driven by the cell that shows the maximum SOC. In our case, it is the cell #1, in blue in Table 22.

7.5.3 Pack capacity ration results per method

Considering that the pack will reach 0% SOC at the end of the low rate discharge step of the RCT test, the remnant capacity as well as the remnant SOC range will allow the calculation of the pack

capacity ration of the remnant capacity step. The obtained value will then be compared to the pack capacity ration, Q_{R_pack} (18.882 mAh.%SOC⁻¹ from the maximum capacity withdrawn from the pack). Since this attribute is rate independent, it should be the same no matter what rate (and its corresponding SOC range) is considered. Figure 98 illustrates the comparison that will be performed. The following tables summarize the Q_R obtained at each rate for each pack-SOC method.

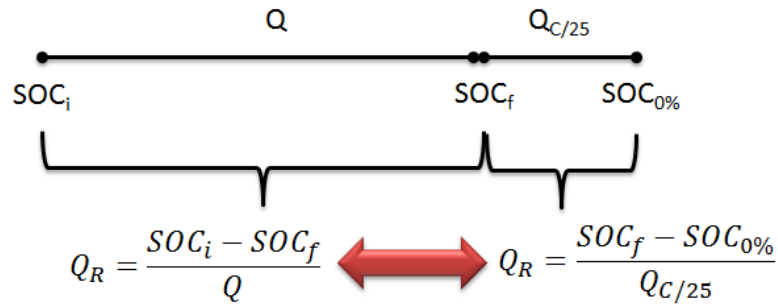


Figure 98 RCT for capacity ration calculation and comparison

7.5.3.1 Method #1: Pack ps-OCV=f(SOC) curve

Rate	Remnant Capacity (Ah)	EOD SOC (%)	Capacity ration (mAh/%SOC)
C/5	0.0681	3.4631	19.66
C/2	0.1267	6.1985	20.44
C	0.1404	6.6530	21.10
3/2C	0.1432	8.2383	17.4
2C	0.1569	7.7818	20.16
5/2C	0.1976	11.1023	17.80

Table 23 Capacity ration from method #1

7.5.3.2 Method #2: RPV/3 and single cell ps-OCV=f(SOC) curve

Rate	Remnant Capacity (Ah)	EOD SOC (%)	Capacity ration (mAh/%SOC)
C/5	0.0681	6.51	10.46
C/2	0.1267	12.52	10.12
C	0.1404	13.05	10.76
3/2C	0.1432	14.66	9.77
2C	0.1569	14.19	11.05
5/2C	0.1976	13.96	14.15

Table 24 Capacity ration from method #2

7.5.3.3 Method #3: Average SOC_s

Rate	Remnant Capacity (Ah)	EOD SOC (%)	Capacity ration (mAh/%SOC)
C/5	0.0681	10.90	6.25
C/2	0.1267	13.66	9.27
C	0.1404	14.05	9.99
3/2C	0.1432	15.52	9.23
2C	0.1569	15.06	10.4
5/2C	0.1976	17.90	11.04

Table 25 Capacity ration from method #3

7.5.3.4 Method #4: Minimum SOC

Rate	Remnant Capacity (Ah)	EOD SOC (%)	Capacity ration (mAh/%SOC)
C/5	0.0681	2.63	25.89
C/2	0.1267	5.08	24.94
C	0.1404	5.56	25.25
3/2C	0.1432	7.12	20.1
2C	0.1569	6.51	24.1
5/2C	0.1976	9.79	20.2

Table 26 Capacity ration from method #4

7.5.3.5 Method #5: Maximum SOC

Rate	Remnant Capacity (Ah)	EOD SOC (%)	Capacity ration (mAh/%SOC)
C/5	0.0681	15.45	4.41
C/2	0.1267	18.07	7.01
C	0.1404	18.40	7.63
3/2C	0.1432	20.41	7.02
2C	0.1569	19.43	8.07
5/2C	0.1976	22.27	8.87

Table 27 Capacity ration from method #5

7.6 Incremental capacity and cell degradation mechanisms analysis

7.6.1 Incremental capacity concept

When working on degradation of commercial LIB, incremental capacity analysis^{2,20} turns out to be very a good way to characterize the state of the cells without having to open them. The incremental capacity (IC) depicts a capacity change associated with a voltage step ($\Delta Q/\Delta V$) on the cell voltage range. Each peak in the $V - \Delta Q/\Delta V$ plot (also called IC curve) features the dynamic between different electrochemically-active phases in the electrodes. In other words, IC curves allow us to probe any gradual changes in the electrochemical behavior of a Li-ion cell during cycle-life test with greater sensitivity than those based on the conventional charge and discharge curves²⁰. The advantage of the IC analysis is achieved by transforming either the voltage plateaus or inflection points on V vs. Q curves into clearly identifiable $\Delta Q/\Delta V$ peaks on the IC curves. By monitoring the evolution of those $\Delta Q/\Delta V$ peaks upon cycling we can yield key information on the behavior of the cell chemistry. Figure 99 shows hypothetical evolutions of the IC curves upon cycling under the major modes of capacity fade^{2,13,32,41}: (a) the loss of lithium inventory, (b) the loss of active material, (c) the increase of polarization resistance, (d) the under-discharge.

In the case of loss of lithium inventory (a), the loss in intensity in one IC peak is made up with the gain in another IC peak but the overall area of peaks (i.e. the capacity) remains constant. This suggests that the amount of active material has not been compromised and that some cyclable Li^+ ions were lost. More details on this phenomenon on Li-ion cells using composite positive electrodes are given by Dubarry et al.¹³ and on LFP Li-ion cells by Safari et al.³². The effect of the loss of active material (b) results in the reduction of intensity of all IC peaks in proportion to their initial value. Besides, if some IC peaks shift towards lower voltages in discharge (or higher voltage in charge), a change of the cell impedance can be easily identified, (c). Finally, if the IC curves get broader upon cycling and/or does not reach $0 \text{ Ah}\cdot\text{V}^{-1}$ at the end of discharge (or at the end of charge), then it indicates some capacity loss due to under-charge (or under-discharge), (d). Information about the kinetics of the electrodes can also be deciphered, usually by a decrease of the slope of the IC peaks, and thus broader peaks. It points out a difficulty for the electrochemical reactions to occur at their corresponding voltage.

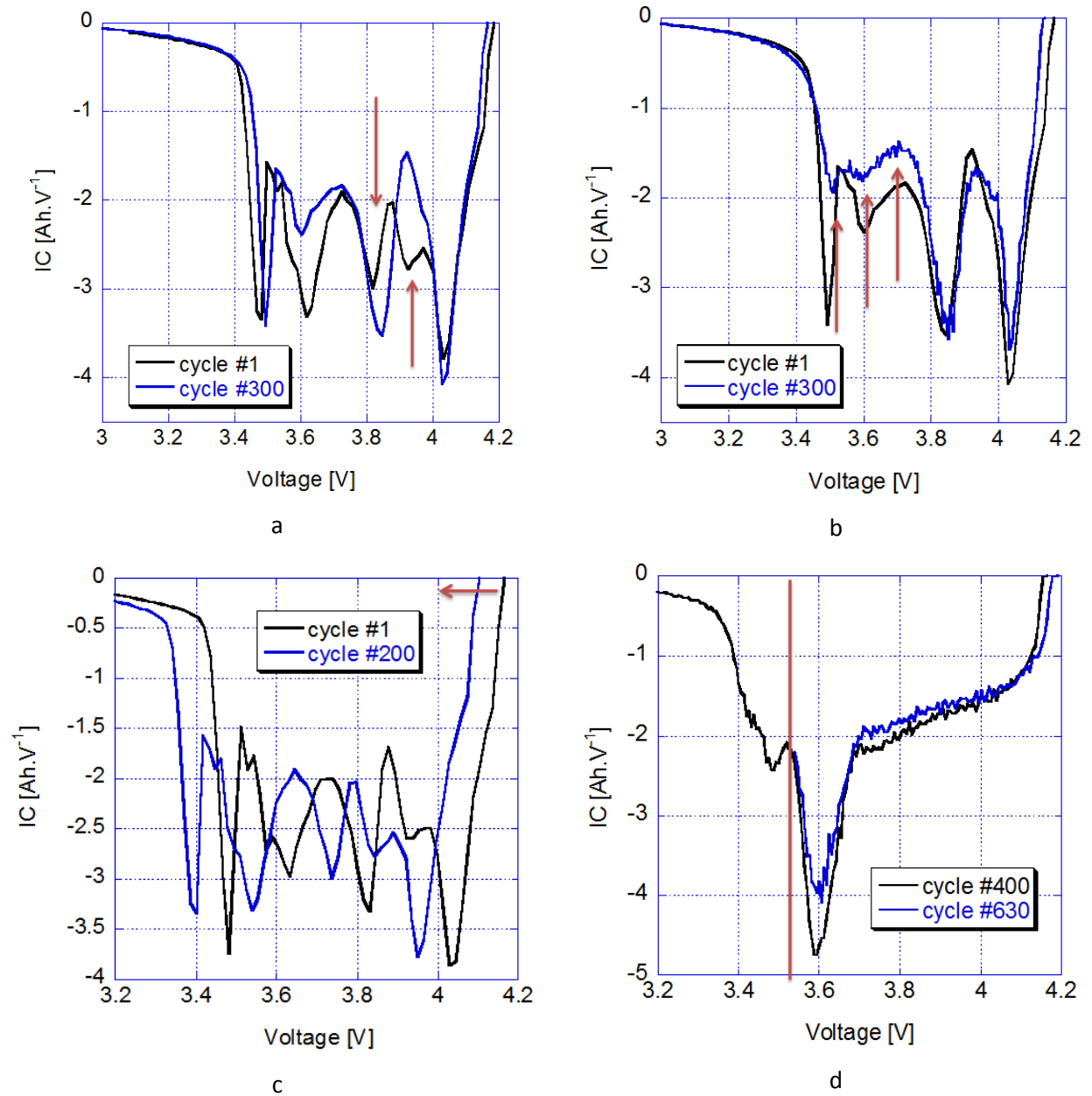


Figure 99 Incremental capacity analysis on major modes of capacity fade

The main difficulty in IC analysis lies in the fact that all of these degradation modes do not happen separately during cycle aging. However, they do not develop simultaneously either and usually occur at different rates, allowing us to keep track of their evolutions. Another delicate task to face when dealing with IC analysis is the peak indexation (i.e. association of electrochemical reactions to each IC peak). As it has been explained in chapter 2, each plateau on the V vs. Q curve corresponds to a specific phase transformation, and yet, when working with Li-ion cells containing binary electrodes, the IC peaks of the positive electrode convolutes with the ones of the negative electrode, making the interpretation

of each of them tough. Further details on the IC peak index have been published³⁰. It is important to note that some of the IC peaks can be used as direct status indicators for an electrode (or a constituent, when using composite electrodes) and some cannot because of the negative and positive electrode convolution.

As an example, Figure 100 displays the peak indexation of the INL cells (using the composite electrode of spinel and NMC materials). Next paragraphs illustrates other cell chemistries.

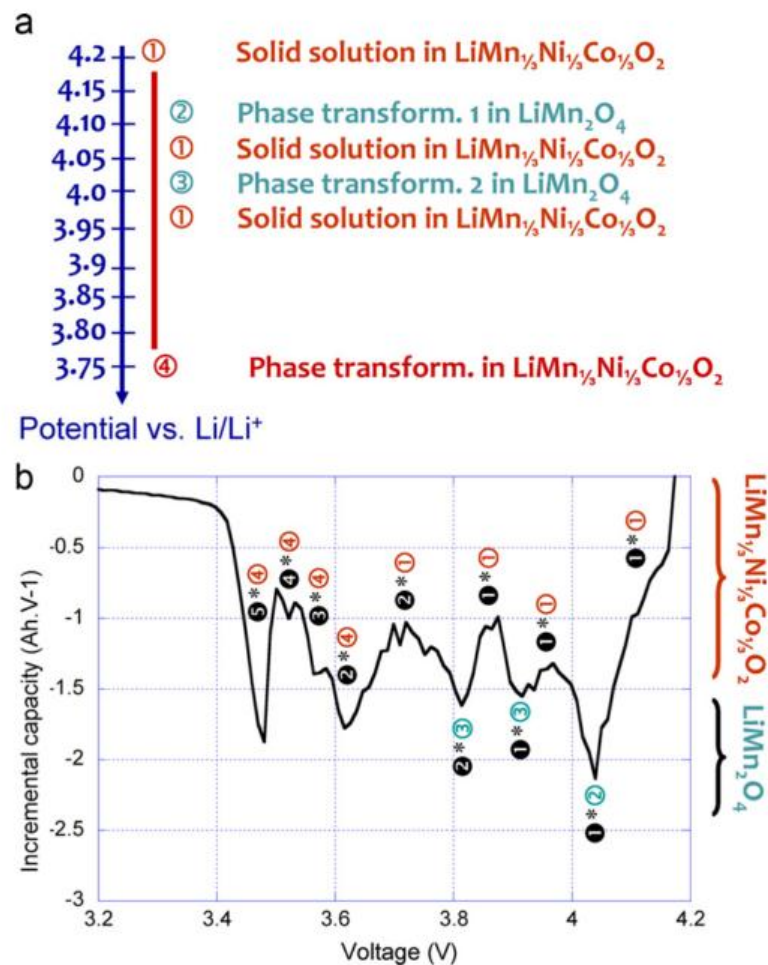


Figure 100 (a) Schematic illustrates the potential scale of the reactions occur in the composite positive electrode that comprises [NMC+Spinel]. (b) Convolution and index of the incremental capacity peaks as a function of cell voltage according to the composite positive electrode against the graphite negative electrode.

7.6.2 Incremental capacity peak indexation

The following figures display the association of each electrochemical reaction occurring at each electrode to an incremental capacity peak for all the other chemistries studied in this thesis work. In the negative electrode, the lithiated graphite undergoes five distinct phase transformations, as denoted by ① to ⑤. In the positive electrode, depending on the cell, different phase transformations and solid solutions happen (Figure 100 summarized these indexes). All of them are then reported on Figure 101 for IHR cells (NMC positive electrode), Figure 102 for IMR cells (NMC + spinel positive electrode) and Figure 103 for IMR cells (spinel positive electrode).

7.6.2.1 IHR

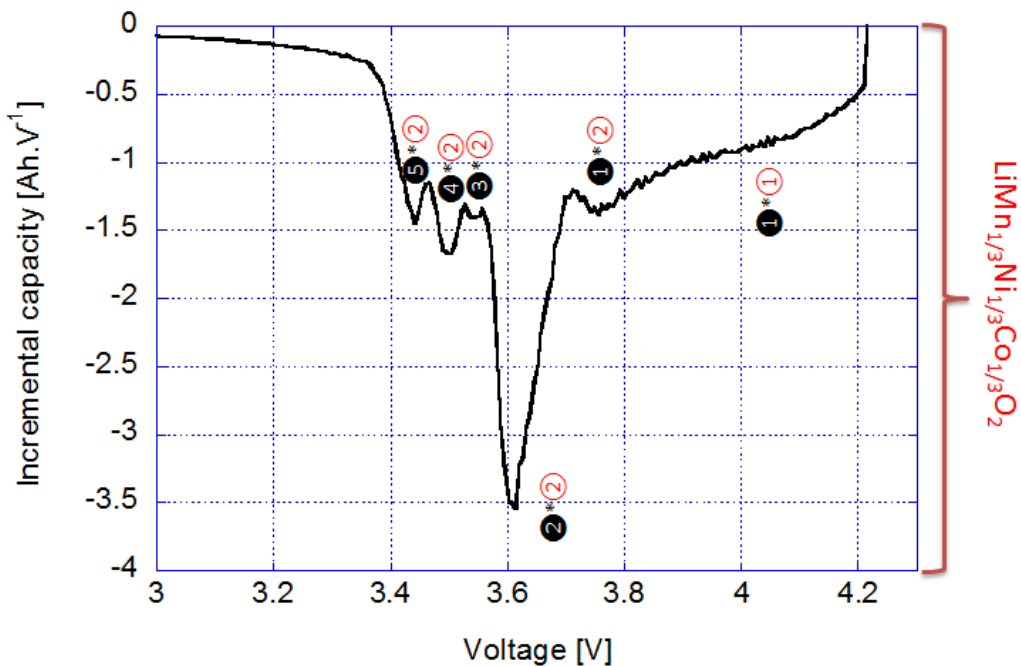


Figure 101 Peak indexation for IHR cell

7.6.2.2 IBR

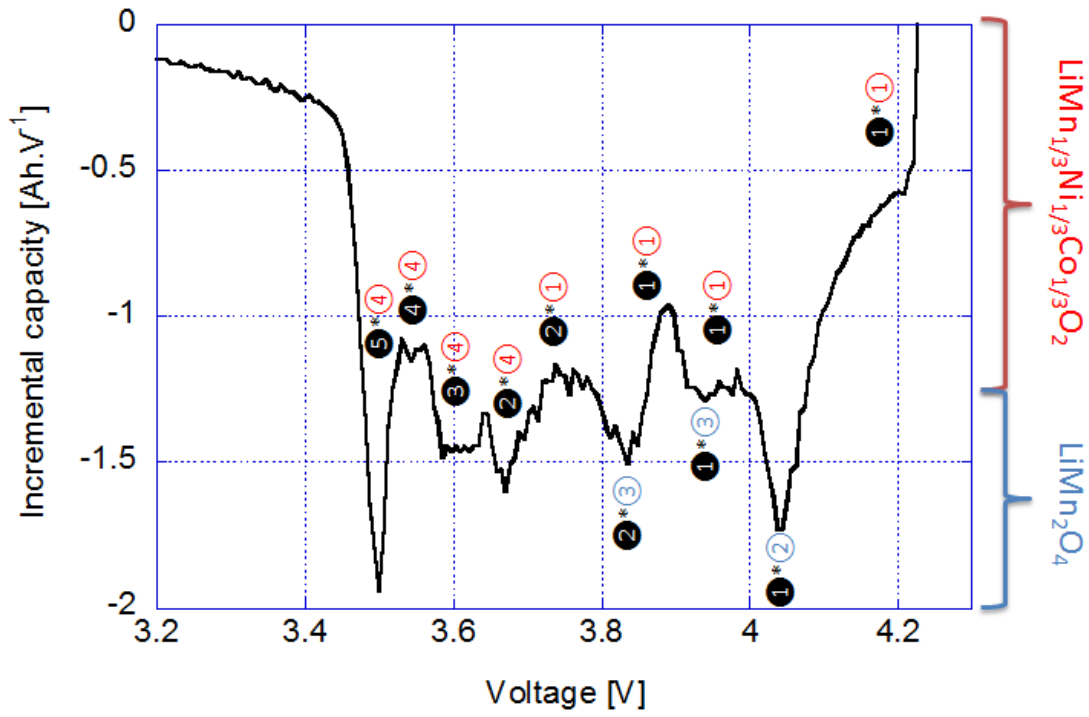


Figure 102 Peak indexation for IBR cells

7.6.2.3 IMR

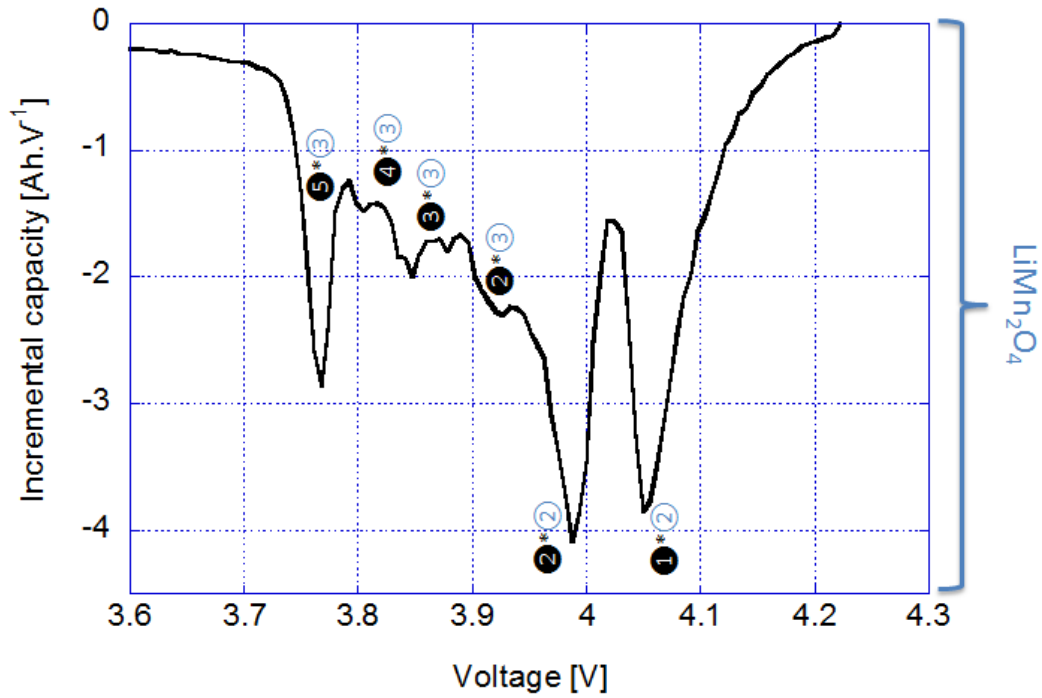


Figure 103 Peak indexation for IMR cells

7.7 Test equipment

Programmable multichannel battery test equipment from Arbin®, Maccor® and BioLogic® were used for all tests.

7.7.1 Arbin

7.7.1.1 BT-2043

Current Range: -100 to 100 mA, -1 to 1 A, -20 to 20 A

Voltage Range: -2 to +20 V

Voltage Accuracy: ?

Current Accuracy: ?



7.7.1.2 HVBT-5560



Current Range: ± 5 A

Voltage Range: ± 5 V

Voltage Accuracy: ?

Current Accuracy: ?

7.7.2 Maccor Series 4300

Current Range: 75 mA to 15 A

Voltage Range: 0 V to 15 V

Voltage Accuracy: ± 3 mV (16 bits)

Current Accuracy: ± 7.5 mA (16 bits)



7.7.3 BioLogic VMP3



Current Range: $\pm 10 \mu\text{A}$, $\pm 100 \mu\text{A}$, $\pm 1 \text{ mA}$, $\pm 10 \text{ mA}$, $\pm 100 \text{ mA}$, $\pm 1 \text{ A}$

Voltage Range: $\pm 2.5 \text{ mV}$, $\pm 5 \text{ mV}$, $\pm 10 \text{ mV}$

Voltage Accuracy: 16 bits ADC + 12 bits DC shift DAC's (max. resolution: 0.0015% of the range down to $7.5 \mu\text{V}$)

Current Accuracy: 16 bits ADC (max. resolution: 0.004% of the range down to 763 pA)

8 References

- 1 Japan, B. A. o. *Monthly battery sales statistics*, <<http://www.baj.or.jp/e/statistics/02.php>> (2011).
- 2 Dubarry, M. & Liaw, B. Y. Identify capacity fading mechanism in a commercial LiFePO₄ cell. *Journal of Power Sources* **194**, 541-549, doi:10.1016/j.jpowsour.2009.05.036 (2009).
- 3 Vetter, J. *et al.* Ageing mechanisms in lithium-ion batteries. *Journal of Power Sources* **147**, 269-281, doi:10.1016/j.jpowsour.2005.01.006 (2005).
- 4 J.-M. Tarascon, M. A. Issues and challenges facing rechargeable lithium batteries. *Nature* **414**, 359-367 (2001).
- 5 R. Koksang, J. B., H. SHi, M.Y. Saidi. Cathode materials for Lithium rocking chair batteries. *Solid State Ionics* **84**, 1-21 (1995).
- 6 Whittingham, M. S. Lithium Batteries and Cathode Materials. *Chem. Rev.* **104**, 4271-4301 (2004).
- 7 N. A. Chaturvedi, R. K., J. Christensen, J. Ahmed, A. Kojic. Algorithms for Advanced Battery-Management Systems. *Institute of Electrical and Electronics Engineers* (2010).
- 8 Economist, T. in *The Economist* (2008).
- 9 Communications, W. *Electropaedia*, <<http://www.mpoweruk.com/index.htm>> (
- 10 Goodenough, J. B. & Kim, Y. Challenges for rechargeable batteries. *Journal of Power Sources* **196**, 6688-6694, doi:10.1016/j.jpowsour.2010.11.074 (2011).
- 11 Buchman, I. *Batteries in a portable world*, <<http://batteryuniversity.com/>> (2001).
- 12 Scrosati, B. & Garche, J. Lithium batteries: Status, prospects and future. *Journal of Power Sources* **195**, 2419-2430, doi:10.1016/j.jpowsour.2009.11.048 (2010).
- 13 Dubarry, M. *et al.* Evaluation of commercial lithium-ion cells based on composite positive electrode for plug-in hybrid electric vehicle applications. Part II. Degradation mechanism under 2C cycle aging. *Journal of Power Sources* **196**, 10336-10343, doi:10.1016/j.jpowsour.2011.08.078 (2011).
- 14 Patterson, M. L. *Anode Materials for Lithium Ion Batteries*, <<http://nano.indiana.edu/documents/MPatterson.pdf>> (2009).
- 15 Huggins, R. A. Alternative materials for negative electrodes in lithium systems. *Solid State Ionics* **61** (2002).
- 16 Jonghoon Kim, J. S. High accuracy state of charge estimation on Li ion battery pack based on screening process. (2010).
- 17 Sabine Piller, M. P., Andreas Jossen. Methods for state-of-charge determination and their applications. *Journal of Power Sources* **96**, 113-120 (2001).
- 18 USABC. *Electric Vehicle Battery Test Procedures Manual*. (USABC, 2009).
- 19 Dubarry, M., Svoboda, V., Hwu, R. & Liaw, B. Y. Capacity loss in rechargeable lithium cells during cycle life testing: The importance of determining state-of-charge. *Journal of Power Sources* **174**, 1121-1125, doi:10.1016/j.jpowsour.2007.06.185 (2007).
- 20 Dubarry, M., Svoboda, V., Hwu, R. & Yann Liaw, B. Incremental Capacity Analysis and Close-to-Equilibrium OCV Measurements to Quantify Capacity Fade in Commercial Rechargeable Lithium Batteries. *Electrochemical and Solid-State Letters* **9**, A454, doi:10.1149/1.2221767 (2006).
- 21 Huggins, R. A. *Advanced Batteries, Materials Science Aspects*. Springer edn, (2009).
- 22 Huggins, R. A. Reference electrodes and Gibbs phase rule. *Solid State Ionics* **136** (2000).
- 23 Anderson, A. *Surface phenomena in Li-ion Batteries*.
- 24 Bouwman, P. J. *lithium intercalation in preferentially oriented submicrons LiCoO₂ films* PhD thesis, Institute of the University of Twente, Netherlands, (2002).

- 25 Christensen, J. & Newman, J. Effect of Anode Film Resistance on the Charge/Discharge Capacity of a Lithium-Ion Battery. *Journal of The Electrochemical Society* **150**, A1416, doi:10.1149/1.1612501 (2003).
- 26 Zhang, J. & Lee, J. A review on prognostics and health monitoring of Li-ion battery. *Journal of Power Sources* **196**, 6007-6014, doi:10.1016/j.jpowsour.2011.03.101 (2011).
- 27 Ng, K. S., Moo, C.-S., Chen, Y.-P. & Hsieh, Y.-C. Enhanced coulomb counting method for estimating state-of-charge and state-of-health of lithium-ion batteries. *Applied Energy* **86**, 1506-1511, doi:10.1016/j.apenergy.2008.11.021 (2009).
- 28 Wang, J., Cao, B., Chen, Q. & Wang, F. Combined state of charge estimator for electric vehicle battery pack. *Control Engineering Practice* **15**, 1569-1576, doi:10.1016/j.conengprac.2007.03.004 (2007).
- 29 Jonghoon Kim, J. S. Screening Process of Li-ion Series Battery Pack for Improved Voltage SOC Balancing. *International Power Electronics Conference* (2010).
- 30 Dubarry, M. *et al.* Evaluation of commercial lithium-ion cells based on composite positive electrode for plug-in hybrid electric vehicle applications. Part I: Initial characterizations. *Journal of Power Sources* **196**, 10328-10335, doi:10.1016/j.jpowsour.2011.08.077 (2011).
- 31 Dubarry, M., B.Y. Liaw. Battery State of Health Monitoring Using Electrochemical Techniques. (2008).
- 32 Safari, M. & Delacourt, C. Aging of a Commercial Graphite/LiFePO₄ Cell. *Journal of The Electrochemical Society* **158**, A1123, doi:10.1149/1.3614529 (2011).
- 33 Pop, V., Bergveld, H. J., Notten, P. H. L., Op het Veld, J. H. G. & Regtien, P. P. L. Accuracy analysis of the State-of-Charge and remaining run-time determination for lithium-ion batteries. *Measurement* **42**, 1131-1138, doi:10.1016/j.measurement.2008.03.009 (2009).
- 34 He, H., Xiong, R. & Guo, H. Online estimation of model parameters and state-of-charge of LiFePO₄ batteries in electric vehicles. *Applied Energy* **89**, 413-420, doi:10.1016/j.apenergy.2011.08.005 (2012).
- 35 Dubarry, M., B.Y. Liaw. Diagnostics of a Battery Pack Reliability and Life via Modeling and Simulation. (2008).
- 36 Dubarry, M., Vuillaume, N. & Liaw, B. Y. Origins and accommodation of cell variations in Li-ion battery pack modeling. *International Journal of Energy Research* **34**, 216-231, doi:10.1002/er.1668 (2010).
- 37 Dubarry, M., Vuillaume, N. & Liaw, B. Y. From single cell model to battery pack simulation for Li-ion batteries. *Journal of Power Sources* **186**, 500-507, doi:10.1016/j.jpowsour.2008.10.051 (2009).
- 38 Dubarry, M. & Liaw, B. Y. Development of a universal modeling tool for rechargeable lithium batteries. *Journal of Power Sources* **174**, 856-860, doi:10.1016/j.jpowsour.2007.06.157 (2007).
- 39 Haifeng Dai, X. W., Zechang Sun, Wang Jiayuan, Gu Weijun. Online cell SOC estimation of Li-ion battery packs using a dual time-scale Kalman filtering for EV applications. *Applied Energy* (2011).
- 40 Plett, G. L. Efficient Battery Pack State Estimation using Bar Delta filtering. *International Battery, Hybrid and Fuel Cell Electric Vehicle Symposium* (2009).
- 41 Christensen, J. & Newman, J. Cyclable Lithium and Capacity Loss in Li-Ion Cells. *Journal of The Electrochemical Society* **152**, A818, doi:10.1149/1.1870752 (2005).
- 42 Groot, J. *State of health estimation of Li ion batteries cycle life test methods* PhD thesis, Chalmers University of Technology, (2012).
- 43 Gering, K. L. *et al.* Investigation of path dependence in commercial lithium-ion cells chosen for plug-in hybrid vehicle duty cycle protocols. *Journal of Power Sources* **196**, 3395-3403, doi:10.1016/j.jpowsour.2010.05.058 (2011).

- 44 Wu, H.-C., Guo, Z.-Z., Wen, H.-P. & Yang, M.-H. Study the fading mechanism of LiMn₂O₄ battery with spherical and flake type graphite as anode materials. *Journal of Power Sources* **146**, 736-740, doi:10.1016/j.jpowsour.2005.03.070 (2005).
- 45 Yunjian, L. *et al.* Electrochemical performance and capacity fading reason of LiMn₂O₄/graphite batteries stored at room temperature. *Journal of Power Sources* **189**, 721-725, doi:10.1016/j.jpowsour.2008.08.044 (2009).
- 46 P. Ramadass, B. H., Ralph White, Branko N. Popov. Capacity fade of sony 18650 cells cycled at elevated temperatures part I cycling performance. *Journal of Power Sources* **112**, 606-613 (2002).
- 47 P. Ramadass, B. H., Ralph White, Branko N. Popov. Capacity fade of sony 18650 cells cycled at elevated temperatures part II Capacity fade analysis. *Journal of Power Sources* **112**, 614-620 (2002).
- 48 P. Ramadass, B. H., Ralph White, Branko N. Popov. Performance study of commercial LiCoO₂ and spinel based li ion cells. *Journal of Power Sources* **111**, 210-220 (2002).
- 49 Dubarry, M. *et al.* Identifying battery aging mechanisms in large format Li ion cells. *Journal of Power Sources* **196**, 3420-3425, doi:10.1016/j.jpowsour.2010.07.029 (2011).
- 50 Premanand, R., Durairajan, A., Haran, B., White, R. & Popov, B. Studies on Capacity Fade of Spinel-Based Li-Ion Batteries. *Journal of The Electrochemical Society* **149**, A54, doi:10.1149/1.1426399 (2002).
- 51 Dubarry, M. *Synthese, etude et optimisation de materiaux d'electrode positive pour batteries au lithium*. PhD thesis, Universite de Nantes, (2004).
- 52 Guy, D., Lestriez, B., Bouchet, R., Gaudefroy, V. & Guyomard, D. Novel architecture of composite electrode for optimization of lithium battery performance. *Journal of Power Sources* **157**, 438-442, doi:10.1016/j.jpowsour.2005.07.036 (2006).
- 53 Lestriez, B. Functions of polymers in composite electrodes of lithium ion batteries. *Comptes Rendus Chimie* **13**, 1341-1350, doi:10.1016/j.crci.2010.01.018 (2010).
- 54 Dominko, R. *et al.* The role of carbon black distribution in cathodes for Li ion batteries. *Journal of Power Sources* **119-121**, 770-773, doi:10.1016/s0378-7753(03)00250-7 (2003).
- 55 Ligneel, E., Lestriez, B., Richard, O. & Guyomard, D. Optimizing lithium battery performance from a tailor-made processing of the positive composite electrode. *Journal of Physics and Chemistry of Solids* **67**, 1275-1280, doi:10.1016/j.jpics.2006.01.093 (2006).
- 56 Ligneel, E., Lestriez, B. & Guyomard, D. Relationships between processing, morphology and discharge capacity of the composite electrode. *Journal of Power Sources* **174**, 716-719, doi:10.1016/j.jpowsour.2007.06.158 (2007).
- 57 P. Arora, Z. Z. Battery separator. *Chem. Rev.*, 4419-4462 (2004).
- 58 Kim, J., Lee, S. & Cho, B. H. Discrimination of Li-ion batteries based on Hamming network using discharging–charging voltage pattern recognition for improved state-of-charge estimation. *Journal of Power Sources* **196**, 2227-2240, doi:10.1016/j.jpowsour.2010.08.119 (2011).
- 59 Shen, Y. Adaptive online state-of-charge determination based on neuro-controller and neural network. *Energy Conversion and Management* **51**, 1093-1098, doi:10.1016/j.enconman.2009.12.015 (2010).
- 60 Plett, G. L. Extended Kalman filtering for battery management systems of LiPB-based HEV battery packs part 1 Background. *Journal of Power Sources* **134**, 252-261, doi:10.1016/j.jpowsour.2004.02.031 (2004).
- 61 Plett, G. L. Extended Kalman filtering for battery management systems of LiPB-based HEV battery packs part 2 Modelling and Identification. *Journal of Power Sources* **134**, 262-276, doi:10.1016/j.jpowsour.2004.02.032 (2004).

- 62 Plett, G. L. Extended Kalman filtering for battery management systems of LiPB-based HEV battery packs part 3 State and parameter estimation. *Journal of Power Sources* **134**, 277-292, doi:10.1016/j.jpowsour.2004.02.033 (2004).
- 63 Oanyong Nam, J. L. Li ion battery SOC estimation method based on the reduced order extended kalman filtering. *American Institute of Aeronautics and Astronautics*.
- 64 Lee, J., Nam, O. & Cho, B. H. Li-ion battery SOC estimation method based on the reduced order extended Kalman filtering. *Journal of Power Sources* **174**, 9-15, doi:10.1016/j.jpowsour.2007.03.072 (2007).
- 65 Lee, S., Kim, J., Lee, J. & Cho, B. H. State-of-charge and capacity estimation of lithium-ion battery using a new open-circuit voltage versus state-of-charge. *Journal of Power Sources* **185**, 1367-1373, doi:10.1016/j.jpowsour.2008.08.103 (2008).
- 66 Junping, W., Jingang, G. & Lei, D. An adaptive Kalman filtering based State of Charge combined estimator for electric vehicle battery pack. *Energy Conversion and Management* **50**, 3182-3186, doi:10.1016/j.enconman.2009.08.015 (2009).
- 67 Santhanagopalan, S. & White, R. E. Online estimation of the state of charge of a lithium ion cell. *Journal of Power Sources* **161**, 1346-1355, doi:10.1016/j.jpowsour.2006.04.146 (2006).
- 68 Alvin J. Salkind, C. F., Pritpal Singh, Terrill Atwater, David E. Reinsner. Determination of state of charge and state of health of batteries by fuzzy logic methodology. *Journal of Power Sources* **80**, 293-300 (1999).
- 69 Dubarry, M., Svoboda, V., Hwu, R. & Liaw, B. Y. Capacity and power fading mechanism identification from a commercial cell evaluation. *Journal of Power Sources* **165**, 566-572, doi:10.1016/j.jpowsour.2006.10.046 (2007).
- 70 Wood, E., Alexander, M. & Bradley, T. H. Investigation of battery end-of-life conditions for plug-in hybrid electric vehicles. *Journal of Power Sources* **196**, 5147-5154, doi:10.1016/j.jpowsour.2011.02.025 (2011).